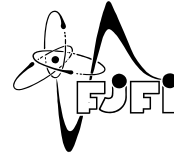




České vysoké učení technické
Fakulta jaderná a fyzikálně inženýrská
Katedra matematiky



Diplomová práce

Numerical Analysis of Multiphase Porous Media Flow in Groundwater Contamination Problems

Numerická analýza vícefázového filtračního proudění
v problematice znečištění podzemních vod

Akademický rok 2005/2006

Autor: Radek Fučík

Školitel: Ing. Jiří Mikyška, Ph.D.

Konzultant: Doc. Dr. Ing. Michal Beneš

Katedra: matematiky

Akademický rok: 2005/2006

ZADÁNÍ DIPLOMOVÉ PRÁCE

Pro: Radek Fučík
Obor: Matematické inženýrství
Zaměření: Matematické modelování
Název práce: Numerická analýza vícefázového filtračního proudění v problematice znečištění podzemních vod / Numerical analysis of multiphase porous media flow in groundwater contamination problems

Osnova:

1. Shrňte své zkušenosti s možnostmi získání analytického řešení zjednodušených jednorozměrných modelů dvoufázového filtračního proudění.
2. Vyšetřete případy, pro něž lze získat řešení zjednodušených modelů v uzavřeném tvaru a diskutujte příčiny možných problémů v případech ostatních.
3. Porovnejte výsledky analytického postupu s výsledky numerických modelů. Proveďte experimentální konvergenční analýzu s použitím stávajících algoritmů.
4. Popište zobecnění jednorozměrného numerického modelu zahrnujícího heterogenní prostředí.
5. Doplňte vaše stávající vzorové simulační výpočty o některé další případy (zejména simulaci infiltrace nevodnaté fáze do prostředí obsahujícím ostré heterogenity).

Doporučená literatura:

1. M. F. Wheeler, Environmental Studies, Springer, 1996
2. J. Bear, A. Verruijt: Modeling Groundwater Flow and Pollution, Reidel, Dodrecht, 1987
3. Helmig R. (1997) Multiphase Flow and Transport Processes in the Subsurface, A Contribution to the Modelling of Hydrosystems. Springer, ISBN3-540-62703-0.
4. McWhorter D. B., Sunada D. K. (1990) Exact Integral Solutions for Two-Phase Flow. Wat. Resour. Res. 26(3), 399-413.
5. McWhorter D. B., Sunada D. K. (1992) Reply. Wat. Resour. Res. 28(5), 1479.

Vedoucí diplomové práce: Ing. Jiří Mikyška

Adresa pracoviště: Katedra matematiky,
FJFI ČVUT Praha,
Trojanova 13, Praha 2

Konzultant: Doc. Dr. Ing. Michal Beneš


Datum zadání diplomové práce: 15.10.2005

Termín odevzdání diplomové práce: **Podle rozhodnutí děkana**

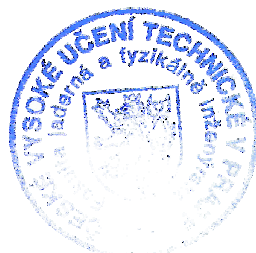
V Praze dne 10.10.2006



Vedoucí katedry



Děkan



Čestné prohlášení

Prohlašuji, že předkládanou diplomovou práci jsem vypracoval samostatně s použitím pouze citované literatury.

V Praze dne 1. května 2006

Radek Fučík



Preface

Mathematical modelling of the groundwater flow and the pollution allows to understand and predict behaviour of the fluids in the subsurface and therefore to protect the quality of the most important resource for all forms of life on Earth. Cleanup of contaminated water aquifers is a very difficult task and it is often beyond human potentialities.

The present work examine the quasi-analytical solution firstly obtained by McWhorter and Sunada in 1990 and provide detailed analysis of the way the solution of the governing partial differential equation of two-phase flow can be obtained from a functional integral equation given by the analytical treatment of the problem. I present an improved algorithm implementation of this solution.

The McWhorter and Sunada analytical solution can be applied to porous media with a discontinuity for a nonzero advection term, which has not been published yet in the available literature. Therefore, the exact solution for heterogeneous media will be useful in the verification of the treatment of the fluid behaviour at the material interfaces in the numerical schemes.

I am very grateful to my advisors Doc. Dr. Ing. Michal Beneš¹, Ing. Jiří Mikyška, Ph.D. ¹ and Prof. Tissa H. Illangasekare² for their introduction into the topic, common leadership, for continuously encouraging my ideas in the work and careful reading of the manuscript.

Last but not least, I would like to thank Doc. Ing. Richard Liska, CSc.¹ for providing information and advice concerning the hyperbolic partial differential equations.

Prague, May 2006

Radek Fučík

¹Czech Technical University in Prague, Faculty of Nuclear Science and Physical Engineering

²Colorado School of Mines, Golden, Colorado

Contents

Preface	i
List of Figures	v
List of Tables	viii
List of Symbols	x
Introduction	1
1 Modelling Immiscible Flow in Porous Media	3
1.1 Porous Medium	3
1.1.1 Definitions	3
1.1.2 Continuum Approach to Porous Medium	5
1.2 Single-Phase Flow	7
1.2.1 Continuity Theorem	7
1.2.2 Darcy Law	8
1.3 Two-Phase Flow	9
1.3.1 Saturation	9
1.3.2 Continuity Theorem	11
1.3.3 Darcy law	11
1.3.4 Capillarity	12
1.3.5 Capillary Pressure	13
1.3.6 Capillary Hysteresis	15
1.3.7 Relative Permeability	16
1.4 Fluid Behaviour at Material Interface	18
1.4.1 Interfacial Conditions	18
1.5 Flow in Homogeneous Porous Medium	20
1.5.1 Total Velocity	21
1.5.2 Rearranging Equations	21
1.5.3 Complete Set of Equations	22

CONTENTS

1.6	One-Dimensional Two-Phase Flow Problem	22
1.6.1	One-Dimensional Transport Equation	23
1.6.2	Problem Formulation	24
2	Exact Solutions in Homogeneous Media	25
2.1	Introduction	25
2.2	Buckley-Leverett Analytical Solution	26
2.2.1	Method of Characteristics	27
2.2.2	Entropy Condition : Convex Hull Construction	30
2.2.3	Mass Balance Condition : Equal Area Rule	31
2.2.4	Analytical Solution	32
2.3	McWhorter-Sunada Exact Solution	33
2.3.1	Problem Formulation	33
2.3.2	Exact Solution Derivation	36
2.3.3	Original Integral Equation	39
2.3.4	Modified Integral Equation	47
2.3.5	Limit value of A	53
2.3.6	Generalization of Formulation	56
2.3.7	Summary	57
2.4	Comparison of Exact Solutions	58
3	Exact Solution for Heterogeneous Media	61
3.1	Introduction	61
3.2	Non-Wetting Phase Infiltration Problem	62
3.2.1	Exact Solution	62
3.2.2	Algorithm	66
3.3	Wetting Phase Influx Problem	68
3.3.1	Exact Solution	68
3.3.2	Admissible Range of Parameters	70
3.3.3	Algorithm	70
3.4	Illustrative Calculations	72
3.4.1	Model Parameters	72
3.4.2	Materials and Fluids with Significant Saturation Jumps across Interface	80
3.4.3	Realistic Materials and Fluids	82
4	One-dimensional Numerical Methods	85
4.1	Two-Phase Flow Equation	85
4.1.1	Spatial Discretization	86
4.1.2	Initial and Boundary Conditions	87
4.1.3	Runge-Kutta Methods for System of ODE	88

4.1.4	Interface Implementation	89
4.2	Applicability in Homogeneous Medium	90
4.2.1	Linearization	90
4.2.2	Applicability of McWhorter and Sunada Exact Solutions .	91
4.2.3	Convergence analysis	92
4.3	Applicability in Heterogeneous Media	106
4.3.1	Convergence analysis	106
4.3.2	Two Phase Flow in Heterogeneous Porous Media	125
	Conclusions	129
	References	131
	Index	134

CONTENTS

List of Figures

1.1	Porous medium illustration	4
1.2	Different scales in a porous medium	5
1.3	Porosity at different scales.	6
1.4	Capillary effects details	12
1.5	Interface tension and wetting angle	13
1.6	Typical capillary pressure curves after Brooks-Corey and after van Genuchten	16
1.7	Relative permeability functions.	17
1.8	Interface between two homogeneous porous media.	19
1.9	Capillary pressure curves.	20
2.1	Typical functions f and f'	28
2.2	Convex hull of the set \mathfrak{S}	30
2.3	Equal area rule	31
2.4	Illustration of the Buckley-Leverett analytical solution	32
2.5	Functions φ and F_1 , viscosity ratio $M = 1$ and $M = 0.05$	44
2.6	Illustration to the approaching of F to F_{BL}	54
2.7	Evolution of A in the iterative process	56
2.8	Congruity of exact solutions.	59
3.1	Heterogeneous medium initial state	63
3.2	Function $h(x) = x(x - 1)^{-1}$	65
3.3	Capillary pressure curves	73
3.4	Illustration to existence of the exact solution.	74
3.5	Admissible values of \mathfrak{S}_i^L and \mathfrak{S}_i^R	75
3.6	Exact solutions, Coarse sand to fine sand flow, Brooks-Corey.	76
3.7	Exact solutions, Coarse sand to fine sand flow, van Genuchten.	77
3.8	Exact solutions, Coarse sand to fine sand flow, Brooks-Corey.	78
3.9	Exact solutions, Coarse sand to fine sand flow, van Genuchten.	79
3.10	Exact solutions.	81
3.11	Admissible values of \mathfrak{S}_i^L and \mathfrak{S}_i^R	82

LIST OF FIGURES

3.12	Exact solutions.	83
4.1	Interface between adjacent nodes	89
4.2	Exact and numerical solutions, homogeneous medium, Brooks-Corey.	94
4.3	Exact and numerical solutions, homogeneous medium, van Genuchten.	100
4.4	Heterogeneous medium initial state	107
4.5	Exact and numerical solutions, heterogeneous CS-FS medium, Brooks-Corey.	112
4.6	Exact and numerical solutions, heterogeneous FS-CS medium, Brooks-Corey.	116
4.7	Exact and numerical solutions, heterogeneous CS-FS medium, van Genuchten.	120
4.8	Exact and numerical solutions, heterogeneous FS-CS medium, van Genuchten.	124
4.9	Test problem setup	126
4.10	Numerical solutions at time $t = 150$ s and $t = 250$ s.	127
4.11	Numerical solutions at time $t = 500$ s, $t = 750$ s and $t = 1650$ s.	128

List of Tables

2.1	Parameter setup used in this chapter.	27
2.2	Critical values \mathcal{S}_0^* model setup 1	43
2.3	Critical values \mathcal{S}_0^* model setup 2	43
2.4	Critical values \mathcal{S}_0^* model setup 3	44
2.5	Number of iterations for required precision	51
2.6	Experimental convergence of F to F_{BL}	55
2.7	Values of A for various values of R and \mathcal{S}_0 ; test setup 1, $\mathcal{S}_i = 0$	59
3.1	Parameter setup, unrealistic materials	72
3.2	Parameter setup, unrealistic materials	80
3.3	Parameter setup, realistic materials	82
4.1	Time steps τ , Brooks-Corey	95
4.2	ECC , $\mathcal{S}_0 = 0.5$, Brooks-Corey	96
4.3	ECC , $\mathcal{S}_0 = 0.7$, Brooks-Corey	96
4.4	ECC , $\mathcal{S}_0 = 0.8$, Brooks-Corey	97
4.5	ECC , $\mathcal{S}_0 = 0.9$, Brooks-Corey	97
4.6	ECC , $\mathcal{S}_0 = 0.5$, Brooks-Corey	98
4.7	ECC , $\mathcal{S}_0 = 0.7$, Brooks-Corey	98
4.8	ECC , $\mathcal{S}_0 = 0.8$, Brooks-Corey	99
4.9	ECC , $\mathcal{S}_0 = 0.9$, Brooks-Corey	99
4.10	Time steps τ , van Genuchten	101
4.11	ECC , $\mathcal{S}_0 = 0.5$, van Genuchten	102
4.12	ECC , $\mathcal{S}_0 = 0.7$, van Genuchten	102
4.13	ECC , $\mathcal{S}_0 = 0.8$, van Genuchten	103
4.14	ECC , $\mathcal{S}_0 = 0.9$, van Genuchten	103
4.15	ECC , $\mathcal{S}_0 = 0.5$, van Genuchten	104
4.16	ECC , $\mathcal{S}_0 = 0.7$, van Genuchten	104
4.17	ECC , $\mathcal{S}_0 = 0.8$, van Genuchten	105
4.18	ECC , $\mathcal{S}_0 = 0.9$, van Genuchten	105
4.19	Parameter setup, unrealistic materials	108

LIST OF TABLES

4.20	Time steps τ , Brooks-Corey, CS \rightarrow FS	109
4.21	<i>ECC</i> , heterogeneous medium, Brooks-Corey	110
4.22	<i>ECC</i> , heterogeneous medium, Brooks-Corey	111
4.23	Time steps τ , Brooks-Corey, FS \rightarrow CS	113
4.24	<i>ECC</i> , heterogeneous medium, Brooks-Corey	114
4.25	<i>ECC</i> , heterogeneous medium, Brooks-Corey	115
4.26	Time steps τ , van Genuchten, CS \rightarrow FS	117
4.27	<i>ECC</i> , heterogeneous medium, van Genuchten	118
4.28	<i>ECC</i> , heterogeneous medium, van Genuchten	119
4.29	Time steps τ , van Genuchten, FS \rightarrow CS	121
4.30	<i>ECC</i> , heterogeneous medium, van Genuchten	122
4.31	<i>ECC</i> , heterogeneous medium, van Genuchten	123
4.32	Test parameter setup.	126

List of Symbols

α	Van Genuchten parameter, [Pa^{-1}]	page 15
λ	Brooks and Corey pore size distribution index, [-]	page 14
λ_α	Mobility of the phase α , [$Pa^{-1}s^{-1}$]	page 11
μ	Dynamic viscosity, [$Pa\ s$]	page 4
Φ	Porosity, [-]	page 6
S_α	Effective saturation of the phase α , [-]	page 10
σ	Surface tension, [$J\ m^{-2}$]	page 12
ρ	Density, [$kg\ m^{-3}$]	page 4
\mathbf{K}	Absolute permeability tensor, [m^{-2}]	page 8
\mathbf{u}	Macroscopic apparent velocity, [$m\ s^{-1}$]	page 8
k_r	Relative permeability, [-]	page 11
m	Van Genuchten parameter, [-]	page 15
n	Van Genuchten parameter, [-]	page 15
p	Fluid pressure, [Pa]	page 8
p_c	Capillary pressure, [Pa]	page 13
p_d	Brooks and Corey entry pressure, [Pa]	page 14
S_α	Saturation of the phase α , [-]	page 10
$S_{r\alpha}$	Residual saturation of the phase α , [-]	page 10

LIST OF TABLES

Introduction

OBJECTIVE OF THIS WORK

Complex multi-dimensional numerical models of multi-phase flow through porous media such as those described in Helmig (1997), or Mikyška et al. (2004) and Mikyška and Illangasekare (2005) require verification to assure that the governing equations are solved correctly and the codes do not contain programming errors. This step of code verification is a necessary step in modelling protocols used in practice (e.g. Anderson & Woessner, 2002). The code simulations are compared to closed form analytical solutions to the governing equations to estimate numerical errors and other inaccuracies of numerical schemes when they are used to simulate simplified flow problems.

Two known solutions to the two-phase flow equations are available for this task, namely the Buckley-Leverett solution of the flow without capillary effects (e.g. described by Helmig, 1997; LeVeque, 2002; or see references in Sunada & McWhorter, 1990) and the exact integral solution derived by McWhorter and Sunada (1990) with subsequent discussions by Chen et al. (1992), McWhorter and Sunada (1992), Fučík 2005 and Fučík et al. (2004a), which allow to study the influence both of the advection and capillary effects in specific one-dimensional settings for the homogeneous porous media.

In this work, the author discusses the exact integral equation for the wetting-phase saturation obtained by McWhorter and Sunada (1990). This equation has to be numerically integrated to yield the saturation distribution along the length of the soil column. In this solution scheme a value for entry saturation is needed as an input boundary condition. The solution to the problem as presented by McWhorter and Sunada (1990) has limitations in situations where the entry wetting-phase saturations are high. The author discusses the use of the McWhorter and Sunada exact solution for all admissible values of the input to total velocity ratio parameter R , including its negative values.

The extension of the original McWhorter and Sunada exact solution allows to derive exact solutions for the heterogeneous porous medium with the nonzero advection term and thus extend exact solutions for the diffusion equation discussed

by van Duijn, 1998.

STRUCTURE OF THIS WORK

This book starts with an introduction to the mathematical modelling of the multiphase flow in homogeneous and heterogeneous porous media. The one-dimensional two-phase flow equation is derived in Chapter 1.

The one-dimensional Buckley-Leverett and McWhorter-Sunada exact solutions for the homogeneous porous media are derived and discussed in Chapter 2. The applicability of the McWhorter-Sunada exact solution is extended to a larger set of admissible input parameters and a new iterative method for solving the respective integral equation developed by the author is presented.

New quasi-analytical solutions for the heterogeneous porous media derived by the author are presented in Chapter 3.

Chapter 4 concentrates on the numerical solutions of the McWhorter and Sunada problem and underlines the applicability of the analytical solution both for the homogeneous and heterogeneous problems.

ACKNOWLEDGEMENTS

The research was realized in collaboration with Center for Experimental Study of Subsurface Environmental Processes (CESEP), Colorado School of Mines, Golden, Colorado.

The author was partly supported by the project "Applied Mathematics in Technical and Physical Sciences" MSM 6840770010, by the project "Environmental modelling" KONTAKT ME878, and by the project "Jindřich-Nečas Center for Mathematical Modelling" LC06052, all of the Ministry of Education of the Czech Republic, and by the National Science Foundation through the award 0222286 (CMG RESEARCH: "Numerical and Experimental Validation of Stochastic Upscaling for Subsurface Contamination Problems Involving Multi-phase Volatile Chlorinated Solvents").

Chapter 1

Modelling Immiscible Flow in Porous Media

This chapter provides an introduction to the mathematical modelling of immiscible multiphase flow in porous media. The author briefly shows how the complex nature of multiphase flow in porous media is described by mathematical modelling and how a domain of validity of this approach is specified.

The author follows Bastian, 1999, Kazda, 1997, Helmig, 1997 and Bear & Verruijt, 1990 in order to describe fundamental approaches in modelling multiphase flow in porous media.

1.1 Porous Medium

1.1.1 Definitions

POROUS MEDIUM

A porous medium is composed of a persistent *solid matrix* (also called *solid phase*) and a *void space* (or a *pore space*). Figure 1.1 shows a two-dimensional cross section of a porous medium filled with water and oil.

In order to develop mathematical models for fluid dynamics within pore space, several assumptions are placed upon the geometry and dimensions of the porous medium (see Bastian, 1999):

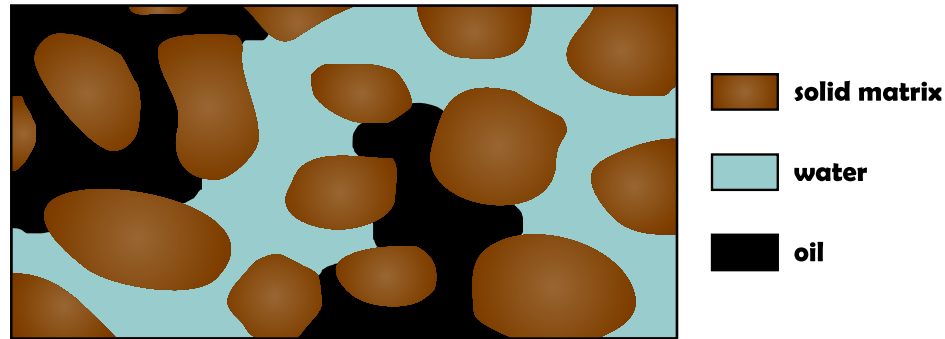


Figure 1.1: Depiction of a porous medium filled with water and oil (two-phase system).

- A. The pore space is interconnected since no flow can take place in a disconnected void space.
- B. The dimensions of the void space must be sufficiently large compared to the dimensions of the fluid molecules and the solid structure can be considered as a hypothetical continuum.
- C. The dimensions of the pore space must be small enough so that the fluid flow is governed by adhesive forces at fluid-solid interfaces and cohesive forces at fluid-fluid interfaces in multiphase systems. This excludes cases like a network of pipes from the definition of porous medium.

Soil, various sands with different grain sizes, fissured rocks, sandstone and Karstic limestone are typical representatives of porous media. However, ceramics, foam rubber, bread, bones or organic tissue are also considered as porous media (see Bear & Verruijt, 1990).

PHASE

A phase is defined as a chemically homogeneous portion of a system under consideration that is separated from other such portions by a definite physical boundary (see the citation on the page 7 in Bastian, 1999).

The necessity of a definite physical boundary between two or more phases implies that no more than one gaseous phase can be present in the multiphase system since gases are always completely miscible. A phase can be formed from one or more fluids and it is usually characterized by the *dynamic viscosity* μ [$Pa\ s$] and the *density* ρ [$kg\ m^{-3}$].

Flow of air (or gaseous mixture), water or NAPL in porous media is studied in the majority of cases. NAPL stands for Non-Aqueous Phase Liquid. These liquids can be further divided into dense NAPL (abbreviated DNAPL), which have higher

density than water and light NAPL (abbreviated LNAPL), whose density is lower than water. The most frequent problem in porous media flow is a groundwater contamination or a protection simulation, where NAPL is usually a liquid such as petroleum products or chlorinated hydrocarbons. These volatile chemicals have very low solubility in water and they satisfy the phase definition. On that account, the division of fluids as above is used.

1.1.2 Continuum Approach to Porous Medium

The previous section adumbrated that considering different dimension scales is very important for modelling porous media flow. Figure 1.2 depicts different magnifications of a porous medium from *macroscale* (left figure) through *microscale* (middle figure) to *molecular scale* (right figure).

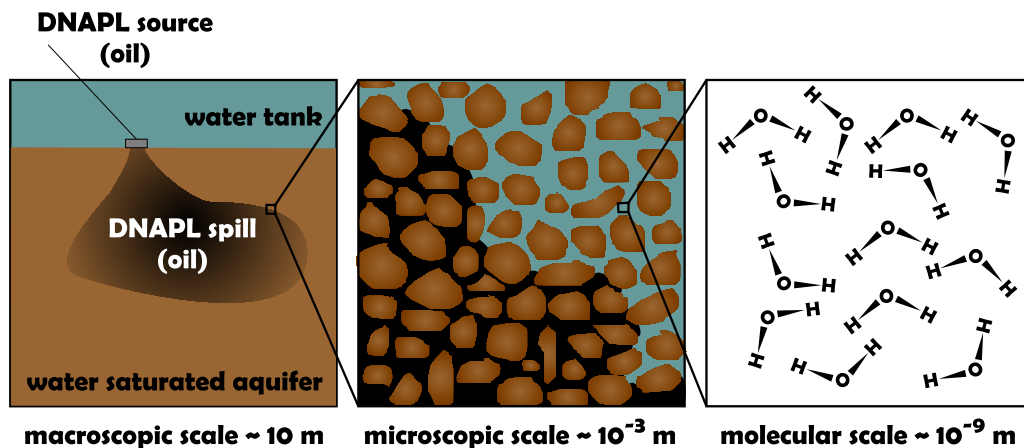


Figure 1.2: Figure of different scales in a porous medium. It illustrates a typical contamination problem, where the contamination source (e.g. oil barrel) lies at the bottom of a water reservoir (e.g. lake). The contaminant (e.g. oil) is leaking out of the source and enters the fully water saturated porous medium.

Every problem concerning fluid dynamics in porous media has to be provided with a set of boundary and initial conditions. It is obvious from Figure 1.2 that for a macroscopic problem the boundary conditions can neither be prescribed at microscale nor at molecular scale due to practically random geometry of the porous medium. In order to develop a mathematical model a description of the porous medium as a continuum at macroscopic scale is needed. Each point in the continuum on the macroscale is assigned average values over *elementary volumes* of quantities on the microscopic level. This process leads to *macroscopic equations* that are in fact independent of the exact description of the microscopic configura-

tion, because only statistical properties of the porous medium and the fluid phases are taken into account.

POROSITY

In this section, a macroscopic property of the porous medium *porosity* Φ is derived by volume averaging.

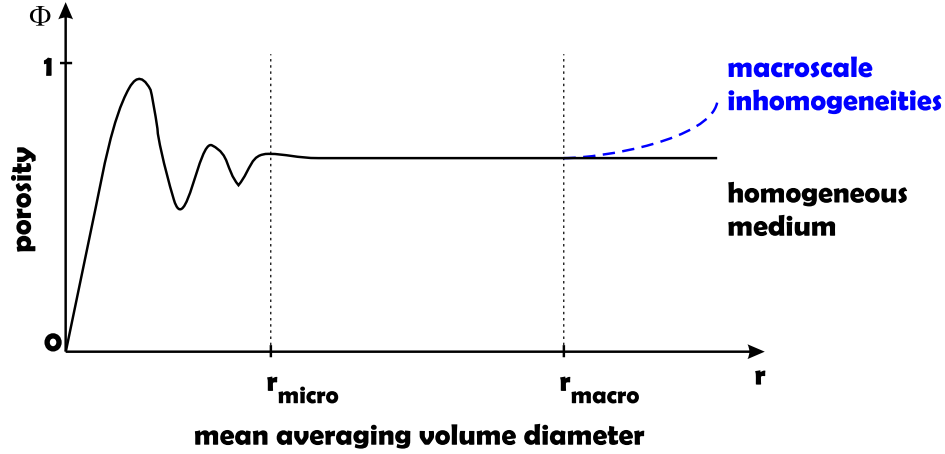


Figure 1.3: Porosity at different scales.

Let Ω be a domain occupied by the porous medium and $meas \Omega$ be its volume. The void space indicator function on the microscopic level is defined as follows

$$\gamma(\mathbf{x}) = \begin{cases} 1 & \mathbf{x} \in \text{void space} \\ 0 & \mathbf{x} \in \text{solid matrix} \end{cases} \quad \forall \mathbf{x} \in \Omega. \quad (1.1)$$

Suppose $B(\mathbf{x}_0, r) \subset \Omega$ is a ball centered at a point $\mathbf{x}_0 \in \Omega$ with radius r . Then the porosity $\Phi(\mathbf{x}_0)$ at position \mathbf{x}_0 with respect to $B(\mathbf{x}_0, r) \subset \Omega$ is defined as

$$\Phi(\mathbf{x}_0) = \frac{1}{meas B(\mathbf{x}_0, r)} \int_{B(\mathbf{x}_0, r)} \gamma(\mathbf{x}) dx. \quad (1.2)$$

The macroscopic quantity porosity is obtained by averaging over the microscopic void space indicator function. The REV has to be chosen so that the value of the averaged quantity does not depend on the size of the averaging volume. A rough plot of porosity values in function of the averaging ball radius is depicted in Figure 1.3. For small values of r the porosity is significantly oscillating, but between certain radii r_{micro} and r_{macro} , the value of $\Phi(\mathbf{x}_0)$ steadies and remains almost constant. For values of r greater than r_{macro} a smooth and monotonous growth

of $\Phi(\mathbf{x}_0)$ is observed. The average volume is called *Representative Elementary Volume* (REV) if the radii r_{micro} and r_{macro} exist such that the value of averaged quantity does not depend on the radius r within the range

$$r_{micro} \ll r \ll r_{macro}$$

(see Bastian, 1999 or Mikyška, 2005).

A REV is a volume, that is sufficiently large to statistically estimate all relevant parameters of the void space configuration (see Bear & Verruijt, 1990) and small enough to be considered as a negligible portion of total volume from the macroscopic scale. If such REV cannot be found then the macroscopic theory of porous media presented in this chapter can not be applied.

Another way to arrive at macroscopic quantities out of microscopic is the homogenization technique which is based on the mathematical theory on asymptotic functional expansion (see Hornung, 1997). Some of its principles has been already discussed in Fučík, 2004.

HOMOGENEOUS VS. HETEROGENEOUS MEDIUM

A porous medium is *homogeneous*, resp. *heterogeneous* with respect to a macroscopic quantity (i.e. porosity, temperature...) if that parameter has the same value, resp. differs throughout the domain.

In the case of this work, only a homogeneous porous media is considered. The term *heterogeneous* porous media is used for media that are composed of more than one homogeneous subdomains of different physical properties (like porosity). Therefore, all relevant quantities of the porous medium are assumed to be constant or piecewisely constant in space.

1.2 Single-Phase Flow

The single-phase fluid flow in the porous medium is described in this section. The mass-conservation law is applied to the fluid in porous medium and then the *Darcy law*, which is a statistical result of momentum balance law in porous media, is analyzed.

1.2.1 Continuity Theorem

Let us consider a porous medium domain Ω with porosity Φ that is filled with a single fluid phase. Macroscopic fluid mass conservation law, the *continuity theorem*, is expressed by the partial differential equation

$$\frac{\partial(\Phi \varrho)}{\partial t} + \nabla \cdot (\varrho \mathbf{u}) = \varrho \mathbf{q} \quad \text{in } \Omega, \quad (1.3)$$

where the quantities have the following meaning :

$\mathbf{u}(t, \mathbf{x})$	$[m s^{-1}]$	<i>Macroscopic apparent velocity.</i> This velocity is observed at macroscale. On the microscopic level the flow takes only place through the pore channels of the porous medium where an average velocity of $\frac{\mathbf{u}}{\phi}$ is observed (see Bastian, 1999).
$\Phi(\mathbf{x})$	$[-]$	Porosity of the porous medium defined in (1.2). Note that it is a function of position for heterogeneous porous media.
$\varrho(t, \mathbf{x})$	$[kg m^{-3}]$	Density of the fluid that can potentially depend on position or time for compressible fluid.
$\mathbf{q}(t, \mathbf{x})$	$[s^{-1}]$	Specific source/sink term.

1.2.2 Darcy Law

By using local averaging techniques (see citation on the page 13 in Bastian, 1999) or homogenization (see Hornung, 1997), the momentum conservation law (Navier-Stokes equations or Euler equations, see Fučík, 2004) can be reduced to a statistical principle:

$$\mathbf{u} = -\frac{\mathbf{K}}{\mu}(\nabla p - \varrho \mathbf{g}), \quad (1.4)$$

where all quantities have the following meaning :

$\mathbf{u}(t, \mathbf{x})$	$[m s^{-1}]$	Macroscopic apparent velocity already defined in (1.3).
$\mathbf{K}(\mathbf{x})$	$[m^{-2}]$	Symmetric tensor of <i>absolute permeability</i> , that can depend on position in the case of heterogeneous medium. Homogeneous (isotropic) porous medium implies $\mathbf{K} = K \mathbf{I}$, where \mathbf{I} is the identity matrix and K is scalar absolute permeability, also called <i>intrinsic soil permeability</i> .
$\mu(t, \mathbf{x})$	$[Pa s]$	<i>Dynamic viscosity</i> of the fluid.
$p(t, \mathbf{x})$	$[Pa]$	Fluid pressure.
\mathbf{g}	$[m s^{-2}]$	Gravitational acceleration vector.

This principle is called the *Darcy Law* after the French physician Henry Darcy, who in 1856 investigated the flow of water in vertical homogeneous sand filters in connection with the fountains of the city of Dijon. It is valid only for slow flows of Newtonian fluid ¹ through a porous medium with rigid solid matrix. The range of its validity can be approximated using the following number *Re*.

¹Newtonian fluid : the stress tensor depends linearly on the deformation tensor.

The Reynolds number Re is a quantity that characterizes fluid velocity \mathbf{u} with respect to fluid *kinematic viscosity* ν [$m^2 s^{-1}$] and representative microscopic length d describing the solid matrix (mean diameter of grain size) of the porous medium. It can be defined by the relationship

$$Re = \frac{d}{\nu} \|\mathbf{u}\|. \quad (1.5)$$

Despite some other definitions of the Reynolds number Re , the Darcy law is valid for values of Re between 1 (fine sand) and 10 (coarse sand). The linear Darcy law in the form (1.4) is therefore valid for most of the practical porous media problems. More complex nonlinear Darcy law has to be employed for greater values of Re , e.g. for modelling flow in a very close vicinity of large pumping or recharging wells, or in very porous matters like cavernous limestone or larger stones, see Bear & Verruijt, 1990.

1.3 Two-Phase Flow

Basics of the two-phase flow in porous medium is studied in this section, but the respective quantities can be used in a multiphase flow formulation as well. The definitions and explanations presented in Helmig, 1997, Bear & Verruijt, 1990 and Bastian, 1999 are resumed.

1.3.1 Saturation

Let us consider REV of a porous medium occupied by several phases. At the microscale every point of the REV is occupied either by the solid phase or by exactly one of the fluid phases. Let γ_α be indicator function of the fluid phase α , defined by

$$\gamma_\alpha(t, \mathbf{x}) = \begin{cases} 1 & \mathbf{x} \text{ belongs to phase } \alpha \text{ at time } t \\ 0 & \text{otherwise} \end{cases} \quad \forall \mathbf{x} \in \Omega. \quad (1.6)$$

(see Bastian, 1999). This α -phase indicator function allows us to define a macroscopical quantity called *saturation* S_α of the phase α by the relation

$$S_\alpha(t, \mathbf{x}_0) = \frac{\int_{REV} \gamma_\alpha(t, \mathbf{x}) d\mathbf{x}}{\int_{REV} \gamma(t, \mathbf{x}) d\mathbf{x}}, \quad (1.7)$$

where $x_0 \in REV$ and the void space indicator function γ is defined in (1.6). The REV volume can be chosen as a ball $B(x_0, r)$ centered in x_0 with a specifically chosen radius r (compare to Section 1.1.2).

The α -phase saturation S_α expresses the volumetric ratio of the phase α to the total void space at a given position \mathbf{x} and a time t and therefore

$$0 \leq S_\alpha \leq 1, \quad (1.8)$$

and

$$\sum_{\alpha} S_\alpha = 1. \quad (1.9)$$

RESIDUAL SATURATION

Since not all volume of the fluid phase can be displaced in multiphase flow from a porous medium due to hysteretic effects (see Helmig, 1997), an α -phase *residual saturation* quantity $S_{r\alpha}$ is introduced. It expresses the minimal saturation of the phase α that will retain in the porous medium due to adhesion effects with respect to the solid matrix. Nevertheless, the remnant phase saturation can be reduced by other means like diminishing the surface tension of the phase (i.e. modifying $S_{r\alpha}$ by chemical substances called *surfactants*) or by phase transition, in this case vaporization (see Bastian, 1999).

Situations with constant residual saturations will be always considered in this work. x Consequently, the relation (1.8) can be adjusted into

$$S_{r\alpha} \leq S_\alpha \leq 1 - \sum_{\beta \neq \alpha} S_{r\beta}. \quad (1.10)$$

EFFECTIVE SATURATION

Mathematical models developed in this work consider residual saturations $S_{r\alpha}$ to be constant in time and space and they are treated as another input parameters to the model. Another quantity *effective saturation* \mathfrak{S}_α is introduced by the relation

$$\mathfrak{S}_\alpha = \frac{S_\alpha - S_{r\alpha}}{1 - \sum_{\beta} S_{r\beta}}. \quad (1.11)$$

This definition permits to modify the relation (1.10) into

$$0 \leq \mathfrak{S}_\alpha \leq 1, \quad (1.12)$$

which gives a more favorable range than the inequality (1.10) from the mathematical point of view. The equation (1.9) is transformed into

$$\sum_{\alpha} \mathfrak{S}_\alpha = 1. \quad (1.13)$$

A new term ϑ in the reverse relationship (1.11) is introduced in the form

$$S_\alpha = S_{r\alpha} + \underbrace{\left(1 - \sum_\beta S_{r\beta}\right)}_{\vartheta} \mathfrak{S}_\alpha, \quad (1.14)$$

to simplify the following text.

1.3.2 Continuity Theorem

The mass balance equation (1.3) can be expressed for each phase α in the form (see Bastian, 1999)

$$\frac{\partial(\Phi \varrho_\alpha S_\alpha)}{\partial t} + \nabla \cdot (\varrho_\alpha \mathbf{u}_\alpha) = \varrho_\alpha \mathbf{q}_\alpha. \quad (1.15)$$

This expression of the continuity theorem includes the saturation quantity as a consequence of the reduction of the void space volume ΦV to a volume $\Phi S_\alpha V$ occupied by the phase α .

The mass balance equation (1.15) can be also formulated using the effective saturation \mathfrak{S}_α simply by substituting relation (1.11) into (1.15)

$$\vartheta \frac{\partial(\Phi \varrho_\alpha \mathfrak{S}_\alpha)}{\partial t} + \nabla \cdot (\varrho_\alpha \mathbf{u}_\alpha) = \varrho_\alpha \mathbf{q}_\alpha, \quad (1.16)$$

if the residual saturations $S_{r\alpha}$ are constant in time.

1.3.3 Darcy law

As in the single phase flow it can be shown by volume averaging or homogenization techniques that the macroscopic α -phase velocity \mathbf{u}_α can be expressed in the α -phase Darcy law

$$\mathbf{u}_\alpha = -\frac{\mathbf{K}_\alpha}{\mu_\alpha} (\nabla p_\alpha - \varrho_\alpha \mathbf{g}), \quad (1.17)$$

if the momentum transfer between phases is negligible. The phase permeability tensor \mathbf{K}_α depends on the saturation of the phase α and can be decomposed into

$$\mathbf{K}_\alpha = k_{r\alpha}(\mathfrak{S}_\alpha) \mathbf{K}, \quad (1.18)$$

where the function $k_{r\alpha}$ is called the *relative permeability* of the phase α and is further discussed in Section 1.3.7. The term \mathbf{K} is called *absolute permeability* or *intrinsic soil permeability* and it is independent of fluid.

The term $\frac{k_{r\alpha}}{\mu_\alpha}$ is frequently called α -phase *mobility* λ_α and the Darcy law (1.17) yields

$$\mathbf{u}_\alpha = -\lambda_\alpha(\mathfrak{S}_\alpha) \mathbf{K} (\nabla p_\alpha - \varrho_\alpha \mathbf{g}). \quad (1.19)$$

1.3.4 Capillarity

Single phase flow is governed by pressure forces arising from the pressure gradient within the void space and the exterior gravitational force. The sharp interfaces between fluid phases in multiphase flows on the microscale give rise to a *capillary force*. This force is evoked by *surface tension* σ [$J m^{-2}$] of both phases (interfacial tension) at their interface, which is caused by both molecular coherence within each of phases and adhesion effects between the phases and the solid matrix.

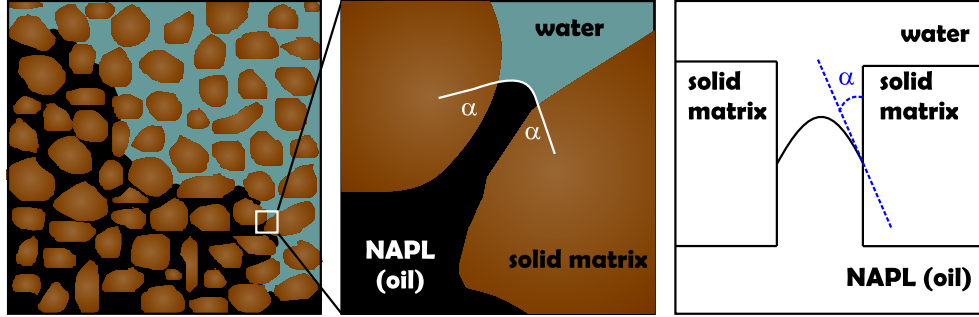


Figure 1.4: Interface between two phases in detail . The contact angle α characterizes the meniscus at the fluid-fluid interface (right figure) and defines the wetting (water) and the non-wetting phase (NAPL).

Figure 1.4 shows the interface in a pore channel between two solid grains. At the fluid-fluid interface the equilibrium of forces leads to a curved form of the interface due to capillarity. Consider two immiscible phases (e.g. water and air). The interaction of three different phases (solid matrix can be considered as a third phase) results in a *contact angle* α as it is depicted in Figure 1.4. The influence of these forces decreases with increasing distance from the interface. *Young's equation* gives the following expression of forces at equilibrium :

$$\sigma_{S-1} = \sigma_{S-2} + \sigma_{1-2} \cos \alpha, \quad (1.20)$$

where σ_{S-1} , σ_{S-2} and σ_{1-2} are respective surface tension forces at solid phase-fluid 1 interface, solid phase-fluid 2 interface and fluid 1 - fluid 2 interface as it is shown in Figure 1.5. From (1.20) the contact angle α can be explicitly expressed as

$$\alpha = \arccos \left(\frac{\sigma_{S-2} - \sigma_{S-1}}{\sigma_{1-2}} \right). \quad (1.21)$$

The contact angle α plays a significant role in the terminology. It is also called the *wetting angle*, because of the following definition. The fluid phase with an

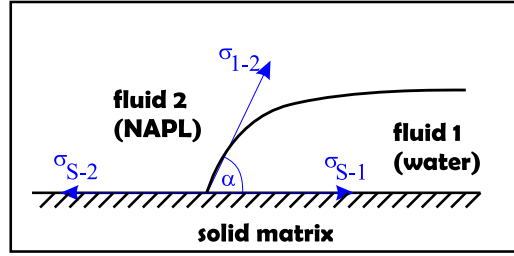


Figure 1.5: Interface tension and wetting angle at equilibrium.

acute contact angle is referred to as the *wetting phase* with respect to the solid matrix (fluid 1 in Figure 1.5), while the fluid phase with an *obtuse* contact angle is the *non-wetting phase* (fluid 2 in Figure 1.5). This notation allows us to develop more general two-phase flow mathematical models with one wetting and one non-wetting phase regardless of factual nature of fluid phases.

In the following text, the subindex *w* is used for quantities related to the wetting phase and analogously *n* for quantities related to the non-wetting phase.

More detailed description of microscopic capillarity effects are in Helmig, 1997 as well as in Bastian, 1999.

1.3.5 Capillary Pressure

The *microscopic capillary pressure* p_c is introduced by the following definition

$$p_c = p_n - p_w \geq 0. \quad (1.22)$$

The curved interface between both phases is preserved by a discontinuity in microscopic pressure of each phase. The capillary pressure is thus the height of the jump and it is always a non-negative quantity, because the pressure p_n of the non-wetting phase is larger than the pressure p_w in the wetting phase at the interface (consequence of the definition of the wetting resp. the non-wetting phase).

In order to incorporate capillarity effects into macroscopic level, an average of the microscopic capillary pressure over REV is taken so that the *macroscopic capillary pressure* is defined almost in the same way as in (1.22), this time using macroscopic pressures p_w and p_n .

$$p_c(t, \mathbf{x}) = p_n(t, \mathbf{x}) - p_w(t, \mathbf{x}). \quad (1.23)$$

Generally, macroscopic capillary pressure is a function of phase saturations, fluid temperature and fluid composition due to changes in surface tension. According to Hassanizadeh & Gray, 1993, the macroscopic relationship (1.23) is

valid only at equilibrium of forces (i.e. both phases are immobile) and it should not be viewed as the definition of the macroscopic capillary pressure p_c . The macroscopic capillary pressure function p_c is seen to be function of the fluid-fluid interfacial areas per unit volume, as well as of the saturation, but it is difficult to incorporate the complex approach made by Hassanizadeh and Gray into existing multiphase flow models, because the capillary pressure - fluid-fluid interfacial area functional dependence is currently unknown. Therefore, only the dependence on saturation is considered in this work.

For two-phase flow, saturations \mathfrak{S}_w and \mathfrak{S}_n are related by $\mathfrak{S}_w + \mathfrak{S}_n = 1$, so that the capillary pressure function can be defined for instance as

$$p_c = p_c(\mathfrak{S}_w). \quad (1.24)$$

There exist two principal non-linear mathematical models for the capillary pressure function (1.24) that are used in modelling multiphase flow in porous media. Both of them are based on experimental results and they approximate macroscopic effects of the capillarity in porous media in dependence on the effective wetting phase saturation \mathfrak{S}_w .

BROOKS-COREY CAPILLARY PRESSURE MODEL

Brooks and Corey, 1964 developed mathematical model for $p_c(\mathfrak{S}_w)$ in the form

$$\mathfrak{S}_w(p_c) = \left(\frac{p_c}{p_d} \right)^\lambda \quad \text{for } p_c \geq p_d. \quad (1.25)$$

The parameter λ describes pore distribution of the grains in porous material. A very small values of λ belongs to single grain size material, while a very large values indicate a highly non-uniform material (see Helmig, 1997). The *entry pressure* p_d [Pa] is considered as the minimal capillary pressure required to displace the wetting phase at its maximal saturation from the largest occurring pore.

This parametrization of the $\mathfrak{S}_w \leftrightarrow p_c$ relations simulates a *DNAPL pooling* (physical barrier) described in Section 1.4.1.

The capillary pressure $p_c(\mathfrak{S}_w)$ can be easily expressed from (1.25)

$$p_c(\mathfrak{S}_w) = p_d \mathfrak{S}_w^{-\frac{1}{\lambda}} \quad \text{for } \mathfrak{S}_w \in (0, 1], \quad (1.26)$$

from which it is obvious that $p_c(1) = p_d$.

VAN GENUCHTEN CAPILLARY PRESSURE MODEL

After van Genuchten, 1980 the capillary pressure is defined by

$$\mathfrak{S}_w(p_c) = (1 + (\alpha p_c)^n)^{-m} \quad \text{for } p_c \geq 0. \quad (1.27)$$

Usually, the parameters m and n are related by $m = 1 - \frac{1}{n}$ and they are characterising the pore structure of the porous medium. The last parameter α is given in $[Pa^{-1}]$. All parameters are estimated to fit the experimental $\mathbb{S}_w \leftrightarrow p_c$ relations.

Expression of $p_c(\mathbb{S}_w)$ follows easily from (1.27) as

$$p_c(\mathbb{S}_w) = \frac{1}{\alpha} \left(\mathbb{S}_w^{-\frac{1}{m}} - 1 \right)^{\frac{1}{n}} \quad \text{for } \mathbb{S}_w \in (0, 1]. \quad (1.28)$$

Unlike the Brooks-Corey capillary pressure, the van Genuchten model does not simulate the barrier effect, because the capillary pressure is always zero for maximal effective wetting phase saturation, i.e. $p_c(1) = 0$.

Note that for small values of effective water saturation \mathbb{S}_w the capillary pressure function $p_c(\mathbb{S}_w)$ as well as its first derivative $p'_c(\mathbb{S}_w)$ are unbounded. This has profound consequences in mathematical formulations and numerical models (see next sections and chapters).

1.3.6 Capillary Hysteresis

Figure 1.6 shows typical shapes of $p_c(\mathbb{S}_w)$ curves. Note that these curves are valid either for a *drainage (displacement) cycle* or a *imbibition (wetting) cycle*. If the porous medium is drained and subsequently filled again (*imbibition*) the capillary pressure-saturation relation will change. According to Bastian, 1999 the $p_c \leftrightarrow \mathbb{S}_w$ relationship depends on the complete history of drainage and imbibition cycle.

It can be significantly observed during the *ink bottle* effect when a capillary tube of axial symmetry having periodical variations in radius has its lower end immersed in water (air-water system), the water will rise through the tube until the hydrostatic pressure in the tube becomes equal to the capillary pressure. If then the tube is raised in the water, some water will drain out and a new equilibrium level will establish.

When the interface meniscus is advancing and it approaches a reduction of the tube it *jumps* through the neck (imbibition). When receding it halts without passing through the neck. This phenomenon explains why a given capillary pressure corresponds to a higher saturation on the drainage curve than on the imbibition curve.

This issue is called the *capillary hysteresis* phenomenon and it is concisely described in Collins, 1976, Bastian, 1999 or Helmig, 1997.

In most fluid-flow problems of practical interest, capillary hysteresis can be neglected because the flow regime usually dictates that one or the other capillary pressure-saturation curve will apply. In the case of this work, only the drainage curve is used, because only contamination (NAPL enters water-saturated domain)

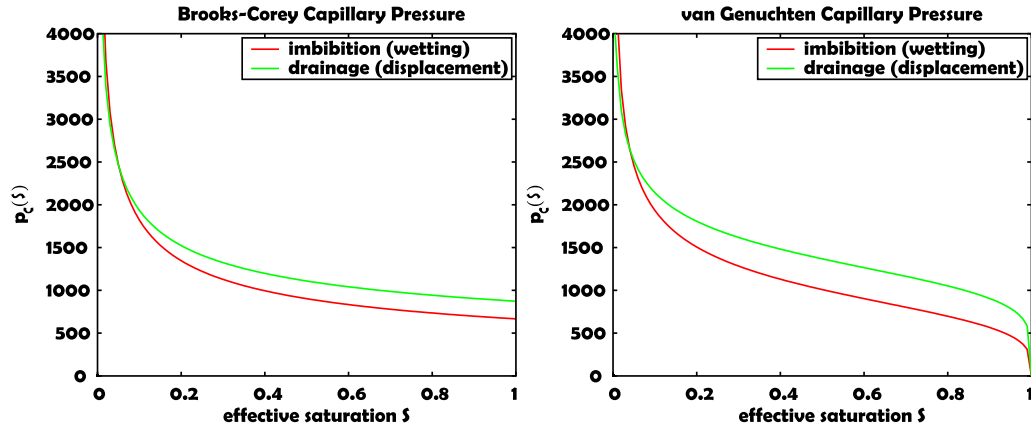


Figure 1.6: Typical capillary pressure curves $p_c(S_w)$ after Brooks-Corey and after van Genuchten for both drainage and imbibition. Parameters correspond to sand # 30 in Turner, 2004 on page 43. Drainage : $\lambda = 2.89$, $p_d = 873 \text{ Pa}$, $n = 5.5$, $\alpha = 0.00077 \text{ Pa}^{-1}$. Imbibition : $\lambda = 2.29$, $p_d = 667 \text{ Pa}$, $n = 4.0$, $\alpha = 0.00110 \text{ Pa}^{-1}$.

or displacement of contaminants (water enters NAPL-saturated domain) in fully saturated zones is discussed in the following text.

1.3.7 Relative Permeability

The relative permeability $k_{r\alpha}$ models the fact that the flow paths of fluid α are hindered by the presence of the other phases. It can be considered as a scaling factor and obeys the constraint

$$0 \leq k_{r\alpha} \leq 1.$$

For the two-phase flow in porous media, the mathematical models for the relative permeability functions k_{rw} and k_{rn} can be deduced from the models of capillarity effects by the relations (see Helmig, 1997):

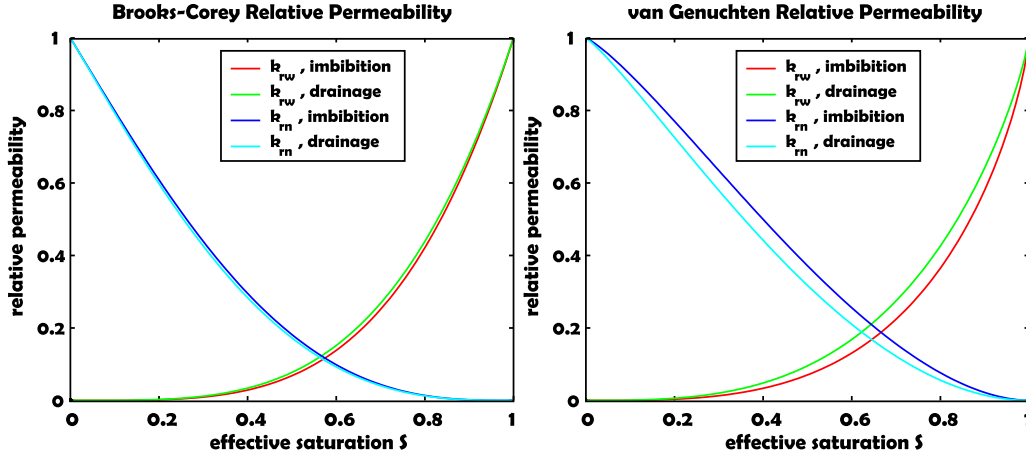


Figure 1.7: Relative permeability functions based on imbibition and drainage capillary curves. Parameters correspond to sand # 30 in Turner, 2004 on page 43. Drainage : $\lambda = 2.89$, $p_d = 873 \text{ Pa}$, $n = 5.5$, $\alpha = 0.00077 \text{ Pa}^{-1}$. Imbibition : $\lambda = 2.29$, $p_d = 667 \text{ Pa}$, $n = 4.0$, $\alpha = 0.00110 \text{ Pa}^{-1}$.

$$k_{rw} = \mathfrak{S}_w^A \left(\frac{\int_0^{\mathfrak{S}_w} [p_c(v)]^{-B} dv}{\int_0^1 [p_c(v)]^{-B} dv} \right)^C, \quad (1.29)$$

$$k_{rn} = (1 - \mathfrak{S}_w)^A \left(\frac{\int_0^{\mathfrak{S}_w} [p_c(v)]^{-B} dv}{\int_0^1 [p_c(v)]^{-B} dv} \right)^C. \quad (1.30)$$

The *Burdine* mathematical model for relative permeability functions are obtained by substituting the Brooks-Corey p_c into (1.29) and (1.30) with $A = B = 2$ and $C = 1$:

$$k_{rw}(\mathfrak{S}_w) = \mathfrak{S}_w^{3+\frac{2}{\lambda}}, \quad (1.31)$$

$$k_{rn}(\mathfrak{S}_w) = (1 - S)^2 (1 - \mathfrak{S}_w^{1+\frac{2}{\lambda}}). \quad (1.32)$$

Therefore, it is common to refer to (1.31) and (1.32) in conjunction with (1.26) as *Brooks-Corey model*².

²This reference is intuitive as the Brooks-Corey parameters λ and p_d are used in the relations

The *Mualem* mathematical model for relative permeability functions are obtained by substituting the van Genuchten capillary pressure p_c into (1.29) and (1.30) with $A = \frac{1}{2}$, $B = 1$ and $C = 2$:

$$k_{rw}(\mathbb{S}_w) = \mathbb{S}_w^{\frac{1}{2}} \left(1 - (1 - \mathbb{S}_w^{\frac{1}{m}})^m \right)^2, \quad (1.33)$$

$$k_{rn}(\mathbb{S}_w) = (1 - \mathbb{S}_w)^{\frac{1}{3}} (1 - \mathbb{S}_w^{\frac{1}{m}})^{2m} \quad (1.34)$$

Analogously, it is usual to refer to (1.33) and (1.34) in conjunction with (1.28) as *van Genuchten model*.

The relationship between the Brooks and Corey model parameters λ and p_d and the van Genuchten model parameters m , n and α is described in Morel-Seytoux *et al.*, 1996.

1.4 Fluid Behaviour at Material Interface

This section describes mathematical treatment of heterogeneous media. The situation, where two different ³ homogeneous porous medium domains meet at a common interface is discussed.

1.4.1 Interfacial Conditions

Let Ω^A and Ω^B be neighbouring homogeneous domains with capillary pressure - saturation functions p_c^A resp. p_c^B . Initially, both domains are fully water-saturated, i.e. the wetting-fluid is present on both sides of the interface, which implies that non-wetting residual water saturations S_{nr} necessarily equal to zero in both subdomains. Therefore

$$p_w \text{ is continuous at the interface.} \quad (1.35)$$

Note that p_n is not defined in the domains since the non-wetting phase is not yet present in the subdomains Ω^A and Ω^B .

It is assumed that the non-wetting phase is approaching the interface through Ω^A . Since no mass is lost or produced at the interface, it is possible to state from the mass conservation law that fluxes

$$Q_w \mathbf{u}_w \cdot \mathbf{n} \text{ and } Q_n \mathbf{u}_n \cdot \mathbf{n} \text{ are continuous across the interface,} \quad (1.36)$$

for relative permeability. The same remark applies to the van Genuchten model as well.

³Each porous medium has different material properties.

where \mathbf{n} is the normal vector to the interface oriented towards Ω^B as it is illustrated in Figure 1.8.

The definition of the *entry pressure* introduced in Section 1.3.5 can be generalized. From now, the *entry pressure* is the value of the capillary pressure in the fully saturated zone, scilicet the value of $p_c(1)$. This definition naturally incorporates the definition of the Brooks-Corey entry pressure p_d .

It is possible to describe the phase saturations behaviour at the interface in the following way. The non-wetting phase will flow through the interface if and only if the capillary pressure p_c^A is higher than the entry pressure $p_c^B(1)$. If this condition holds, then the capillary pressure is continuous across the interface, i.e. $p_c^A = p_c^B$. This condition implies that there is always jump in saturation across the boundary as it is shown in Figure 1.9. If the p_c^A is not higher than the entry pressure $p_c^B(1)$, the non-wetting phase is prevented from entering the domain B.

This behaviour is observed in experiments (see Mikyška, 2005 or Bastian, 1999), when the non-wetting phase infiltrating fully wetting phase saturated domain accumulates at the interface of two homogeneous porous medium. When the amount of the non-wetting phase is sufficiently large, the non-wetting phase pressure increases at certain level and the non-wetting phase enters the other domain.

Altogether, the *extended capillary pressure condition* is given by

$$\mathbb{S}_w^B = \begin{cases} 1 & \text{if } p_c^A(\mathbb{S}_w^A) \leq p_c^B(1), \\ (p_c^B)^{-1}(p_c^A(\mathbb{S}_w^A)) & \text{else.} \end{cases} \quad (1.37)$$

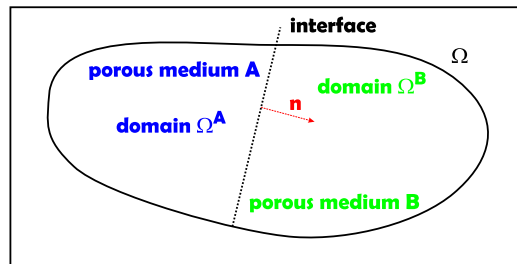


Figure 1.8: Interface between two homogeneous porous media.

The van Genuchten model for the capillary pressure-saturation relationship involves zero entry pressure and thus the $p_c(\mathbb{S}_w)$ function is always invertible in (1.37). There is no barrier effect for the van Genuchten model as it was already discussed in Section 1.3.5.

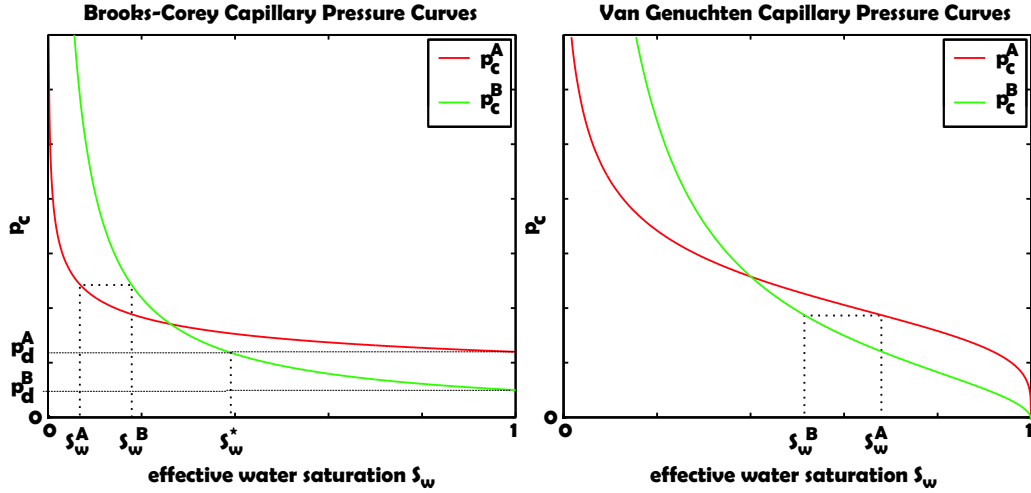


Figure 1.9: Capillary pressure curves for a porous medium with a discontinuity.

1.5 Flow in Homogeneous Porous Medium

The complete two-phase flow model applied throughout the work is stated in this section. The flow of two immiscible and incompressible fluids in homogeneous isotropic porous medium is considered, i.e. ρ_α and Φ are constant in time and space and absolute permeability tensor reads $\mathbf{K} = K\mathbf{I}$.

All relevant equations (1.13), (1.16), (1.17) and (1.23) under these assumptions are resumed in the following way

$$1 = \mathfrak{S}_w + \mathfrak{S}_n, \quad (1.38)$$

$$p_c = p_n - p_w, \quad (1.39)$$

$$\mathbf{u}_w = -K \lambda_w (\nabla p_w - \rho_w \mathbf{g}), \quad (1.40)$$

$$\mathbf{u}_n = -K \lambda_n (\nabla p_n - \rho_w \mathbf{g}), \quad (1.41)$$

$$\vartheta \Phi \frac{\partial \mathfrak{S}_w}{\partial t} = -\nabla \cdot \mathbf{u}_w + \mathbf{q}_w, \quad (1.42)$$

$$\vartheta \Phi \frac{\partial \mathfrak{S}_n}{\partial t} = -\nabla \cdot \mathbf{u}_n + \mathbf{q}_n, \quad (1.43)$$

where the definition of the α -phase mobility λ_α introduced in Section 1.3.7 is employed.

New variables are introduced to eliminate explicit presence of p_w and p_n in the set of equations (see Bastian, 1999).

1.5.1 Total Velocity

A quantity called *total velocity* \mathbf{u} can be introduced by the relationship

$$\mathbf{u} = \mathbf{u}_w + \mathbf{u}_n. \quad (1.44)$$

It expresses the total velocity of the whole fluid content within the porous medium at each point.

Addition of equations (1.42) and (1.43) yields

$$\vartheta\Phi \underbrace{\frac{\partial}{\partial t} (\mathfrak{S}_w + \mathfrak{S}_n)}_1 = -\nabla \cdot \underbrace{(\mathbf{u}_w + \mathbf{u}_n)}_{\mathbf{u}} + \mathbf{q}_w + \mathbf{q}_n, \quad (1.45)$$

from (1.38)

which yields

$$\nabla \cdot \mathbf{u} = \mathbf{q}_w + \mathbf{q}_n. \quad (1.46)$$

This equation includes the equation (1.38) in the summary above.

1.5.2 Rearranging Equations

In order to reduce the total number of equations, the definition of the capillary pressure (1.39) is incorporated in this subsection.

Substitution of $p_w = p_n - p_c$ in the equation (1.40) and $\mathbf{u}_n = \mathbf{u} - \mathbf{u}_w$ into (1.41) and then multiplication of the equation (1.40) resp. (1.41) by λ_n resp. λ_w . yield

$$\lambda_n \mathbf{u}_w = -\lambda_w \lambda_n K (\nabla p_n - \nabla p_c - \varrho_w \mathbf{g}) \quad (1.47)$$

$$\lambda_w \mathbf{u} - \lambda_w \mathbf{u}_w = -\lambda_w \lambda_n K (\nabla p_n - \varrho_n \mathbf{g}). \quad (1.48)$$

Subtraction of (1.47) and (1.48) yields

$$(\lambda_w + \lambda_n) \mathbf{u}_w = \lambda_w \mathbf{u} + \lambda_w \lambda_n K (\nabla p_c + (\varrho_w - \varrho_n) \mathbf{g}). \quad (1.49)$$

Since $\lambda_w + \lambda_n > 0$ for all $\mathfrak{S}_w \in [0, 1]$, we can replace the equation (1.40) by

$$\mathbf{u}_w = \frac{\lambda_w}{\lambda_w + \lambda_n} \mathbf{u} + \frac{\lambda_w \lambda_n}{\lambda_w + \lambda_n} K (\nabla p_c + (\varrho_w - \varrho_n) \mathbf{g}). \quad (1.50)$$

Analogously, it is possible to obtain

$$\mathbf{u}_n = \frac{\lambda_n}{\lambda_w + \lambda_n} \mathbf{u} - \frac{\lambda_w \lambda_n}{\lambda_w + \lambda_n} K (\nabla p_c + (\varrho_w - \varrho_n) \mathbf{g}). \quad (1.51)$$

The term

$$f_\alpha = \frac{\lambda_\alpha}{\lambda_w + \lambda_n}, \quad (1.52)$$

is called the α -phase *fractional flow function* and it is a function of effective saturation due to the definition of relative permeability functions. As the capillary pressure function p_c depends only on the effective wetting phase saturation, the capillary pressure gradient ∇p_c can be replaced by

$$\nabla p_c = p'_c(\mathbf{S}_w)\nabla \mathbf{S}_w = -p'_c(1 - \mathbf{S}_n)\nabla \mathbf{S}_n, \quad (1.53)$$

where

$$p'_c(\mathbf{S}_w) = \frac{d}{d\mathbf{S}_w} p_c(\mathbf{S}_w).$$

1.5.3 Complete Set of Equations

Finally, new equations can be collected in the following list

$$\nabla \cdot \mathbf{u} = \mathbf{q}_w + \mathbf{q}_n, \quad (1.54)$$

$$\mathbf{u}_w = \frac{\lambda_w}{\lambda_w + \lambda_n} \mathbf{u} + \frac{\lambda_w \lambda_n}{\lambda_w + \lambda_n} K (\nabla p_c + (\varrho_w - \varrho_n) \mathbf{g}), \quad (1.55)$$

$$\mathbf{u}_n = \frac{\lambda_n}{\lambda_w + \lambda_n} \mathbf{u} - \frac{\lambda_w \lambda_n}{\lambda_w + \lambda_n} K (\nabla p_c + (\varrho_w - \varrho_n) \mathbf{g}), \quad (1.56)$$

$$\vartheta \Phi \frac{\partial \mathbf{S}_w}{\partial t} = -\nabla \cdot \mathbf{u}_w + \mathbf{q}_w, \quad (1.57)$$

$$\vartheta \Phi \frac{\partial \mathbf{S}_n}{\partial t} = -\nabla \cdot \mathbf{u}_n + \mathbf{q}_n. \quad (1.58)$$

The explicit presence of both phase pressures p_w and p_n is eliminated from the model equations. However, they are hidden in the total velocity term by the relation

$$\mathbf{u} = -(\lambda_w + \lambda_n) K \left(\nabla p_n - f_w \nabla p_c - \frac{\lambda_w \varrho_n + \lambda_n \varrho_w}{\lambda_w + \lambda_n} \mathbf{g} \right), \quad (1.59)$$

that results from adding the equations (1.40) and (1.41) with respect to (1.39).

1.6 One-Dimensional Two-Phase Flow Problem

One of the main objectives of this work is to study exact solutions of one-dimensional two-phase flow problems in porous media. Exact solutions can be

obtained under following constraints. Let two immiscible and incompressible phases flow through one dimensional domain of a homogeneous porous medium with no gravitational force and without sinks or sources throughout the domain. This situation can be represented by a long thin pipe of length L filled with porous material. The pipe is situated horizontally since no gravitational effects are assumed. All position dependent quantities introduced in the previous sections are considered constant in every cross-section of the pipe (the one dimensional assumption) and thus calculated only at each point $x \in [0, L]$.

1.6.1 One-Dimensional Transport Equation

Since no sinks or sources are placed in the domain $[0, L]$, the equation (1.54) yields

$$u(t, x) = C(t), \quad (1.60)$$

where u is the one-dimensional total velocity and $C(t)$ is an arbitrary function independent of the position x . Therefore, it follows that

$$u = u(t).$$

To simplify the following text, a new term $\mathfrak{D} = \mathfrak{D}(\mathbb{S}_w)$ is introduced by the definition

$$\mathfrak{D}(\mathbb{S}_w) = -K \frac{\lambda_w(\mathbb{S}_w)\lambda_n(\mathbb{S}_w)}{\lambda_w(\mathbb{S}_w) + \lambda_n(\mathbb{S}_w)} \frac{dp_c}{d\mathbb{S}_w}(\mathbb{S}_w). \quad (1.61)$$

The symbol \mathfrak{D} stands for *diffusion* or *diffusive term*, also commonly called *the capillary diffusive term*. It is always a non negative quantity because $p'_c(\mathbb{S}_w)$ is non positive function since $p_c(\mathbb{S}_w)$ decreases in $(0, 1]$.

The equations (1.55) and (1.57) can be expressed as one

$$\vartheta\Phi \frac{\partial \mathbb{S}_w}{\partial t} = -u \frac{\partial f_w(\mathbb{S}_w)}{\partial x} + \frac{\partial}{\partial x} \left(\mathfrak{D}(\mathbb{S}_w) \frac{\partial \mathbb{S}_w}{\partial x} \right), \quad (1.62)$$

and analogously the equations (1.56) and (1.58) give

$$\vartheta\Phi \frac{\partial \mathbb{S}_n}{\partial t} = -u \frac{\partial f_n(1 - \mathbb{S}_n)}{\partial x} + \frac{\partial}{\partial x} \left(\mathfrak{D}(1 - \mathbb{S}_n) \frac{\partial \mathbb{S}_n}{\partial x} \right). \quad (1.63)$$

Formally, the *two-phase flow equation* can be given in the form

$$\vartheta\Phi \frac{\partial \mathbb{S}_\alpha}{\partial t} = -u \frac{\partial f_\alpha}{\partial x} + \frac{\partial}{\partial x} \left(\mathfrak{D} \frac{\partial \mathbb{S}_\alpha}{\partial x} \right). \quad (1.64)$$

The α -phase velocity is expressed as

$$u_\alpha = u f_\alpha - \mathfrak{D} \frac{\partial \mathbb{S}_\alpha}{\partial x}. \quad (1.65)$$

1.6.2 Problem Formulation

Three main problems can be described by the equation (1.64).

First of them is a two-phase flow problem without capillary effects included in the model. This pure hyperbolic two-phase flow problem is described by

$$\vartheta\Phi \frac{\partial \mathbb{S}_\alpha}{\partial t} = -u \frac{\partial f_\alpha}{\partial x}. \quad (1.66)$$

There exists an analytical solution derived by *Buckley and Leverett* using modified method of characteristics which is discussed in the next chapter (see Section 2.2).

If the total velocity is zero, i.e. $u = 0$, a nonlinear equation of a parabolic type is obtained

$$\vartheta\Phi \frac{\partial \mathbb{S}_\alpha}{\partial t} = \frac{\partial}{\partial x} \left(\mathfrak{D} \frac{\partial \mathbb{S}_\alpha}{\partial x} \right). \quad (1.67)$$

This situation is referred to as *bi-directional displacement*, because the fluid phase velocities are opposite at each point $x \in [0, L]$,

$$0 = u \quad \Rightarrow \quad u_w = -u_n.$$

The third problem is the equation (1.64) itself

$$\vartheta\Phi \frac{\partial \mathbb{S}_\alpha}{\partial t} = -u \frac{\partial f_\alpha}{\partial x} + \frac{\partial}{\partial x} \left(\mathfrak{D} \frac{\partial \mathbb{S}_\alpha}{\partial x} \right). \quad (1.68)$$

Both advective and diffusive terms are present in the equation and it is referred to as *unidirectional displacement* since $u \neq 0$.

McWhorter and Sunada, 1990 developed a closed form exact solution for the two-phase flow equation with diffusion (1.67) and also with diffusion and advection (1.68). The main contribution of this work is a deep analysis of the McWhorter and Sunada exact solution and clarification of some outstanding issues published in Sunada & McWhorter, 1990, Z.-X. Chen & Witherspoon, 1992 and Sunada & McWhorter, 1992.

DUAL FORMULATIONS

Both problem formulations (1.62) and (1.63) represent *dual problem formulations* to each other in the following way. Exact solutions are derived under an assumption, that the Dirichlet boundary conditions $\mathbb{S}_\alpha(t, 0) = \mathbb{S}_0$ and $\mathbb{S}_\alpha(t, L) = \mathbb{S}_i$ with $L = \infty$, satisfy $\mathbb{S}_i < \mathbb{S}_0$. If the problem formulation requires $\mathbb{S}_i > \mathbb{S}_0$, simply the other formulation is used and the inequality is satisfied because $\mathbb{S}_i^\# < \mathbb{S}_0^\#$, where $\mathbb{S}_i^\#$ and $\mathbb{S}_0^\#$ are the dual saturations to the original problem defined as

$$\mathbb{S}_i^\# = 1 - \mathbb{S}_i, \quad (1.69)$$

$$\mathbb{S}_0^\# = 1 - \mathbb{S}_0. \quad (1.70)$$

Chapter 2

Exact Solutions in Homogeneous Media

2.1 Introduction

OVERVIEW

A derivation of exact solutions of the two-phase flow one dimensional problems in porous medium is presented in this chapter. For that purpose, a general form of the two-phase flow equation (1.68) is presented in the form

$$\Phi \vartheta \frac{\partial \mathfrak{S}}{\partial t} = -u(t) \frac{\partial f(\mathfrak{S})}{\partial x} + \frac{\partial}{\partial x} \left(D(\mathfrak{S}) \frac{\partial \mathfrak{S}}{\partial x} \right), \quad (2.1)$$

where $\mathfrak{S} = \mathfrak{S}(t, x)$ ($0 \leq \mathfrak{S} \leq 1$) is a non-specified ¹ effective saturation, $f = f(\mathfrak{S})$ is a fractional flow function. In the case of this work, the relative permeability models so that the diffusive term is a non-negative function such that $D(0) = 0$ and $D(1) = 0$ due to $\lambda_w(0) = \lambda_n(1) = 0$ in the definition of \mathfrak{D} in (1.61).

The mathematical derivation of exact solutions in the general form including analysis and respective algorithms is provided in this chapter.

APPLICATION TO POROUS MEDIA TRANSPORT PROBLEMS

In this section we specify, how the general exact solutions of the two-phase flow equation (2.1) can be applied to the problems (1.66), (1.67) or (1.68). We present description of the functions f and D for the wetting-phase and the non-wetting phase displacement.

¹ \mathfrak{S} can be either wetting phase or non-wetting phase effective saturation.

In the situation where the non-wetting phase is displaced from the domain, the wetting phase is introduced to the domain at $x = 0$. Therefore we redefine variables in the general equation (2.1) in the following way

$$\begin{aligned} \mathcal{S} &\equiv \mathcal{S}_w \\ f(\mathcal{S}) &= f_w(\mathcal{S}_w) \\ D(\mathcal{S}) &= \mathfrak{D}(\mathcal{S}_w). \end{aligned} \tag{2.2}$$

The resulting equation is the equation (1.62).

In the other case the wetting phase is displaced from the domain via inflow of the wetting phase at $x = 0$. The redefinition of the variables in the general equation (2.1) is as follows

$$\begin{aligned} \mathcal{S} &\equiv \mathcal{S}_n \\ f(\mathcal{S}) &= f_n(1 - \mathcal{S}_n) \\ D(\mathcal{S}) &= \mathfrak{D}(1 - \mathcal{S}_n). \end{aligned} \tag{2.3}$$

This substitution still preserves the positive sign before the diffusive term in the equation (2.1) because of the expression of the non-wetting phase velocity \mathbf{u}_n in (1.56) and the execution of the derivative $\nabla p_c(1 - \mathcal{S}_n)$ in (1.53). As a result we obtain the equation (1.63).

TEST PROBLEMS

The setups in Table 2.1 are used in this chapter to illustrate usage and analysis of the exact solutions. The wetting phase is always water in the computational experiments while various realistic or theoretical NAPLs are used.

The first test setup consists of the Brooks-Corey model functions (1.26), (1.31) and (1.32) and artificially selected values of the soil parameters (see Helmig, 1997). Since NAPLs that are more viscous than water make the problems described in this work more obvious, the value of $\mu_n = 0.020 \text{ kg m}^{-1} \text{ s}^{-1}$ is selected in the test setup 1.

The other test setups 2 and 3 model realistic soil parameters (sand #30 in Turner, 2004, p.43) and realistic NAPL Soltrol 220.

2.2 Buckley-Leverett Analytical Solution

The strictly hyperbolic two-phase flow equation (1.66) is a version of the equation (2.1) without diffusive term ($D \equiv 0$) and it can be solved analytically. Let the total

2.2. BUCKLEY-LEVERETT ANALYTICAL SOLUTION

	Par.	Units	Setup 1	Setup 2	Setup 3
Porosity	Φ	[-]	0.3	0.4	
Intrinsic Permeability	K	$[m^2]$	$1 \cdot 10^{-10}$	$2.26 \cdot 10^{-10}$	
Residual Water Sat.	S_{wr}	[-]	0	0.144	
Residual NAPL Sat.	S_{nr}	[-]	0	0.069	
Water Viscosity	μ_w	$[kg\ m^{-1}s^{-1}]$	0.001	0.001	
DNAPL Viscosity	μ_n	$[kg\ m^{-1}s^{-1}]$	0.020	0.0035	
Model Functions			BC	BC	vG
Brooks-Corey (BC)	P_0	$[Pa]$	1000	668	-
	λ	[-]	2	2.29	-
van Genuchten (vG)	α	$[Pa^{-1}]$	-	-	$\frac{1}{909}$
	m	[-]	-	-	0.75

Table 2.1: Parameter setup used in this chapter.

velocity $u = u(t)$ be an arbitrary integrable non-negative function. Buckley and Leverett used modified method of characteristics to derive analytical solution to the following Riemann problem (see LeVeque, 2002, Collins, 1976, Huyakorn & Pinder, 1983)

$$\Phi \vartheta \frac{\partial \mathbb{S}}{\partial t} + u(t) \frac{\partial f(\mathbb{S})}{\partial x} = 0, \quad (2.4)$$

or

$$\Phi \vartheta \frac{\partial \mathbb{S}}{\partial t} + u(t) f'(\mathbb{S}) \frac{\partial \mathbb{S}}{\partial x} = 0. \quad (2.5)$$

The boundary and initial conditions for all $t \in (0, \infty)$ resp. $x \in (0, \infty)$ are

$$\mathbb{S}(t, 0) = \mathbb{S}_0, \quad (2.6)$$

$$\mathbb{S}(0, x) = \mathbb{S}_i. \quad (2.7)$$

The modification of the method of characteristics is necessary due to existence of an inflexion point of the function f in most of the common models as it is depicted in Figure 2.1. This situation is referred to as the *Buckley-Leverett* problem and it is sufficiently described in literature only for $\mathbb{S}_0 = 1$, $\mathbb{S}_i = 0$ and u constant in time. Bastian, 1999 describes the derivation of the solution for any $0 \leq \mathbb{S}_i \leq \mathbb{S}_0 \leq 1$, but he still considers constant total velocity u .

2.2.1 Method of Characteristics

The analytical solution to the Riemann problem (2.4) is derived using the method of characteristics and the theory concerning the non-convex flux functions dis-

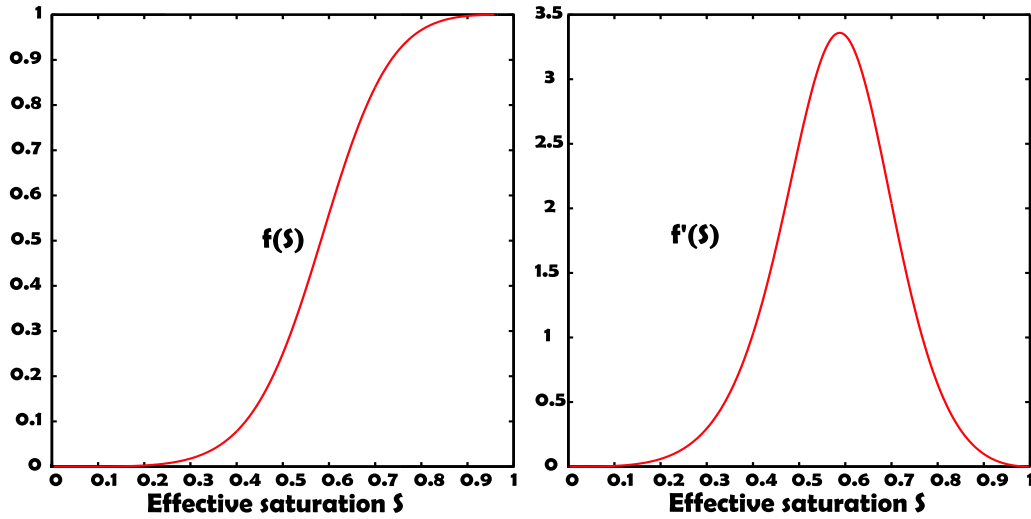


Figure 2.1: Typical fractional flow function f with inflexion (left) and its first derivative f' (right), model Brooks-Corey.

cussed in LeVeque, 1990.

A characteristics is a line in the (x, t) -plane, whereon the solution $\mathbb{S}(t, x)$ is constant. Let $\eta = \eta(x, t)$ be unknown function such that

$$\tilde{\mathbb{S}}(\eta(t, x)) = \mathbb{S}(t, x). \quad (2.8)$$

Derivative of the expression (2.8) by η yields

$$\frac{d\tilde{\mathbb{S}}}{d\eta} = \frac{\partial \mathbb{S}}{\partial t} \frac{dt}{d\eta} + \frac{\partial \mathbb{S}}{\partial x} \frac{dx}{d\eta} = 0, \quad (2.9)$$

because it is assumed that the solution $\mathbb{S}(t, x)$ is constant along the characteristic described by $\eta(t, x)$.

Comparing the coefficients in (2.9) and (2.4), a system of ordinary differential equations

$$\frac{d\tilde{\mathbb{S}}}{d\eta} = 0, \quad (2.10)$$

$$\frac{dt}{d\eta} = \frac{1}{\Phi \vartheta'} \quad (2.11)$$

$$\frac{dx}{d\eta} = \frac{1}{\Phi \vartheta} u(t) f'(\tilde{\mathbb{S}}), \quad (2.12)$$

is obtained and thus it yields

$$\frac{dx}{dt} = \frac{1}{\Phi\vartheta} u(t) f'(\tilde{\mathfrak{S}}). \quad (2.13)$$

A smooth *rarefaction wave* is obtained for convex flow functions f for the situation $\mathfrak{S}_0 > \mathfrak{S}_i$ by integrating the relationship (2.13) in the form

$$x(t, \tilde{\mathfrak{S}}) = f'(\tilde{\mathfrak{S}}) \int_0^t u(\tau) d\tau. \quad (2.14)$$

The convexity or concavity of the function f means that its first derivative is a monotonous function and thus it can be inverted to obtain the solution $\mathfrak{S}(t, x)$. Since this is not the case in the Buckley-Leverett problem (see Figure 2.1), only *weak solutions* exist.

For the discussion on the weak solution theory, refer to LeVeque, 2002, LeVeque, 1990.

Note that the solution of the Riemann problem (2.4) involves both a shock and rarefaction wave and is called *compound wave*.

To determine the weak solution to a nonconvex scalar conservation law, one needs to consider the following form of the *entropy condition* (see citations on page 353 in LeVeque, 2002)

Theorem 1 (Entropy condition (Oleinik)). *A weak solution $\mathfrak{S}(t, x)$ is the vanishing-viscosity solution to a general scalar conservation law (2.4) if all discontinuities have the property that*

$$\frac{f(\mathfrak{S}) - f(\mathfrak{S}_0)}{\mathfrak{S} - \mathfrak{S}_0} \geq s \geq \frac{f(\mathfrak{S}) - f(\mathfrak{S}_i)}{\mathfrak{S} - \mathfrak{S}_i}, \quad (2.15)$$

for all $\mathfrak{S}_i \leq \mathfrak{S} \leq \mathfrak{S}_0$, where

$$s = \frac{f(\mathfrak{S}_t) - f(\mathfrak{S}_0)}{\mathfrak{S}_t - \mathfrak{S}_0} \quad (2.16)$$

is the (fractional) shock speed and \mathfrak{S}_t is the postshock value that is constant in time defined by the relationship

$$f'(\mathfrak{S}_t) = \frac{f(\mathfrak{S}_t) - f(\mathfrak{S}_i)}{\mathfrak{S}_t - \mathfrak{S}_i}. \quad (2.17)$$

The term *fractional shock speed* is used because the shock speed v_{shock} is defined as

$$v_{shock}(t) = s u(t) \quad (2.18)$$

in this case and it is a time dependent variable. If the function f has no inflexion then $\mathfrak{S}_t = \mathfrak{S}_i$ and the shock speed $v_{shock}(t)$ is exactly the *Rankine-Hugoniot condition* (see Bastian, 1999).

$$v_{RH} = \frac{f(\mathfrak{S}_0) - f(\mathfrak{S}_i)}{\mathfrak{S}_0 - \mathfrak{S}_i} u(t). \quad (2.19)$$

There are two possible interpretations of the equation (2.17). The first one is a consequence of the entropy condition while the second one is a result of the mass balance equation, also called *equal area rule*.

2.2.2 Entropy Condition : Convex Hull Construction

The entropy-satisfying solution to the Riemann problem (2.4) can be determined from the graph of $f(\mathfrak{S})$ in the following way. Only the relationship $\mathfrak{S}_i \leq \mathfrak{S}_0$ is considered, because the other case can be simply reformulated e.g. from the wetting phase displacement formulation to the non-wetting phase formulation, where the relationship $\mathfrak{S}_i \leq \mathfrak{S}_0$ holds (see the *dual formulation* in Section 1.6.1).

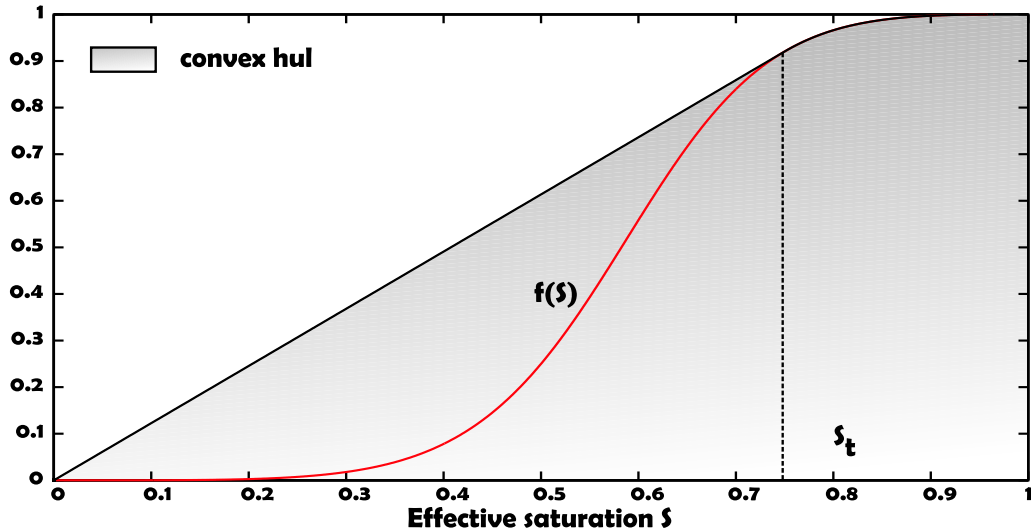


Figure 2.2: Convex hull construction of the set \mathfrak{S} , model Brooks-Corey, $\mathfrak{S}_0 = 1$, $\mathfrak{S}_i = 0$.

It is possible to construct the *convex hull* of the set \mathfrak{S}

$$\mathfrak{S} = \{(\mathfrak{S}, y) : \mathfrak{S}_i \leq \mathfrak{S} \leq \mathfrak{S}_0, y \leq f(\mathfrak{S})\}.$$

The convex hull of a set is the smallest convex set that contains the original set as it is depicted in Figure 2.2 for $\mathfrak{S}_i = 0$ and $\mathfrak{S}_0 = 1$. The upper boundary of the convex

hull is composed of a tangential from the *origin* $[\mathfrak{S}_i, f(\mathfrak{S}_i)]$ to the graph at point $[\mathfrak{S}_t, f(\mathfrak{S}_t)]$. The notation of \mathfrak{S}_t therefore corresponds to the tangent point to the graph f and is also called the *Welge* tangent saturation (see Sunada & McWhorter, 1990). The point \mathfrak{S}_t is exactly the postshock value defined by the equation (2.17). The straight line represents a shock jumping from $\mathfrak{S} = \mathfrak{S}_i$ to $\mathfrak{S} = \mathfrak{S}_t$. The segment where the convex hull boundary follows the graph $f(\mathfrak{S})$ is the rarefaction wave. Moreover the slope of the line equals to the fractional shock speed s defined in Theorem 1.

If f is convex, then the convex hull construction gives either a single line segment (single shock) or the function f itself (single rarefaction) if f is concave.

2.2.3 Mass Balance Condition : Equal Area Rule

The mass conservation law and the method of characteristics imply that the area delimited by the function

$$x(t) = \frac{1}{\Phi \mathfrak{S}} f'(\mathfrak{S}) \int_0^t u(\tau) d\tau \quad \mathfrak{S}_i \leq \mathfrak{S} \leq \mathfrak{S}_0,$$

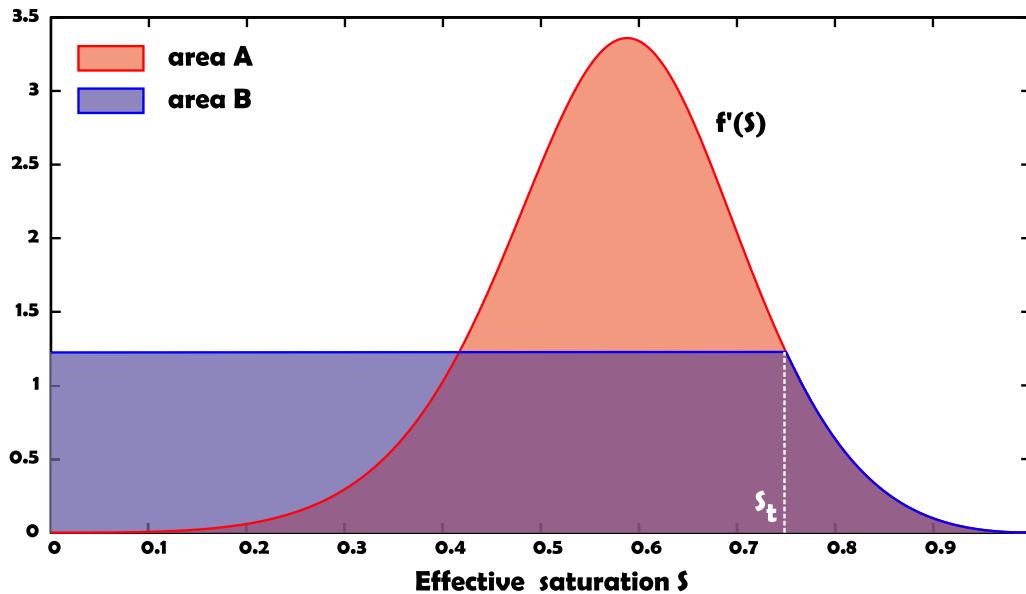


Figure 2.3: Equal area rule illustration, model Brooks-Corey, $\mathfrak{S}_0 = 1$, $\mathfrak{S}_i = 0$.

must be the same as the area between the solution $\mathfrak{S}(t, x)$ and \mathfrak{S}_i . Figure 2.3 depicts the situation for $\mathfrak{S}_i = 0$ and $\mathfrak{S}_0 = 1$. Using the notation in Figure 2.3, the

equal area rule is expressed as

$$\text{meas}(A) = \text{meas}(B).$$

This condition is referred to as the *equal area rule* and can be expressed by the relation

$$\int_{S_i}^{S_0} f'(s)ds = f'(S_t)(S_t - S_i) + \int_{S_t}^{S_0} f'(s)ds.$$

Evaluating the integrals on both sides, one gets exactly the same condition as in the equation (2.17) in Theorem 1, i.e.

$$f(S_t) - f(S_i) = f'(S_t)(S_t - S_i).$$

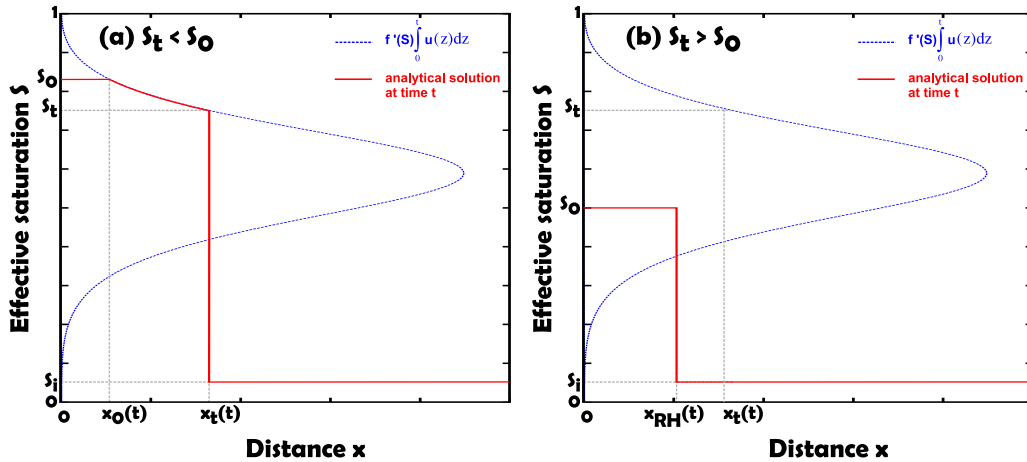


Figure 2.4: Illustration of the Buckley-Leverett analytical solution, model Brooks-Corey. If $S_0 > S_t$ the solution of the Riemann problem contains a rarefaction wave and a shock-wave (case (a),left picture), while the solution consists of a single shockwave if $S_0 < S_t$ (case (b), right picture). Note that the factor $\frac{1}{\phi^3}$ is included in the term $u(z)$.

2.2.4 Analytical Solution

The value of S_t is computed from the equation (2.17). If $S_t < S_0$ the solution of the Riemann problem (2.5) contains a shockwave as well as a rarefaction wave, see Figure 2.4 (a). There is only a shockwave with Rankine-Hugoniot shock speed

$v_{RH}(t)$ if $\mathfrak{S}_t > \mathfrak{S}_0$. The shock front position $x_{RH}(t)$ can be expressed as

$$x_{RH}(t) = \frac{1}{\Phi \vartheta} \frac{f(\mathfrak{S}_0) - f(\mathfrak{S}_t)}{\mathfrak{S}_0 - \mathfrak{S}_t} \int_0^t u(\tau) d\tau, \quad (2.20)$$

Let $x_0(t)$ and $x_t(t)$ are time-dependent variables defined by

$$x_0(t) = \frac{1}{\Phi \vartheta} f'(\mathfrak{S}_0) \int_0^t u(\tau) d\tau, \quad (2.21)$$

$$x_t(t) = \frac{1}{\Phi \vartheta} f'(\mathfrak{S}_t) \int_0^t u(\tau) d\tau, \quad (2.22)$$

Then the solution is obtained for a given time t in the following form :

$$\begin{aligned} \text{Case } \mathfrak{S}_0 \geq \mathfrak{S}_t : \quad & x = f'(\mathfrak{S}) \int_0^t u(\tau) d\tau \quad \text{for } \mathfrak{S}_t \leq S \leq \mathfrak{S}_0, \\ & \mathfrak{S}(t, x) = \mathfrak{S}_0 \quad \text{for } \forall x \leq x_0(t), \\ & \mathfrak{S}(t, x) = \mathfrak{S}_t \quad \text{for } \forall x > x_t(t). \end{aligned}$$

$$\begin{aligned} \text{Case } \mathfrak{S}_0 < \mathfrak{S}_t : \quad & \mathfrak{S}(t, x) = \mathfrak{S}_0 \quad \text{for } \forall x \leq x_{RH}(t), \\ & \mathfrak{S}(t, x) = \mathfrak{S}_t \quad \text{for } \forall x > x_{RH}(t). \end{aligned}$$

2.3 McWhorter-Sunada Exact Solution

McWhorter and Sunada published their article on exact integral solution of two-phase flow equation in 1990 resp. 1992. Despite presented derivations and examples illustrating usage of their exact solution, the work contains a lot of confusions. The author's contribution to the subject would be to explain how the exact solution can be derived, to correct some impetuous conclusions and to offer better insights into the subject through the modified iterative methods.

2.3.1 Problem Formulation

The McWhorter and Sunada exact solution to the two-phase flow problem is derived in this section.

TRANSPORT EQUATION

Consider one-dimensional problem already introduced in Section 1.6.1 in general terms (see (2.1))

$$\Phi \vartheta \frac{\partial \mathbb{S}}{\partial t} = -u(t) \frac{\partial f(\mathbb{S})}{\partial x} + \frac{\partial}{\partial x} \left(D(\mathbb{S}) \frac{\partial \mathbb{S}}{\partial x} \right), \quad (2.23)$$

where $\mathbb{S} = \mathbb{S}(t, x)$ for all $x \in [0, \infty]$ and $t \in [0, \infty]$.

INITIAL CONDITION

At $t = 0$, the domain $[0, \infty)$ is uniformly occupied by the phase α with its effective saturation \mathbb{S}_i ,

$$\mathbb{S}(0, x) = \mathbb{S}_i \quad \text{for all } x \in (0, \infty). \quad (2.24)$$

Note that the subscript i stands for *initial effective saturation*.

DIRICHLET BOUNDARY CONDITIONS

In order to obtain a unique solution of the two-phase flow equation (2.23), boundary conditions are needed at $x = 0$ and $x = \infty$. Both conditions are of the Dirichlet type

$$\mathbb{S}(t, 0) = \mathbb{S}_0, \quad (2.25)$$

$$\mathbb{S}(t, \infty) = \mathbb{S}_i, \quad (2.26)$$

where \mathbb{S}_i is the initial effective saturation. The inlet effective saturation \mathbb{S}_0 is related to the total velocity term u and therefore the Dirichlet boundary condition (2.25) corresponds to the *total velocity condition* (2.31) presented in the next subsection.

TOTAL VELOCITY CONDITION

The displacing phase is introduced to the domain at $x = 0$ with velocity² u_{dp} given by

$$u_{dp}(t, 0) = Ag(t) = A t^{-\frac{1}{2}}, \quad (2.27)$$

with $A > 0$. Reasons why the function g must have the form $g(t) = t^{-\frac{1}{2}}$ will be discussed later in the exact solution derivation text.

The other phase velocities at the inlet ($x = 0$) and the outlet ($x = \infty$) are unknown, although one can suppose the boundary at $x = \infty$ as semi-permeable characterized by a scalar coefficient $R \in [0, 1]$. The total velocity u is independent of the position in one-dimensional case and it is defined as

$$u = u_w + u_n. \quad (2.28)$$

²The displacing phase velocity is either u_w or u_n , generally denoted as u_{dp} .

Depending on the permeability of the boundary at infinity, it is assumed that

$$u(t) = R Ag(t), \quad (2.29)$$

where $R \in [0, 1]$ because the total velocity can vary from $Ag(t)$ to 0. The total velocity is maximal $u(t) = Ag(t)$ (i.e. $R = 1$) in the situation where the outlet from the domain is not prevented at $x = \infty$, i.e. in the *unidirectional displacement*. On the other hand the total velocity vanishes (i.e. $R = 0$), if the displaced phase can be drained out only at $x = 0$, it is the situation of the *bidirectional displacement*. Introducing a semi-permeable membrane at $x = \infty$, it is possible to obtain all values of $R \in [0, 1]$ and therefore the original problem formulation proposed by Sunada & McWhorter, 1990 can be generalized in that way.

Using the expression (1.65) in a generalized form

$$u_{dp} = u f - D \frac{\partial \mathbb{S}}{\partial x}, \quad (2.30)$$

it is possible to formulate the *total velocity condition* from (2.27) in the terms of \mathbb{S}

$$Ag(t) = R Ag(t) f(\mathbb{S}_0) - D(\mathbb{S}_0) \frac{\partial \mathbb{S}}{\partial x}(t, 0), \quad (2.31)$$

where the boundary condition (2.25) : $\mathbb{S}(t, 0) = \mathbb{S}_0$ is applied.

The condition (2.30) can be formulated either for the case of the non-wetting phase displacement ($dp = w$) according to (1.55) as

$$u_w = u f_w(\mathbb{S}_w) - D(\mathbb{S}_w) \frac{\partial \mathbb{S}_w}{\partial x},$$

or for the case of the wetting phase displacement ($dp = n$) from (1.56) as

$$u_n = u f_n(1 - \mathbb{S}_n) - D(1 - \mathbb{S}_n) \frac{\partial \mathbb{S}_n}{\partial x}.$$

SUMMARY

The partial differential equation

$$\Phi \vartheta \frac{\partial \mathbb{S}}{\partial t} = -A R t^{-\frac{1}{2}} \frac{\partial f(\mathbb{S})}{\partial x} + \frac{\partial}{\partial x} \left(D(\mathbb{S}) \frac{\partial \mathbb{S}}{\partial x} \right), \quad (2.32)$$

is solved for the unknown function $\mathbb{S} = \mathbb{S}(t, x)$ with boundary and initial conditions for all $x \in (0, \infty)$ and $t \in [0, \infty)$

$$\mathbb{S}(t, 0) = \mathbb{S}_0, \quad (2.33)$$

$$\mathbb{S}(t, \infty) = \mathbb{S}_i, \quad (2.34)$$

$$\mathbb{S}(0, x) = \mathbb{S}_i, \quad (2.35)$$

$$(2.36)$$

where

$$\mathbb{S}_0 > \mathbb{S}_i. \quad (2.37)$$

The total velocity condition (2.31) yields

$$\frac{\partial \mathbb{S}}{\partial x}(t, 0) = -A t^{-\frac{1}{2}} \frac{1 - R f(\mathbb{S}_0)}{D(\mathbb{S}_0)}. \quad (2.38)$$

2.3.2 Exact Solution Derivation

The exact solution is derived in this section. In order to understand the necessity of the form $g(t) = t^{-\frac{1}{2}}$ of the input velocity resp. the total velocity term, the general form of the input flux

$$u(t) = R u_{dp}(t, 0) = R A g(t)$$

will be used in the following text.

FUNDAMENTAL ASSUMPTION

Suppose the solution exists in a form

$$\mathbb{S} = \mathbb{S}(\lambda), \quad (2.39)$$

where

$$\lambda = x g(t). \quad (2.40)$$

This substitution is possible if and only if the following *fundamental assumption* holds:

$$\text{Let } \mathbb{S} = \mathbb{S}(\lambda) \text{ be strictly monotone function of } \lambda. \quad (2.41)$$

This assumption permits to invert the dependence (2.39) and assume that

$$\lambda = \lambda(\mathfrak{S}). \quad (2.42)$$

Partial differentiation of (2.40) yields

$$\frac{\partial \mathfrak{S}}{\partial t}(t, x) = \frac{\lambda[\mathfrak{S}(t, x)] g'(t)}{\lambda'[\mathfrak{S}(t, x)] g(t)}, \quad (2.43)$$

$$\frac{\partial \mathfrak{S}}{\partial x}(t, x) = \frac{g(t)}{\lambda'[\mathfrak{S}(t, x)]}, \quad (2.44)$$

where $g'(t)$ resp. $\lambda'(\mathfrak{S})$ stands for the derivative $\frac{dg(t)}{dt}$ resp. $\frac{d\lambda(\mathfrak{S})}{d\mathfrak{S}}$.

FUNCTION F

The *fractional flow function* $F = F(t, x)$ is defined as

$$F(t, x) = R \frac{f[\mathfrak{S}(t, x)] - f(\mathfrak{S}_i)}{1 - R f(\mathfrak{S}_i)} - \frac{D[\mathfrak{S}(t, x)]}{Ag(t) (1 - R f(\mathfrak{S}_i))} \frac{\partial \mathfrak{S}}{\partial x}(t, x). \quad (2.45)$$

The substitution (2.44) makes possible to assume that $F = F(\mathfrak{S})$,

$$F(\mathfrak{S}) = R \frac{f(\mathfrak{S}) - f(\mathfrak{S}_i)}{1 - R f(\mathfrak{S}_i)} - \frac{1}{A(1 - R f(\mathfrak{S}_i))} \frac{D(\mathfrak{S})}{\lambda'(\mathfrak{S})}. \quad (2.46)$$

ODE DERIVATION

According to the expression of the function F (2.46), the partial differential equation (2.32) can be modified into

$$\Phi \vartheta \frac{\partial \mathfrak{S}}{\partial t} + Ag(t) (1 - R f(\mathfrak{S}_i)) \underbrace{\frac{\partial}{\partial x} \left(R \frac{f(\mathfrak{S}) - f(\mathfrak{S}_i)}{1 - R f(\mathfrak{S}_i)} - \frac{D(\mathfrak{S})}{Ag(t) (1 - R f(\mathfrak{S}_i))} \frac{\partial \mathfrak{S}}{\partial x} \right)}_{F(t, x)} = 0, \quad (2.47)$$

where the added constant $f(\mathfrak{S}_i)$ vanishes after applying the partial differentiation and thus the equation (2.47) is equivalent to (2.32).

Application of the substitution (2.40) yields

$$\Phi \vartheta \frac{g'(t)}{g^3(t)} \lambda(\mathfrak{S}) + A(1 - R f(\mathfrak{S}_i)) F'(\mathfrak{S}) = 0. \quad (2.48)$$

If the time dependence of the terms in the equation (2.48) is removed, an ordinary differential equation only in terms dependent on \mathfrak{S} is obtained. The relevant condition is

$$\frac{g'(t)}{g^3(t)} = C_1. \quad (2.49)$$

It is solved by

$$g(t) = (-2 C_1 t + C_2)^{-\frac{1}{2}}. \quad (2.50)$$

It is possible to incorporate any negative value of C_1 in A because $u(t) = Ag(t)$, and thus one may choose for instance $C_1 = -\frac{1}{2}$.

Under these assumptions, the equation (2.48) is transformed into

$$F'(\mathfrak{S}) = \frac{\Phi \vartheta}{2A(1 - R f(\mathfrak{S}_i))} \lambda(\mathfrak{S}). \quad (2.51)$$

Differentiation of this equation with respect to \mathfrak{S} allows to substitute $\lambda'(\mathfrak{S})$ from (2.46), and finally, the second order ordinary differential equation

$$F''(\mathfrak{S}) = -\frac{\Phi \vartheta}{2A^2(1 - R f(\mathfrak{S}_i))^2} \frac{D(\mathfrak{S})}{F(\mathfrak{S}) - \varphi(\mathfrak{S})} \quad (2.52)$$

is obtained, where

$$\varphi(\mathfrak{S}) = R \frac{f(\mathfrak{S}) - f(\mathfrak{S}_i)}{1 - R f(\mathfrak{S}_i)}$$

is the normalized fractional flow function.

CONDITIONS FOR FUNCTION F

If $g(0) = \infty$ then the value of $F(0, x)$ is

$$F(0, x) = R \frac{f[\mathfrak{S}(0, x)] - f(\mathfrak{S}_i)}{1 - R f(\mathfrak{S}_i)}$$

and the initial condition (2.24) yields

$$F(\mathfrak{S}_i) = 0, \quad (2.53)$$

independently of the values of $D(\mathfrak{S}_i)$ or $\frac{\partial \mathfrak{S}}{\partial x}(t, \infty)$, if $D(\mathfrak{S}_i)$ and $\frac{\partial \mathfrak{S}}{\partial x}(t, \infty)$ are bounded. The infinite condition $g(0) = \infty$ implies that the only possible form of the input flux function $g(t)$ is $g(t) = t^{-\frac{1}{2}}$ and thus it incorporates $C_2 = 0$ in (2.50).

Boundary condition (2.25) and the total velocity condition (2.31) substituted into $F(t, 0)$ in (2.45) yields

$$F(\mathfrak{S}_0) = 1. \quad (2.54)$$

The boundary condition (2.25) ensure time independency of \mathfrak{S}_0 while the total velocity condition (2.31) incorporates the α -phase velocity prescribed at $x = 0$ through the term $\frac{\partial \mathfrak{S}}{\partial x}(t, 0)$ explicitly expressed in (2.38).

Moreover, the condition (2.25) can be used in the relationship (2.42)

$$\lambda(\mathfrak{S}_0) = 0 \quad g(t)$$

and the equation (2.51) to formulate an extra condition

$$F'(\mathfrak{S}_0) = 0. \quad (2.55)$$

Altogether, the second order differential equation (2.52) with three conditions for F is obtained. However, the problem is not overdetermined because the third condition is used to establish relationship between A and \mathfrak{S}_0 .

SOLUTION OF PDE

Once the function $F(\mathfrak{S})$ is known, it is possible to easily compute the inverted solution from (2.51)³

$$\frac{2A(1 - R f(\mathfrak{S}_i))}{\Phi \vartheta} F'(\mathfrak{S}) = \lambda = x t^{-\frac{1}{2}}, \quad (2.56)$$

which is in a similar form to the Buckley-Leverett analytical solution (see Section 2.2.4), i.e.

$$x(t, \mathfrak{S}) = \frac{(1 - R f(\mathfrak{S}_i))}{\Phi \vartheta} \frac{dF(\mathfrak{S})}{d\mathfrak{S}} \int_0^t A \tau^{-\frac{1}{2}} d\tau. \quad (2.57)$$

This formula is valid for all values of $\mathfrak{S} \in [\mathfrak{S}_i, \mathfrak{S}_0]$ because the function $\frac{dF(\mathfrak{S})}{d\mathfrak{S}}$ can be inverted as the consequence of to the fundamental assumption (2.41).

In order to demonstrate the relationship between the Buckley-Leverett and McWhorter-Sunada exact solutions, the Buckley-Leverett fractional flow function F_{BL} has to be defined as

$$F_{BL} = \begin{cases} \varphi(\mathfrak{S}) & \forall \mathfrak{S} \geq \mathfrak{S}_t, \\ \varphi(\mathfrak{S}_t) \frac{\mathfrak{S} - \mathfrak{S}_i}{\mathfrak{S}_t - \mathfrak{S}_i} & \forall \mathfrak{S} < \mathfrak{S}_t, \end{cases} \quad (2.58)$$

where \mathfrak{S}_t is again the Welge tangent saturation computed from (2.17). It is obvious that the function F_{BL} does not agree to the fundamental assumption (2.41) with respect to the relationship (2.46) due to its linear part, but formally the solution (2.57) with F_{BL} substituted for F is the same as in Section 2.2.4.

2.3.3 Original Integral Equation

DERIVATION OF INTEGRAL EQUATION

³Compare to the Buckley-Leverett solution in Section 2.2.4

The ODE (2.52) can not be solved directly because the relationship between A and \mathfrak{S}_0 is not determined yet. It is advised from Sunada & McWhorter, 1990 to integrate the ODE to

$$F(\mathfrak{S}) = 1 - \frac{\Phi \vartheta}{2A^2(1 - Rf(\mathfrak{S}_i))^2} \int_{\mathfrak{S}}^{\mathfrak{S}_0} \frac{(v - \mathfrak{S}) D(v)}{F(v) - \varphi(v)} dv, \quad (2.59)$$

where conditions (2.55)

$$F'(\mathfrak{S}_0) = 0,$$

and (2.54)

$$F(\mathfrak{S}_0) = 1,$$

were already included. The last condition (2.53)

$$F(\mathfrak{S}_i) = 0,$$

permits to write

$$F(\mathfrak{S}_i) = 0 = 1 - \frac{\Phi \vartheta}{2A^2(1 - Rf(\mathfrak{S}_i))^2} \int_{\mathfrak{S}_i}^{\mathfrak{S}_0} \frac{(v - \mathfrak{S}_i) D(v)}{F(v) - \varphi(v)} dv, \quad (2.60)$$

and consequently

$$A^2 = \frac{\Phi \vartheta}{2(1 - Rf(\mathfrak{S}_i))^2} \int_{\mathfrak{S}_i}^{\mathfrak{S}_0} \frac{(v - \mathfrak{S}_i) D(v)}{F(v) - \varphi(v)} dv. \quad (2.61)$$

With (2.61), it is possible to rewrite integral equation (2.59) to

$$F(\mathfrak{S}) = 1 - \frac{\int_{\mathfrak{S}}^{\mathfrak{S}_0} \frac{(v - \mathfrak{S}) D(v)}{F(v) - \varphi(v)} dv}{\int_{\mathfrak{S}_i}^{\mathfrak{S}_0} \frac{(v - \mathfrak{S}_i) D(v)}{F(v) - \varphi(v)} dv}. \quad (2.62)$$

Differentiating this integral equation, the desired function $F'(\mathfrak{S})$ is obtained in the form

$$F'(\mathfrak{S}) = \frac{\int_{\mathfrak{S}}^{\mathfrak{S}_0} \frac{D(v)}{F(v) - \varphi(v)} dv}{\int_{\mathfrak{S}_i}^{\mathfrak{S}_0} \frac{(v - \mathfrak{S}_i) D(v)}{F(v) - \varphi(v)} dv}. \quad (2.63)$$

The magnitude of the *diffusion term* $D(\mathcal{S})$ does not influence the function F (multiplicative constants can be reduced in (2.62) as well as in (2.63)), it affects only the value of A .

SOLVING INTEGRAL EQUATION

According to Sunada & McWhorter, 1990, the unknown function $F(\mathcal{S})$ is computed from the integral equation (2.62) by iterations.

$$F_{k+1}(\mathcal{S}) = 1 - \frac{\int_{\mathcal{S}_0}^{\mathcal{S}} \frac{(v-\mathcal{S}) D(v)}{F_k(v)-\varphi(v)} dv}{\int_{\mathcal{S}_i}^{\mathcal{S}_0} \frac{(v-\mathcal{S}_i) D(v)}{F_k(v)-\varphi(v)} dv}. \quad (2.64)$$

It is suggested to use $F_0 \equiv 1$ as a first guess. The function F_k is considered to be a solution of (2.59) when successive iterations are sufficiently small in a norm. The L_∞ norm is employed in the case of this work. The iterative process is terminated if

$$\|F_k - F_{k+1}\|_{L_\infty} < \varepsilon_F. \quad (2.65)$$

Integrals in (2.64) are evaluated numerically, therefore the exact solution is often named as *quasi-analytical* solution.

The iterative process is rapid and convergent for all values of \mathcal{S}_0 in the case of the bidirectional flow ($R = 0$). However, serious difficulties occur when \mathcal{S}_0 and R are close to 1 as the following first iteration analysis demonstrates.

FIRST ITERATION ANALYSIS

If

$$\frac{\partial \mathcal{S}}{\partial x} \leq 0, \quad (2.66)$$

the function F fulfils (see the definition (2.46), resp. (2.45)) the inequality

$$F(\mathcal{S}) \geq \varphi(\mathcal{S}), \quad (2.67)$$

for all $\mathcal{S} \in [0, 1]$. The inequality (2.67) permits to analytically demonstrate causes of the iterative process failures for the case of the Brooks-Corey model functions (1.26), (1.31) and (1.32).

As the author already suspected in recent works Fučík *et al.*, 2004b or Fučík *et al.*, 2004a, the original iterative process fails as the denominator in the integrand $\frac{D(v)}{F(v)-\varphi(v)}$ in (2.62) becomes arbitrarily small or zero if the values of \mathcal{S}_0 and R are selected close to 1. It is possible to present analytical explanation of this

phenomenon. It can be shown that $F(S) > \varphi(S)$ for all $S \in (S_i, S_0)$ and so this relationship must stand for all approximations F_k of the function F .

The first iteration of the function F is obtained by substituting $F_0 \equiv 1$ into the right hand side of the integral equation (2.64). The Brooks-Corey model functions (1.26), (1.31) and (1.32) permit to express the first iteration F_1 analytically as follows

$$F_1(S) = 1 - \frac{S_0^{3+\frac{1}{\lambda}}(3\lambda S_0 - 4\lambda S - S) + \lambda S^{4+\frac{1}{\lambda}}}{S_0^{3+\frac{1}{\lambda}}(3\lambda S_0 - 4\lambda S_i - S_i) + \lambda S_i^{4+\frac{1}{\lambda}}}. \quad (2.68)$$

The second iteration of the function F can not be computed for certain values of S_0 by substituting F_1 into the right hand side of the integral equation (2.64) because the function F_1 intersects the function φ and the integrand $\frac{D(v)}{F(v)-\varphi(v)}$ becomes unbounded as it is illustrated in Figure 2.5, where $S_i = 0$, $R = 1$ and $S_0 \in \{0.5, 0.7, 0.9, 1\}$.

Definitions of functions D and f imply that the first iteration of F_1 is always independent of any other variables except λ , which enables analytical analysis of the subject. Any admissible value of λ does not affect the situation in any remarkable way.

Although μ_w and μ_n do not influence F_1 , they have an important impact on the instability occurrence through the function φ , as depicts Figure 2.5. The *viscosity ratio* parameter $M = \frac{\mu_w}{\mu_n}$ is the key variable that affects the stability of the whole iterative process because it shifts the inflexion point of the function φ towards S_0 or S_i (see Figure 2.5) and therefore the singularity may occur at any point of the interval (S_i, S_0) and not only in the vicinity of S_0 .

The other parameter that influences the formation of the instability after the first iteration is the initial saturation S_i which occurs in both functions φ and F_1 .

The original iterative process fails for values of S_0 from a close neighborhood of 1 as it is demonstrated in details in Table 2.2, Table 2.3 and Table 2.4.

The *critical boundary* denoted by S_0^* represents the highest value of S_0 for which the original iterative process (2.64) is stable. It is obvious that the instability issue of the original process is not peripheral for high viscous non-wetting fluids.

For example, the original iterative process fails for values of S_0 superior to 0.82 in the case of realistic DNAPL Soltrol 220 (test setup 2), where $\mu_n = 0.0035 \text{ kg m}^{-1} \text{ s}^{-1}$ (i.e. $M = 0.286$) and $S_i = 0$.

As a consequence of the first iteration analysis the original iterative process can not be used for the values of $S_0 \geq S_0^*$, where S_0^* is defined as

$$S_0^* = \inf \left\{ S_0 : F_1^{S_0}(S) > \varphi(S) \quad \forall S \in (S_i, S_0) \right\}, \quad (2.69)$$

where $F_1^{S_0}$ is a first iteration of the function F for a given S_0 .

\mathbb{S}_i	viscosity ratio M				
	0.001	0.01	1	100	1000
0.00	0.33593	0.52734	0.91578	0.99728	0.99984
0.10	0.30390	0.49330	0.90798	0.99824	0.99976
0.20	0.30468	0.45937	0.89843	0.99656	0.99966
0.30	0.41142	0.45790	0.88378	0.99602	0.99957
0.40	0.52743	0.54003	0.86640	0.99527	0.99970
0.50	0.63696	0.64037	0.84570	0.99413	0.99928
0.60	0.73642	0.73730	0.82968	0.99230	0.99896
0.70	0.82395	0.82414	0.84648	0.98904	0.99842
0.80	0.89818	0.89821	0.90151	0.98261	0.99843

Table 2.2: Critical values \mathbb{S}_0^* for the model setup 1 depending on \mathbb{S}_i and $M = \frac{\mu_w}{\mu_n}$.

\mathbb{S}_i	viscosity ratio M				
	0.001	0.01	1	100	1000
0.00	0.32018	0.51366	0.91241	0.99715	0.99982
0.10	0.30390	0.47880	0.90463	0.99824	0.99973
0.20	0.30312	0.44335	0.89335	0.99641	0.99980
0.30	0.41347	0.45295	0.87831	0.99584	0.99954
0.40	0.52946	0.54032	0.85929	0.99503	0.99970
0.50	0.63889	0.64208	0.83886	0.99384	0.99920
0.60	0.73798	0.73886	0.82460	0.99191	0.99890
0.70	0.82500	0.82520	0.84648	0.98849	0.99832
0.80	0.89872	0.89877	0.90195	0.98281	0.99843

Table 2.3: Critical values \mathbb{S}_0^* for the model setup 2 depending on \mathbb{S}_i and $M = \frac{\mu_w}{\mu_n}$.

IMPLEMENTATION

The implementation of the numerical algorithm for solving the original integral equation (2.48) is based on the first order Newton-Cotes formulae for numerical approximation of integrals. The function F is discretized to a vector with M components. The code below computes the function $F'(\mathbb{S})$ and the value of A depending on input parameters \mathbb{S}_0 , \mathbb{S}_i , R and input functions $D(\mathbb{S})$ and $f(\mathbb{S})$. In some particular cases

$$\frac{D(\mathbb{S})}{F(\mathbb{S}) - \varphi(\mathbb{S})}$$

\mathbb{S}_i	viscosity ratio M				
	0.001	0.01	1	100	1000
0.00	0.27734	0.52319	0.98449	0.99998	0.99999
0.10	0.23359	0.47792	0.98143	0.99998	0.99999
0.20	0.32031	0.44921	0.97714	0.99997	0.99999
0.30	0.44731	0.49277	0.97163	0.99996	0.99999
0.40	0.56977	0.58690	0.96410	0.99995	0.99999
0.50	0.68108	0.68798	0.95483	0.99993	0.99999
0.60	0.77875	0.78123	0.94492	0.99991	0.99999
0.70	0.86109	0.86193	0.93784	0.99988	0.99999
0.80	0.92667	0.92687	0.94645	0.99982	0.99999

Table 2.4: Critical values \mathbb{S}_0^* for the model setup 3 depending on \mathbb{S}_i and $M = \frac{\mu_w}{\mu_n}$.

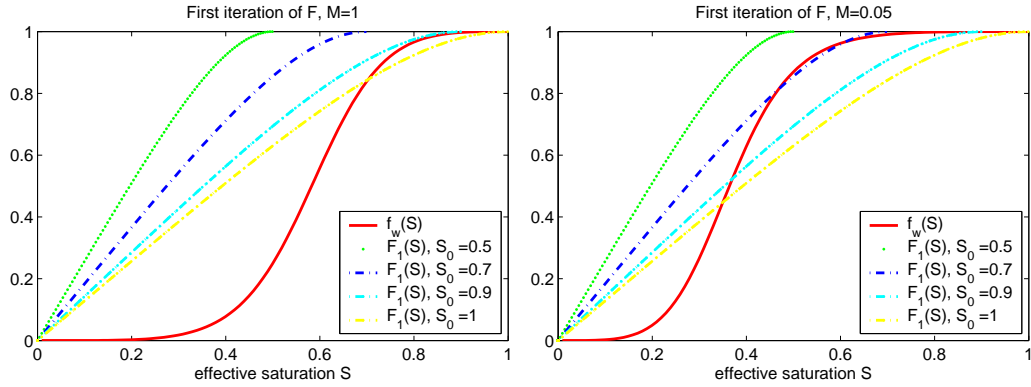


Figure 2.5: Depiction of the function φ and F_1 for different selections of \mathbb{S}_0 illustrate why the original iterative process fails even after the first iteration. As an illustration, a non-wetting phase displacement problem with $R = 1$ and $\mathbb{S}_i = 0$ (i.e. $\varphi \equiv f$) is studied. Whenever the function φ intersects the first iteration F_1 , a singularity in the integrand $\frac{D(v)}{F(v) - \varphi(v)}$ in (2.62) occurs. Brooks-Corey model setup: $\lambda = 2$.

has an undefined value for $\mathbb{S} = \mathbb{S}_0$ so we have to compute the limit

$$\lim_{\mathbb{S} \rightarrow \mathbb{S}_0} \frac{D(\mathbb{S})}{F(\mathbb{S}) - \varphi(\mathbb{S})}.$$

and implement its value in the C function `limitS0()`.

Theorem 2. Let F be an arbitrary continuous function such that $F(\mathbb{S}_0) = 1$ and $F'(\mathbb{S}_0) = 0$. If

$$D(\mathbb{S}) = V(\mathbb{S})(1 - \varphi(\mathbb{S}))$$

and for all $\mathbb{S} \in (0, 1)$

$$0 < \varphi(\mathbb{S}) < 1,$$

then for all $0 < \mathbb{S}_0 < 1$

$$\lim_{\mathbb{s} \rightarrow \mathbb{S}_0^-} \frac{D(\mathbb{S})}{F(\mathbb{S}) - \varphi(\mathbb{S})} = V(\mathbb{S}_0).$$

Proof. It follows from $F'(\mathbb{S}_0) = 0$ that

$$(\forall \varepsilon > 0)(\exists \delta > 0)(\forall h, 0 < h < \delta) (|F(\mathbb{S}_0) - F(\mathbb{S}_0 - h)| < \varepsilon h).$$

The term $\frac{D}{F-\varphi}$ can be simplified into

$$\frac{D}{F - \varphi} = V \frac{1}{1 - \frac{1-F}{1-\varphi}},$$

where $F(\mathbb{S}_0) = 1$. Since $1 - \varphi(\mathbb{S}) > 0$ for all $\mathbb{S} \in [\mathbb{S}_i, \mathbb{S}_0]$, it follows that

$$\left| \frac{1 - F(\mathbb{S}_0 - h)}{1 - \varphi(\mathbb{S}_0 - h)} \right| < \varepsilon h \frac{1}{1 - \varphi(\mathbb{S}_0 - h)},$$

for all $0 < h < \delta$. Therefore

$$\lim_{\mathbb{s} \rightarrow \mathbb{S}_0^-} \frac{D(\mathbb{S})}{F(\mathbb{S}) - \varphi(\mathbb{S})} = V(\mathbb{S}_0).$$

□

The function D defined in Section 1.6.1 satisfies the Theorem 2 assumptions, and therefore the C function `limitS0()` returns exactly the value of $V(\mathbb{S}_0)$. Note that this value can be infinite for the van Genuchten model for a particular parameter selection.

IMPLEMENTATION IN THE C LANGUAGE

```
// McWhorter-Sunada exact solution, algorithm, (C) Radek Fučík 2005
// Department of Mathematics,
// Faculty of Nuclear Science and Physical Engineering
// Czech Technical University in Prague,
// Trojanova 13,120 00 Prague, Czech Republic
#include <math.h> // fabs, sqrt
```

CHAPTER 2. EXACT SOLUTIONS IN HOMOGENEOUS MEDIA

```
#define M 100 // number of vector components
typedef double real; // representation of real numbers
typedef long nat; // representation of natural numbers
typedef double vector[M+1]; // vector of real numbers

// Input variables
real R = 0.8; // - R
real Si = 0.0; // - Si
real S0 = 0.9; // - S0

// Definition of input functions:
real D(real S) {return ?;} // - function D(S)
real f(real S) {return ?;} // - function f(S)
real limitS0() {return ?;} // - limit D/(1-phi) when S0->1

// Auxiliary functions:
real S(int j) { return Si+(S0-Si)/M*j; } // - discretization of S
real phi(real u) // - function phi(S)
{
    return R*(f(u)-f(Si))/(1.0-R*f(Si));
}

// McWhorter Integral Equation Solver
real McWhorter(vector &F,vector &dF,real Epsilon_F)
{
    // - Eps ... accuracy of successive iterations
    vector prevF, IG, IsG; // - dF ... first derivative of function F
    nat k;
    real r=1.0,h,c;
    for (k=0;k<=M;k++) {F[k]=1.0;prevF[k]=1.0;} // - initialization
    while (r>Epsilon_F)
    {
        IG[M] = 0; IsG[M] = 0;
        c = limitS0();
        for (k=M-1;k>=0;k--) // - numerical computation of integrals
        {
            h=S(k+1)-S(k);
            IG[k]=IG[k+1]+h*c/2.0;
            IsG[k]=IsG[k+1]+h*S(k+1)*c/2.0;
            c = (k==0) ? 0 : D(S(k))/(F[k]-phi(S(k)));
            IG[k] +=h*c/2.0;
            IsG[k]+=h*S(k)*c/2.0;
        }
        r=0;c=IsG[0]-Si*IG[0];
        for (k=0;k<=M;k++) // - evaluation of new iteration of F and dF
        {
            prevF[k]=F[k];
            F[k]=(1.0-(IsG[k]-S(k)*IG[k])/c);
            dF[k]=IG[k]/c;
            if (fabs(F[k]-prevF[k])>r)
                r=fabs(F[k]-prevF[k]);
        }
    }
    return sqrt(c/2.0)/(1.0-R*f(Si)); // - return the value of A
}

int main() // Calling of the function McWhorter
{
    // - the solution S(t,x) is computed
    vector F, dF; // from the function dF
    real A;
    A = McWhorter(F,dF,1e-15);
    return 1;
}
```


2.3.4 Modified Integral Equation

MODIFIED ITERATIVE PROCESS

As it was already demonstrated in the first iteration analysis, solution of the above presented original integral equation is not always possible.

The author proposes the following modified iterative method to bypass the formation of the instability in the numerical iterative process. Denoting the significant part of the integrand in (2.62) as

$$G = \frac{D}{F - \varphi}, \quad (2.70)$$

the equation (2.62) can be rewritten in a more suitable way

$$F(\mathfrak{S}) = \frac{D(\mathfrak{S})}{G(\mathfrak{S})} + \varphi(\mathfrak{S}) = 1 - \frac{\int_{\mathfrak{S}}^{\mathfrak{S}_0} (v - \mathfrak{S}) G(v) dv}{\int_{\mathfrak{S}_i}^{\mathfrak{S}_0} (v - \mathfrak{S}_i) G(v) dv}, \quad (2.71)$$

which allows us to deduce two types of iterative schemes; the *variant A* is given by

$$G_{k+1}(\mathfrak{S}) = D(\mathfrak{S}) + G_k(\mathfrak{S}) \left(\varphi(\mathfrak{S}) + \frac{\int_{\mathfrak{S}}^{\mathfrak{S}_0} (v - \mathfrak{S}) G_k(v) dv}{\int_{\mathfrak{S}_i}^{\mathfrak{S}_0} (v - \mathfrak{S}_i) G_k(v) dv} \right), \quad (2.72)$$

and the *variant B* is given by

$$G_{k+1}(\mathfrak{S}) = [D(\mathfrak{S}) + G_k(\mathfrak{S}) \varphi(\mathfrak{S})] \left(1 - \frac{\int_{\mathfrak{S}}^{\mathfrak{S}_0} (v - \mathfrak{S}) G_k(v) dv}{\int_{\mathfrak{S}_i}^{\mathfrak{S}_0} (v - \mathfrak{S}_i) G_k(v) dv} \right)^{-1}. \quad (2.73)$$

The author suggests to use

$$G_0 \equiv \frac{D}{1 - \varphi}$$

as the first iteration which is equivalent to $F_0 \equiv 1$ proposed in Sunada & McWhorter, 1990.

SOLUTION OF INTEGRAL EQUATION

The function F , resp. F_k is easily computed from

$$F(\mathfrak{S}) = \frac{D(\mathfrak{S})}{G(\mathfrak{S})} + \varphi(\mathfrak{S}), \quad (2.74)$$

since $G(\mathfrak{S}) > 0$ for all $\mathfrak{S} \in (\mathfrak{S}_i, \mathfrak{S}_0)$. Nevertheless, the numerical implementation allows to determine values of its first derivative F' based on (2.63)

$$F'(\mathfrak{S}) = \frac{\int_{\mathfrak{S}}^{\mathfrak{S}_0} G(v) dv}{\int_{\mathfrak{S}_i}^{\mathfrak{S}_0} (v - \mathfrak{S}_i) G(v) dv},$$

because the integrals are already numerically evaluated during the iterative process.

DISCRETIZATION

The integrals in (2.72) and (2.73) are evaluated numerically taking advantage of the form of the integrand as follows.

Let $\{G^j\}_{j=0}^M$ be equidistant discretization of the function G in the interval $[\mathfrak{S}_i, \mathfrak{S}_0]$ defined as

$$G^j = G(\mathfrak{S}_i + j h), \quad (2.75)$$

where $h = \frac{\mathfrak{S}_0 - \mathfrak{S}_i}{M}$. The numerical solution of the integral equations (2.72) and (2.73) requires to compute the integral

$$\int_{\mathfrak{S}_i + j h}^{\mathfrak{S}_i + (j+1)h} (v - \mathfrak{S}_i - l h) G(v) dv. \quad (2.76)$$

The numerical approximation of the integral (2.76) is denoted as $I^j(l)$. The linear interpolation of $\{G^j\}_{j=0}^M$ in the interval $[\mathfrak{S}_i, \mathfrak{S}_0]$ allows to express the value of $I^j(l)$ as

$$I^j(l) = \frac{h^2}{6}(3j - 3l + 1)(G^j + G^{j+1}) + \frac{h^2}{6}G^{j+1}. \quad (2.77)$$

It is possible to numerically evaluate the integrals in the modified iterative schemes (2.72) and (2.73) as follows

$$\int_{\mathfrak{S}_i + l h}^{\mathfrak{S}_0} (v - \mathfrak{S}_i - l h) G(v) dv = \sum_{j=0}^{M-1} I^j(l). \quad (2.78)$$

Since both $F(\mathbb{S}_i) = 0$ and $\varphi(\mathbb{S}_i) = 0$ by definition, it follows from (2.70) that the value of $G(\mathbb{S}_i)$ is undefined. The value $G(\mathbb{S}_i) = 0$ is always used in the iterative process.

IMPLEMENTATION

The implementation of the modified iterative schemes (2.72) and (2.73) is based on the discretization presented in the previous subsection. The function G is discretized to a vector with M components. The code below computes the function $F'(\mathbb{S})$ and the value of A depending on input parameters \mathbb{S}_0 , \mathbb{S}_i , R and input functions $D(\mathbb{S})$ and $f(\mathbb{S})$. In order to correctly setup the initial value of G_0 , implementation of the function

$$V = \frac{D}{1 - \varphi},$$

is required. The function D defined in Section 1.6.1 (see also Theorem (2)) can be reduced in such a way.

IMPLEMENTATION IN THE C LANGUAGE

```
// McWhorter-Sunada exact solution, modified algorithm, (C) Radek Fučík 2005
// Department of Mathematics,
// Faculty of Nuclear Science and Physical Engineering
// Czech Technical University in Prague,
// Trojanova 13,120 00 Prague, Czech Republic
#include <math.h>           // fabs, sqrt

#define M 100              // number of vector components
typedef double real;       // representation of real numbers
typedef long nat;         // representation of natural numbers
typedef double vector[M+1]; // vector of real numbers

// Input variables
real R = 0.8;             // - R
real Si = 0.0;           // - Si
real S0 = 0.9;           // - S0

// Definition of input functions:
real D(real S) {return ?;} // - function D(S)
real f(real S) {return ?;} // - function f(S)
real phi(real u)          // - function phi(S)
{
    return R*(f(u)-f(Si))/(1.0-R*f(Si));
}
real V(real S) { return D(S)/(1-phi(S)); } // Simplified first guess G_0

// Auxiliary function:
// - discretization of S
real S(int j) { return Si+(S0-Si)/M*j; }

real ModifiedMethod(vector &F, vector &dF, vector &d2F, real Epsilon_A, int type)
{
    vector G,fi,d;
    nat k;
```

CHAPTER 2. EXACT SOLUTIONS IN HOMOGENEOUS MEDIA

```
real prevA, A, h=(S0-Si)/M, IG, IsG, diff, I0, Ik, dIk;
for (k=0; k<=M; k++)
{
  G[k]=V(S(k));          // first guess
  d[k] = D(S(k));        // pre-allocating values of D(S)
  fi[k] = phi(S(k));     // pre-allocating values of phi(S)
}
F[M]=1.0;
dF[M]=0;
I0 = h*h/6.0*G[M]*(3.0*M-1.0);
for (k=1; k<=M-1; k++) I0+=k*G[k]*h*h;

while (diff>Epsilon_A)
{
  diff=0; IG=0; IsG=0;
  for (k=M-1; k>=1; k--)
  {
    Ik = h*h*(G[k] + G[M]*(3.0*M-3.0*k-1.0)/6.0)+IsG-k*IG;
    dIk = h/2.0*(G[k] + G[M]) + IG/h;
    IG = G[k]*h*h+IG;
    IsG = k*G[k]*h*h+IsG;

    switch (type)
    {
      default :
      // variant A :
      case 0 : G[k] = d[k] + G[k]*(fi[k] + Ik/I0); break;
      // variant B :
      case 1 : G[k] = (d[k] + G[k]*fi[k])/(1.0 - Ik/I0); break;
    }
    F[k] = 1.0-Ik/I0;
    dF[k] = dIk/I0;
    d2F[k] = -G[k]/I0;
  }
  d2F[M] = -G[M]/I0;
  I0 = h*h/6.0*G[0] + h*h/6.0*G[M]*(3.0*M-1.0) + IsG;
  A = sqrt(I0/2.0)/(1.0-R*f(Si));
  diff=fabs(A-prevA);
  prevA = A;
}
return A;
}

int main()
{
  // function F, F' and F''
  vector F, dF, d2F;
  real A;
  // variant A
  A = ModifiedMethod(F, dF, d2F, 1e-15, 0);
  // variant B
  A = ModifiedMethod(F, dF, d2F, 1e-15, 1);
  return 1;
}
```

MODIFIED ITERATIVE SCHEME ANALYSIS

In this section, the unidirectional case ($R = 1$) is picked to better illustrate the functionality of the modified method on the edge of the validity of the fundamental

2.3. MCWHORTER-SUNADA EXACT SOLUTION

assumption (2.41).

A monotone growth of successive estimates of G is observed in all computations, i.e. $G_k \leq G_{k+1}$ in $[\mathbb{S}_i, \mathbb{S}_0]$ and fast convergence for all cases, where the original iterative method does not fail as it is illustrated in Table 2.5.

Number of iterations, test setup 1, $\mathbb{S}_i = 0$								
\mathbb{S}_0	0.4	0.5	0.6	0.7	0.8	0.9	0.99	0.999
(2.64)	13	12	18	-	-	-	-	-
(2.72)	574	628	637	1645	8342	89684	7.53e7	$> 10^9$
(2.73)	36	115	411	1645	8348	89681	7.55e7	$> 10^9$

Number of iterations, test setup 2, $\mathbb{S}_i = 0$								
\mathbb{S}_0	0.4	0.5	0.6	0.7	0.8	0.9	0.99	0.999
(2.64)	13	13	13	14	27	-	-	-
(2.72)	636	711	772	807	1655	17913	1.56e7	$> 10^9$
(2.73)	29	31	87	320	1652	17925	1.60e7	$> 10^9$

Number of iterations, test setup 3, $\mathbb{S}_i = 0$								
\mathbb{S}_0	0.4	0.5	0.6	0.7	0.8	0.9	0.99	0.999
(2.64)	14	14	14	14	15	27	-	-
(2.72)	1527	1747	1937	2103	2198	2027	121888	7.06e6
(2.73)	36	38	46	99	294	1493	121891	7.07e6

Number of iterations, test setup 2, $\mathbb{S}_i = 0.2$								
\mathbb{S}_0	0.4	0.5	0.6	0.7	0.8	0.9	0.99	0.999
(2.64)	20	19	18	18	-	-	-	-
(2.72)	38	25199	29088	32236	31501	17723	1.53e7	$> 10^9$
(2.73)	7	136	88	323	1654	failed	1.53e7	$> 10^9$

Number of iterations, test setup 3, $\mathbb{S}_i = 0.2$								
\mathbb{S}_0	0.4	0.5	0.6	0.7	0.8	0.9	0.99	0.999
(2.64)	22	21	20	19	19	46	-	-
(2.72)	20523	24836	29106	33519	38123	40250	119475	6.83e6
(2.73)	630	157	failed	68	292	1477	119467	failed

Table 2.5: Number of iterations required to obtain the function F and the value of A with precision $\varepsilon_A = 10^{-15}$. Original iterative scheme (2.64), the variant A (2.72) and variant B (2.73) of the modified iterative scheme are used. In some situations if $\mathbb{S}_i > 0$ the modified iterative method variant B 2.73 fails randomly.

The modified method still works even if the original method fails, successive approximations of G are decreasing in the L_∞ norm, but the number of iterations needed to reach required precision of the function G increases considerably as both \mathbb{S}_0 and R approach 1. Although there are negligible variations in successive estimates F_k in this situation, the estimates of A converge very slowly. With respect to such behaviour of the iterative process the author suggests to use difference of the successive estimates of A as the criterion to terminate the iterative process, formally as

$$|A_k - A_{k+1}| < \varepsilon_A. \quad (2.79)$$

The test models with high viscous NAPL are used to demonstrate robustness of the modified iterative scheme in situations, where the original iterative scheme fails even after the first iteration as it was already explained in the previous sections.

If $\mathbb{S}_i > 0$, the variant B (2.73) of the modified iterative process fails randomly due to numerical division by zero, because the integrals in the fraction in (2.73) give exactly the same value in the computer precision for \mathbb{S} very close to \mathbb{S}_i . Otherwise if $\mathbb{S}_i = 0$, the process is stable because the diffusivity term $D(0) = 0$ zeroize the value of $G(\mathbb{S})$ in the proximity of \mathbb{S}_i . It is obvious that the value of $G(\mathbb{S}_i)$ is undefined for all $\mathbb{S}_i \in [0, \mathbb{S}_0]$ since $F(\mathbb{S}_i) = \varphi(\mathbb{S}_i) = 0$ by definition. The author suggests to exclude the value of $G(\mathbb{S}_i)$ from the discretization of the function G in the numerical computation since $F(\mathbb{S}_i) = 0$.

Table 2.5 shows that the number of iterations required to reach certain precision of successive estimates of A increases as $\mathbb{S}_0 \rightarrow 1$ for both variant A and B of the modified iterative scheme.

This is due to extremely small difference between the function φ and F in the neighborhood of 1 as McWhorter and Sunada claimed in Sunada & McWhorter, 1990. It is possible to verify numerically and graphically the approaching of the function F to the Buckley-Leverett function F_{BL} introduced in (2.58) in Table 2.6 and Figure 2.6. Moreover, this convergence is realized also for the first and second derivatives of F , i.e. $F' \rightarrow F'_{BL}$ and $F'' \rightarrow F''_{BL}$ as $\mathbb{S}_0 \rightarrow 1$ (see Figure 2.6).

The number of iterations increases as $\mathbb{S}_0 \rightarrow 1$ because the more these two functions approach each other, the more the numerical evaluation of the integrals in the iterative scheme is inaccurate due to finite precision of the computer arithmetic. Furthermore, the limit function F_{BL} does not obey the fundamental assumption as it was already stated and its second derivative F''_{BL} is a discontinuous function. Note that the function F'' can be expressed as

$$F''(\mathbb{S}) = -\frac{G(\mathbb{S})}{\int_{\mathbb{S}_i}^{\mathbb{S}_0} (v - \mathbb{S}_i) G(v) dv}. \quad (2.80)$$

The convergence of F to F_{BL} as $\mathfrak{S}_0 \rightarrow 1$ can be studied only by the means of numerical experiments since all other analytical techniques are insufficient.

An extreme number of iterations is required to achieve convergence of A as \mathfrak{S}_0 is close to 1 (see Figure 2.7), but after certain value of \mathfrak{S}_0 , the modified iterative process will not converge due to loss of the numerical precision as it is demonstrated in the Figure 2.7. However, the estimates of the function F with its first and second derivative changes negligibly in such iterative process due to the fact, that the fraction

$$\frac{\int_{\mathfrak{S}}^{\mathfrak{S}_0} (v - \mathfrak{S}) G_k(v) dv}{\int_{\mathfrak{S}_i}^{\mathfrak{S}_0} (v - \mathfrak{S}_i) G_k(v) dv}, \quad (2.81)$$

suppresses any effects of the increase of A on the function F . Note that the value of A is represented by the integral in the denominator in (2.81) by the relationship (2.61).

Consequently, the integral equation (2.62) cannot be solved numerically for values of \mathfrak{S}_0 greater than a certain limit unless one is able to compute with infinitesimally small numbers.

2.3.5 Limit value of A

As it was already stated in the previous sections, the important part of the computational process is the value of A in dependence of \mathfrak{S}_0 . The iterative process requires a huge number of iterations to arrive at certain precision of successive estimates of A for imposition of \mathfrak{S}_0 and R close to 1 while the estimates of the function F vary negligibly. Therefore the author pursues Sunada & McWhorter, 1990, Sunada & McWhorter, 1992 and Z.-X. Chen & Witherspoon, 1992 discussion of the limit

$$\lim_{\mathfrak{S}_0 \rightarrow 1} A(\mathfrak{S}_0). \quad (2.82)$$

Only the unidirectional displacement case $R = 1$ is considered in this section.

McWhorter and Sunada claimed in Sunada & McWhorter, 1990 that the limit (2.82) is infinite as the consequence of $F \rightarrow \varphi$ in some neighborhood of \mathfrak{S}_0 . However, this statement has been impugned in Z.-X. Chen & Witherspoon, 1992 where the authors declared the limit always finite as a consequence of boundedness of the integrand

$$\frac{(v - \mathfrak{S}_i) D(v)}{F(v) - \varphi(v)}, \quad (2.83)$$

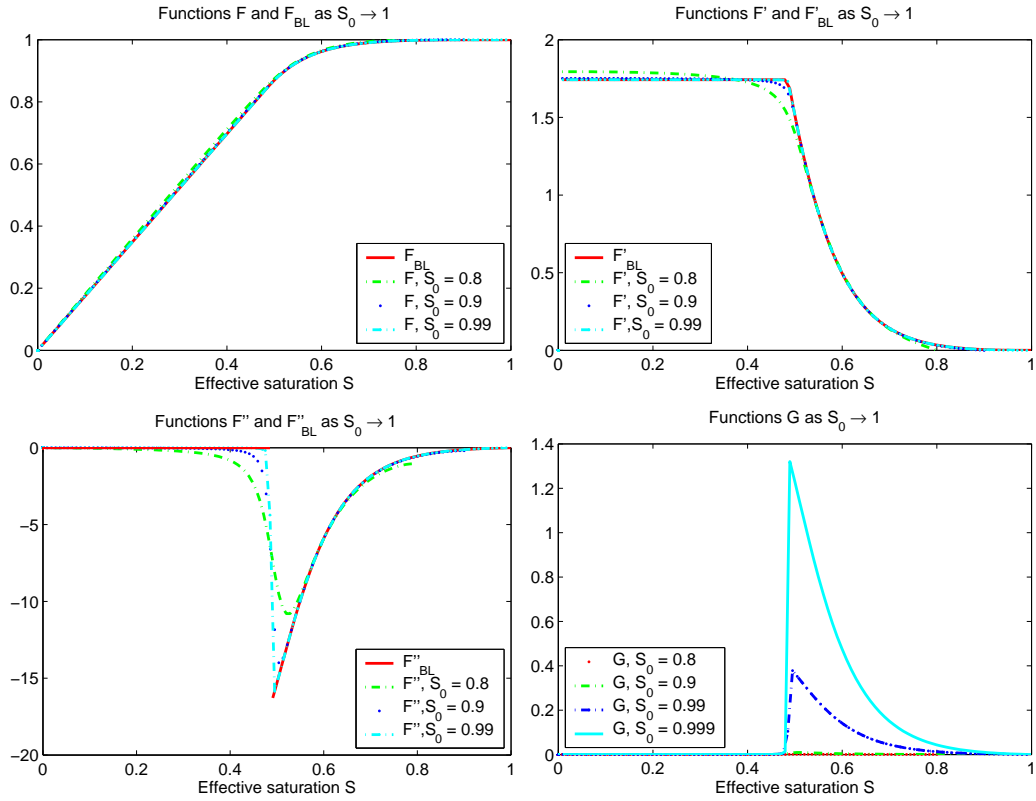


Figure 2.6: Experimental approaching of the functions F to F_{BL} , F' to F'_{BL} and F'' to F''_{BL} as $S_0 \rightarrow 1$; test setup 1 with $S_i = 0$, variant A (2.72) of the modified iterative scheme. The last figure depicts the evolution of the function G as $S_0 \rightarrow 1$. Note that the function G and F'' are related by (2.80), i.e. they differ only by a factor consisting of A^2 .

as $S_0 \rightarrow 1$. In the reply to this comment, McWhorter and Sunada confirmed in Sunada & McWhorter, 1992 that the limit (2.82) is always finite because the integrand (2.83) is bounded for $v = S_0$.

On the contrary, the author's work shows that as S_0 approaches 1, the value of A increases without bounds as it is demonstrated in Figure 2.7. Experimental observations concerning the approaching of F'' are applied to F''_{BL} as $S_0 \rightarrow 1$ as follows.

The substitution $\lambda = \lambda(S)$ permits to express the partial derivative of $\frac{\partial S}{\partial x}(t, x)$ in (2.44). The term $\lambda'(S)$ can be evaluated by differentiating of the expression (2.46) by S

$$\frac{\Phi \vartheta}{2A(1 - f(S_i))} \lambda'(S) = F''(S). \quad (2.84)$$

Variant A (2.72) of the modified iterative scheme				
\mathcal{S}_0	$\ F - F_{BL}\ _{L_1}$	$\ F' - F'_{BL}\ _{L_1}$	$\ F'' - F''_{BL}\ _{L_1}$	Number of iterations
0.6	5.46e-2	2.48e-1	1.71	637
0.7	2.30e-2	1.07e-1	1.21	1645
0.8	5.76e-3	2.89e-2	5.62e-1	8342
0.9	1.00e-3	5.43e-3	1.951e-1	89684
0.99	3.75e-5	2.19e-4	3.09e-2	10000000 ^{*)}
0.999	1.20e-5	7.15e-5	1.64e-2	10000000 ^{*)}
0.9999	1.06e-5	6.34e-5	1.55e-2	10000000 ^{*)}
Variant B (2.73) of the modified iterative scheme				
\mathcal{S}_0	$\ F - F_{BL}\ _{L_1}$	$\ F' - F'_{BL}\ _{L_1}$	$\ F'' - F''_{BL}\ _{L_1}$	Number of iterations
0.6	5.46e-2	2.48e-1	1.71	411
0.7	2.30e-2	1.07e-1	1.21	1645
0.8	5.76e-3	2.89e-2	5.62e-1	8348
0.9	1.00e-3	5.43e-3	1.95e-1	89681
0.99	3.75e-5	2.19e-4	3.09e-2	10000000 ^{*)}
0.999	1.20e-5	7.15e-5	1.67e-2	10000000 ^{*)}
0.9999	1.06e-5	6.34e-5	1.55e-2	10000000 ^{*)}

^{*)} ... the $\varepsilon_A = 10^{-15}$ precision was not reached yet after 10^8 iterations

Table 2.6: Experimental convergence of $F \rightarrow F_{BL}$ as $\mathcal{S}_0 \rightarrow 1$ for test setup 1, $\mathcal{S}_i = 0$ and $\varepsilon_A = 10^{-15}$.

The substitution of the expression of $\lambda'(\mathcal{S})$ into (2.44) yields

$$\frac{\partial \mathcal{S}}{\partial x}(t, x) = \frac{\Phi \vartheta Ag(t)}{2A^2(1 - f(\mathcal{S}_i))F''(\mathcal{S})}. \quad (2.85)$$

The total velocity condition (2.38) can be written in the terms depending on \mathcal{S}_0 only as follows

$$Ag(t) = Ag(t)f(\mathcal{S}_0) - Ag(t)\frac{\Phi \vartheta D(\mathcal{S}_0)}{2A^2(1 - f(\mathcal{S}_i))F''(\mathcal{S}_0)}, \quad (2.86)$$

This equation can be further simplified using for instance the non-wetting phase displacement situation (2.2) into

$$1 = \frac{\Phi \vartheta K k_{rw}(\mathcal{S}_0) p'_c(\mathcal{S}_0)}{2\mu_w \vartheta \Phi A^2 (1 - f_w(\mathcal{S}_i))F''(\mathcal{S}_0)}, \quad (2.87)$$

and thus one can state

$$\lim_{\mathcal{S}_0 \rightarrow 1} A^2(\mathcal{S}_0) = \lim_{\mathcal{S}_0 \rightarrow 1} \frac{\Phi \vartheta K k_{rw}(\mathcal{S}_0) p'_c(\mathcal{S}_0)}{2\mu_w \vartheta \Phi (1 - f_w(\mathcal{S}_i))F''(\mathcal{S}_0)}. \quad (2.88)$$

Based on the numerical experiments, the function F behaves asymptotically as F_{BL} at least to its second derivative. Under this assumption the limit (2.88) is infinite for both the Brooks-Corey and van Genuchten model functions, i.e.

$$\lim_{S_0 \rightarrow 1} A^2(S_0) = \infty, \quad (2.89)$$

which agrees to the experimental observations in Figure 2.7 and to Sunada & McWhorter, 1990 as well.

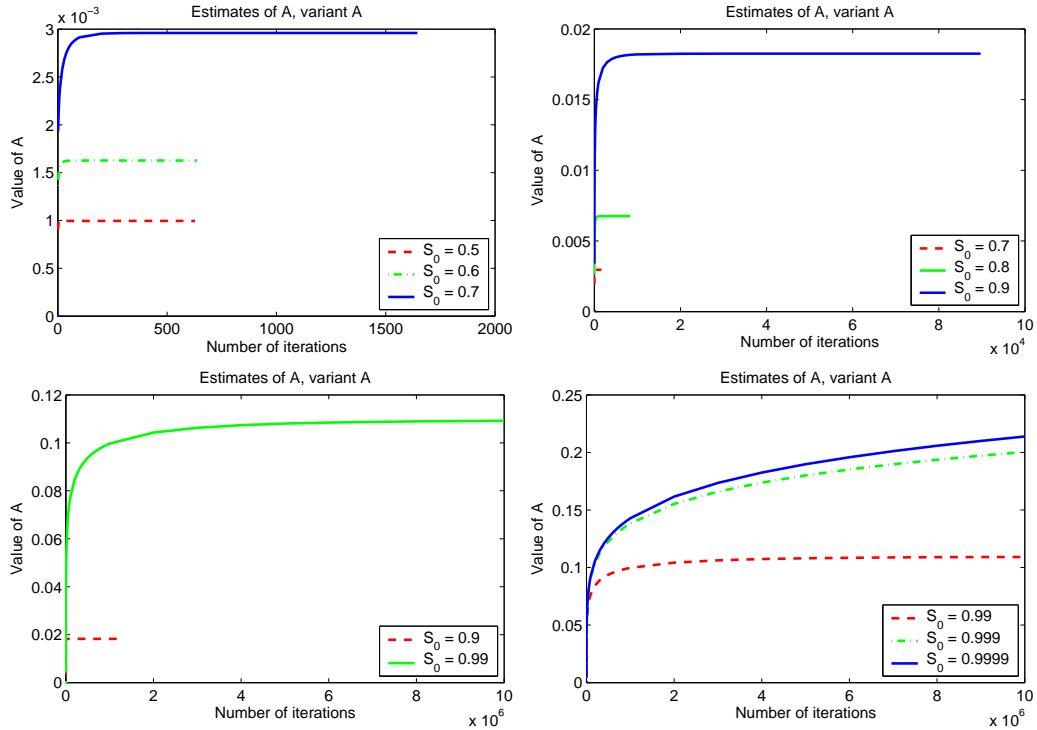


Figure 2.7: Evolution of A in the modified iterative process, variant A; test setup 1, $S_i = 0$. As S_0 approaches 1, the iterative process requires higher number of iterations to reach convergence of A . In the very proximity of S_0 to 1, the value of A is far from convergence even after 10^8 iterations. The variant B situation is analogous.

2.3.6 Generalization of Formulation

NEGATIVE VALUE OF R

The author studied various setups for the McWhorter and Sunada analytical solution and he discovered that the formulation of the McWhorter and Sunada

problem discussed in Section 2.3.1 can be further generalized by allowing the parameter R to shift towards negative values. This generalization is necessary in order to apply the exact solutions to the heterogeneous porous medium (see the next chapter).

The formulation of the McWhorter and Sunada problem involves influx of the displacing phase (denoted by the subscript *in* in this subsection) with velocity

$$u_{in} = At^{-\frac{1}{2}}. \quad (2.90)$$

The displaced phase (denoted by the subscript *out*) already present in the medium flows out of the medium either at $x = \infty$ or at $x = 0$ depending on the ratio parameter R , defined as

$$R = \frac{u}{u_{in}}, \quad (2.91)$$

where u is the total velocity defined as $u = u_{in} + u_{out}$.

Assuming the displaced phase is injected instead of being drained out at $x = \infty$, a negative value of R can be prescribed resulting that the displacing phase can be injected in the counter-current flow direction of the displaced phase.

The original McWhorter and Sunada iterative algorithm (2.64) admits all negative values of R , while both of the variants of the modified iterative scheme (2.72) and (2.73) fail for R lower than a $R_{crit} < 0$. This is due to non-positivity of the function φ in the modified iterative method with causes improper evaluation of the iterations G_k . However, the original iterative scheme is designed such that the integrals in the equation remains always non-negative for all values of R .

NEGATIVE VALUE OF A

Another generalization can be made with respect to the value of A . Consider the McWhorter and Sunada problem in the semi-infinite domain $(-\infty, 0)$ with the boundary and initial conditions (2.25) and (2.24) in the form

$$\mathbb{S}(0, x) = \mathbb{S}_i \quad \text{for all } x \in (-\infty, 0), \quad (2.92)$$

$$\mathbb{S}(t, 0) = \mathbb{S}_0 \quad \text{for all } t > 0, \quad (2.93)$$

$$\mathbb{S}(t, -\infty) = \mathbb{S}_i \quad \text{for all } t > 0. \quad (2.94)$$

The formal derivation of the McWhorter and Sunada solution with $A < 0$ is still applicable as a consequence of the square of A in (2.61).

2.3.7 Summary

The restrictions of applicability of the original and modified iterative scheme are resumed in the following list :

Restrictions of applicability of the iterative schemes

Original method (2.64) :	(\mathcal{S}_0, R) not close to (1, 1), depending on $\frac{\mu_w}{\mu_n}$
Modified method, variant A (2.72):	$R_{crit} \leq R \leq 1$
Modified method, variant B (2.73):	$R_{crit} \leq R \leq 1$ and only for $\mathcal{S}_i = 0$

2.4 Comparison of Exact Solutions

The demonstration of how the modified iterative method (2.72) resp. (2.73) shows the relationship between McWhorter and Buckley-Leverett analytical solutions is provided in this section. Computations for the test setup 1 (see Table 2.1, page 27), $\mathcal{S}_i = 0$ with various values of R and \mathcal{S}_0 are proceeded.

The value of A corresponding to the McWhorter exact solution for $R = 1$ is used in order to compare the McWhorter exact solution (2.56) to the Buckley-Leverett analytical solution (see Section 2.2.4).

The Figure 2.8 depicts how the bi-directional displacement ($R=0$, diffusive term only in (2.1)), partially unidirectional displacement ($R=0.8$, both advective and diffusive terms in (2.1)) and unidirectional displacement ($R=1$, both advective and diffusive terms in (2.1)) are related to the Buckley-Leverett solution of the advective equation (2.4). The more \mathcal{S}_0 approaches 1, the less the diffusive term in (2.1) affects the solution. Table 2.7 contains values of A for various values of R and \mathcal{S}_0 .

The modified iterative process permits to obtain solutions for strong advective terms in (2.1) and compare them to the Buckley-Leverett solution while the original iterative process fails already in situations where the diffusive term still prevails; since the critical value \mathcal{S}_0^* for the test setup 1 with $\mathcal{S}_i = 0$ is $\mathcal{S}_0^* = 0.69$, Figure 2.8 parts B), C) and D) depict only solutions, that are obtainable by the modified iterative method (for the case $R = 1$).

2.4. COMPARISON OF EXACT SOLUTIONS

Dependency of A on S_0 and R						
S_0	$R=0$	$R=0.2$	$R=0.4$	$R=0.6$	$R=0.8$	$R=1$
0.40	1.37e-4	1.42e-4	1.48e-4	1.55e-4	1.64e-4	1.75e-4
0.50	1.75e-4	1.85e-4	1.98e-4	2.16e-4	2.43e-4	9.94e-4
0.60	1.97e-4	2.11e-4	2.29e-4	2.57e-4	3.05e-4	1.62e-3
0.70	2.08e-4	2.23e-4	2.45e-4	2.78e-4	3.41e-4	2.95e-3
0.80	2.12e-4	2.28e-4	2.51e-4	2.86e-4	3.57e-4	6.75e-3
0.90	2.13e-4	2.30e-4	2.53e-4	2.89e-4	3.62e-4	1.82e-2
0.99	2.14e-4	2.30e-4	2.53e-4	2.89e-4	3.62e-4	1.09e-1

Table 2.7: Values of A for various values of R and S_0 ; test setup 1, $S_i = 0$.

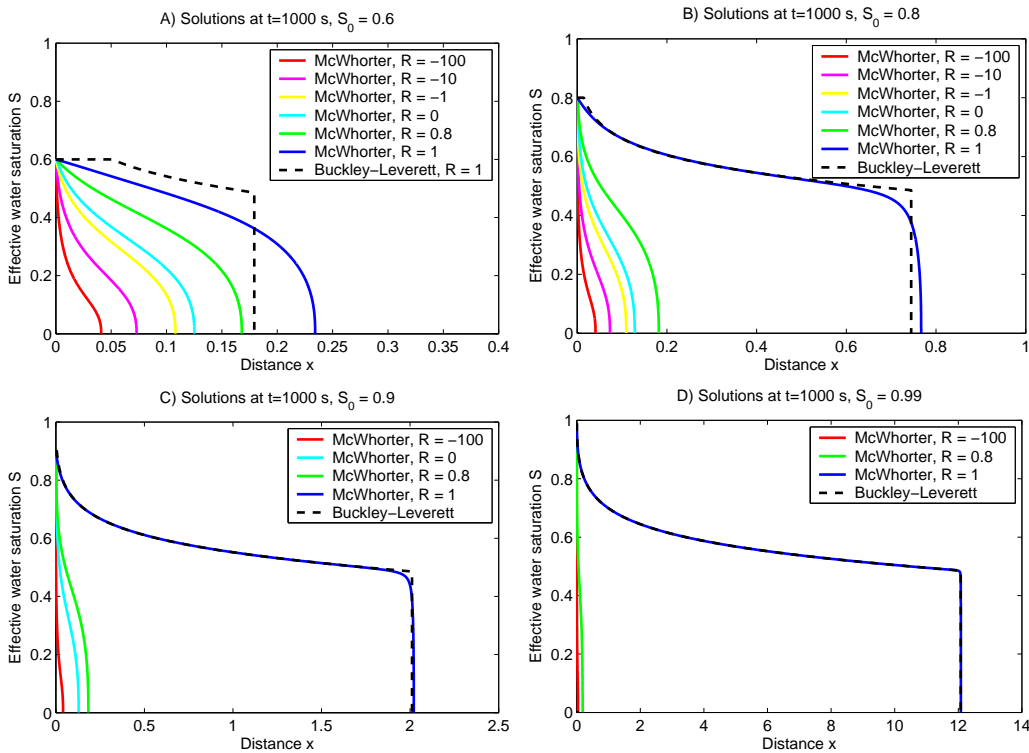


Figure 2.8: McWhorter exact solutions (the variant A) and Buckley-Leverett analytical solutions for various S_0 ; test setup 1, $S_i = 0$. As $S_0 \rightarrow 1$, the unidirectional displacement solution ($R=1$) approaches the Buckley-Leverett solution, while the front of the bi-directional displacement solution ($R=0$) advances negligibly.

Chapter 3

Exact Solution for Heterogeneous Media

3.1 Introduction

The author extends the ideas of van Duijn & de Neef, 1998, concerning exact solutions of two-phase flow in heterogeneous porous media. In that paper, van Duijn and de Neef discuss similarity solutions for capillary redistribution problems without external forces, i.e. the equation (2.23) with $u \equiv 0$:

$$\Phi \vartheta \frac{\partial \mathcal{S}}{\partial t} = \frac{\partial}{\partial x} \left(D(\mathcal{S}) \frac{\partial \mathcal{S}}{\partial x} \right). \quad (3.1)$$

Extension of their idea to the advection-diffusion equation

$$\Phi \vartheta \frac{\partial \mathcal{S}}{\partial t} = -u \frac{\partial f(\mathcal{S})}{\partial x} + \frac{\partial}{\partial x} \left(D(\mathcal{S}) \frac{\partial \mathcal{S}}{\partial x} \right), \quad (3.2)$$

is provided by applying the McWhorter and Sunada exact solution discussed in Chapter 2. According to available scientific resources, this approach has not been published yet.

The quasi-analytical solution of the McWhorter and Sunada problem 2.23 can be obtained for a large range of entry parameters by virtue of the original iterative method 2.64 and the modified iterative methods 2.72 and 2.73.

The exact solution derivation and respective algorithms are presented for each of the cases separately in order to describe the exact solution for both non-wetting phase and wetting phase infiltration.

3.2 Non-Wetting Phase Infiltration Problem

The non-wetting phase infiltration problem is defined as the intrusion of the non-wetting phase in the positive direction along the x axis with nonnegative total velocity u defined by (2.28) as $u = u_n + u_w$. Therefore assume $u_n(t, x) \geq 0$ for all $t \geq 0$ and $x \in (-\infty, \infty)$.

3.2.1 Exact Solution

Van Duijn and de Neef, 1998 derive the similarity solution as a combination of two solutions in semi-infinite domains by implementing the interface conditions (1.36) and the extended capillary pressure condition (1.37). The author applies their idea to the McWhorter and Sunada problem formulation, which is identical to their equations in the case of the bidirectional displacement with no advection term (the total velocity $u \equiv 0$ in (3.2), $R = 0$).

PROBLEM EQUATIONS

Denote the other parameters characterising the material in Ω^R , resp. Ω^L by superscript R resp. L . Under this notation the system of the two-phase flow equations yields

$$\Phi^R \vartheta^R \frac{\partial \mathfrak{S}_n}{\partial t} = -u^R \frac{\partial f_n^R(1 - \mathfrak{S}_n)}{\partial x} + \frac{\partial}{\partial x} \left(\mathfrak{D}^R(1 - \mathfrak{S}_n) \frac{\partial \mathfrak{S}_n}{\partial x} \right), \quad (3.3)$$

$$\Phi^L \vartheta^L \frac{\partial \mathfrak{S}_n}{\partial t} = -u^L \frac{\partial f_n^L(1 - \mathfrak{S}_n)}{\partial x} + \frac{\partial}{\partial x} \left(\mathfrak{D}^L(1 - \mathfrak{S}_n) \frac{\partial \mathfrak{S}_n}{\partial x} \right). \quad (3.4)$$

The McWhorter and Sunada exact solution for the bidirectional case ($R < 1$) involves positive velocity of the displacing phase at $x = 0$ while the displaced phase flows out of the domain at $x = 0$ (therefore with negative velocity at $x = 0$).

Suppose a one-dimensional unbounded domain $\Omega = (-\infty, +\infty)$ divided at $x = 0$ into two semi-infinite domains Ω^L and Ω^R of different material properties. The situation at $t = 0$ is depicted in Figure 3.1.

RIGHT DOMAIN PROBLEM

Consider the non-wetting phase intrusion problem (the wetting phase displacement) in the domain Ω^R with boundary and initial conditions given by

$$\mathfrak{S}_n(t, 0) = \mathfrak{S}_0^R \quad \text{for all } t > 0, \quad (3.5)$$

$$\mathfrak{S}_n(t, \infty) = \mathfrak{S}_i^R \quad \text{for all } t > 0, \quad (3.6)$$

$$\mathfrak{S}_n(0, x) = \mathfrak{S}_i^R \quad \text{for all } x > 0. \quad (3.7)$$

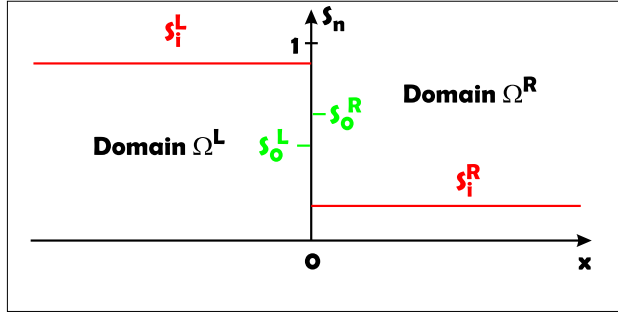


Figure 3.1: Initial state of the porous medium with a discontinuity.

According to the derivation of the McWhorter and Sunada exact solution, the non-wetting phase velocity at $x = 0$ is given by

$$u_n^R(t, 0) = A^R t^{-\frac{1}{2}}, \quad (3.8)$$

where $A^R > 0$ and the total velocity u^R satisfies for all $t \geq 0$ and $x \geq 0$

$$u^R(t, x) = u_n^R(t, x) + u_w^R(t, x) = R^R u_n^R(t, 0) = R^R A^R t^{-\frac{1}{2}}. \quad (3.9)$$

The McWhorter and Sunada exact solution for positive value of the non-wetting phase influx velocity $u_n^R(t, 0)$ can be derived only for

$$\mathfrak{S}_0^R > \mathfrak{S}_i^R, \quad (3.10)$$

which is obvious from the duality of the formulation discussed in Section (1.6.1). If $\mathfrak{S}_0^R < \mathfrak{S}_i^R$, then the McWhorter and Sunada solution can be still obtained using the dual formulation (i.e. the non-wetting phase displacement), but the non-wetting phase velocity $u_n^R(t, 0)$ will be then negative.

LEFT DOMAIN PROBLEM

The non-wetting phase flows out of the domain Ω^L with velocity given by (3.8), while the wetting phase flows in with negative velocity which yields from (3.9)

$$u_w^R(t, 0) = A^R (R^R - 1) t^{-\frac{1}{2}}. \quad (3.11)$$

It was already discussed in Section 2.3.6 that the McWhorter and Sunada problem admits negative values of A and R . Preserving the formal formulation of the McWhorter and Sunada problem, the the following formulation is used in the domain Ω^L :

$$\mathfrak{S}_n(t, 0) = \mathfrak{S}_0^L \quad \text{for all } t > 0, \quad (3.12)$$

$$\mathfrak{S}_n(t, -\infty) = \mathfrak{S}_i^L \quad \text{for all } t > 0, \quad (3.13)$$

$$\mathfrak{S}_n(0, x) = \mathfrak{S}_i^L \quad \text{for all } x < 0. \quad (3.14)$$

The McWhorter and Sunada exact solution for the non-wetting phase displacement with negative value of A^L can be derived only for

$$\mathfrak{S}_0^L < \mathfrak{S}_i^L, \quad (3.15)$$

because the effective wetting phase saturation \mathfrak{S}_w is related to the effective non-wetting phase saturation \mathfrak{S}_n as $\mathfrak{S}_w = 1 - \mathfrak{S}_n$.

The influx wetting phase velocity in the non-wetting phase displacement problem is set as

$$u_w^L(t, 0) = A^L t^{-\frac{1}{2}}, \quad (3.16)$$

where $A^L < 0$. The total velocity in the domain Ω^L , defined as

$$u^L(t, x) = u_w^L(t, x) + u_n^L(t, x) = R^L u_w(t, 0) = R^L A^L t^{-\frac{1}{2}}, \quad (3.17)$$

must be equal to the total velocity in the domain Ω^R such that

$$u^R = u^L, \quad (3.18)$$

because the phase velocities are continuous across the interface (see (1.36)).

INTERFACE CONDITIONS

It is possible to state the three interface conditions that combine the McWhorter and Sunada exact solutions for the domains Ω^L and Ω^R .

Using the expressions (3.9), (3.17) and (3.18), the *first condition* can be expressed in the form

$$R^L A^L = R^R A^R, \quad (3.19)$$

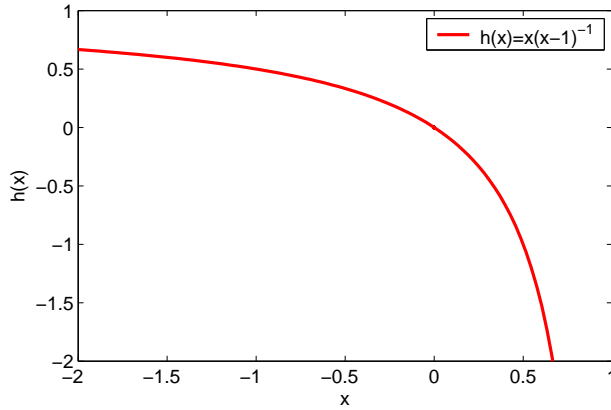
where the expressions on both sides of the equation are nonnegative.

The continuity of the wetting phase velocity u_w across the interface yields $u_w^L(t, 0) = u_w^R(t, 0)$, so that the *second condition* is obtained from (3.11) and (3.16)

$$A^L = A^R(R^R - 1), \quad (3.20)$$

It follows from (3.19) and (3.20) that

$$R^R = -\frac{R^L}{1 - R^L}, \quad (3.21)$$


 Figure 3.2: Function $h(x) = x(x - 1)^{-1}$.

or

$$R^L = -\frac{R^R}{1 - R^R}, \quad (3.22)$$

so that one of the parameters must be non-positive and the other one non-negative, see Figure 3.2 that depicts the function $h(x) = x(x - 1)^{-1}$.

The *third condition* is the *extended capillary pressure condition* that yields from (1.37) for the case of permeable interface

$$p_c^R(1 - \mathfrak{S}_0^R) = p_c^L(1 - \mathfrak{S}_0^L). \quad (3.23)$$

The relationship (3.23) is not always satisfied, particularly in the case of the Brooks and Corey capillary pressure function (1.26) with nonzero entry pressure. Therefore one can define the critical effective wetting phase saturation \mathfrak{S}_w^{*L} as

$$\mathfrak{S}_w^{*L} = \begin{cases} (p_c^L)^{-1}(p_c^R(1)) & \text{if } p_c^R(1) > p_c^L(1) \\ 1 & \text{else} \end{cases}. \quad (3.24)$$

The critical saturation $1 - \mathfrak{S}_w^{*L}$ expresses the boundary value for the left saturation \mathfrak{S}_0^L , for which it is possible to use the relationship (3.23) to obtain \mathfrak{S}_0^R , i.e.

$$\mathfrak{S}_i^L > \mathfrak{S}_0^L \geq 1 - \mathfrak{S}_w^{*L}, \quad (3.25)$$

where (3.15) is incorporated. If the value of \mathfrak{S}_0^L is lower than $1 - \mathfrak{S}_w^{*L}$, the non-wetting phase interfacial capillary pressure in Ω^L is smaller than the entry pressure $p_c^R(1)$ in the domain Ω^R and the non-wetting phase can not enter the right-hand side domain until the capillary pressure $p_c^L(1 - \mathfrak{S}_0)$ is large enough (the *barrier*

effect). This situation can not be incorporated in the exact solution derivation since a nonzero interfacial velocity of both phases is assumed for all $t \geq 0$.

Altogether, the inequalities (3.25) and (3.10) yield a limiting condition for the initial saturations \mathfrak{S}_i^R and \mathfrak{S}_i^L in the form

$$p_c^R(1 - \mathfrak{S}_i^R) < p_c^L(1 - \mathfrak{S}_i^L). \quad (3.26)$$

3.2.2 Algorithm

An algorithm is presented in this section, that incorporates the McWhorter and Sunada exact solution with the following input and output parameters and functions:

McWhorter and Sunada input and output variables		
Input:	\mathfrak{S}_0	effective saturation at $x = 0$
	\mathfrak{S}_i	effective initial saturation
	R	total velocity to displacing phase velocity ratio
Output:	F'	first derivative of F used to compute $\mathfrak{S}(t, x)$ in (2.56)
	A	positive velocity parameter

In order to satisfy the total velocity interface condition (3.19), various values of $\mathfrak{S}_0^L \in [1 - \mathfrak{S}_0^{*L}, \mathfrak{S}_i^L)$ are prescribed and the right domain boundary saturation \mathfrak{S}_0^R is computed from (3.23). However, the total velocity interface condition (3.19) can not be used in the algorithm for the zero total velocity case $R = 0$ because the condition is always true. Therefore, the relationship (3.21) is used and the total velocity interface condition is reformulated as

$$A^R = A^L(R^L - 1). \quad (3.27)$$

NON-WETTING PHASE INFILTRATION PROBLEM ALGORITHM

0. Let R^L be given. Let \mathfrak{S}_i^L and \mathfrak{S}_i^R be given such that the relationship (3.26) holds.
1. Choose some $\mathfrak{S}_0^L \in [1 - \mathfrak{S}_0^{*L}, \mathfrak{S}_i^L)$.
2. Compute the McWhorter and Sunada exact solution for the non-wetting phase displacement (the \mathfrak{S}_w formulation) with the setup parameters corresponding to the left-hand side domain and with

$$\mathfrak{S}_i := 1 - \mathfrak{S}_i^L, \quad (3.28)$$

$$\mathfrak{S}_0 := 1 - \mathfrak{S}_0^L, \quad (3.29)$$

$$R := R^L. \quad (3.30)$$

Set $A^L := -A$ and $F^L(\mathfrak{S}_n) := F'(1 - \mathfrak{S}_w)$.

3. Compute the right domain boundary saturation \mathfrak{S}_0^R from

$$p_c^L(1 - \mathfrak{S}_0^L) = p_c^R(1 - \mathfrak{S}_0^R).$$

4. Compute the McWhorter and Sunada exact solution for the wetting phase displacement (the \mathfrak{S}_n formulation) with the setup parameters corresponding to the right domain and with

$$\mathfrak{S}_i := \mathfrak{S}_i^R, \quad (3.31)$$

$$\mathfrak{S}_0 := \mathfrak{S}_0^R, \quad (3.32)$$

$$R := -\frac{R^L}{1 - R^L} = R^R. \quad (3.33)$$

Set $A^R := A$ and $F^R(\mathfrak{S}_n) := F'(\mathfrak{S}_n)$.

5. If the total velocity interface condition (3.27) holds or the estimates of A^R and $A^L(R^L - 1)$ are below some bound ε_u

$$|A^R - A^L(R^L - 1)| < \varepsilon_u,$$

terminate the algorithm, otherwise skip back to step 1.

The author suggests to use the bisection method in the step 1. The dependence

$$\kappa(\mathfrak{S}_0^L) = A^R - A^L(R^L - 1) \quad (3.34)$$

is strictly monotonous as a consequence of the monotonicity of the dependence $A = A(\mathfrak{S}_0)$, see the illustration in Section 3.4, Figure 3.4.

However, in some particular cases, the value of \mathfrak{S}_0^L such that $\kappa(\mathfrak{S}_0^L) = 0$ does not exist due to small values of A in one of the subdomains for all admissible \mathfrak{S}_0 . This issue can not be analytically resolved, only experimental observations are currently available.

The solution of the two-phase flow in heterogeneous medium problem (3.3) and (3.4) is subsequently obtained from

$$\frac{2A^R(1 - R^R f_n^R(1 - \mathbb{S}_i^R))}{\Phi^R \mathfrak{S}^R} F'^R(\mathbb{S}_n) = x t^{-\frac{1}{2}} \quad \text{for all } \mathbb{S}_n \in [\mathbb{S}_i^R, \mathbb{S}_0^R], \quad (3.35)$$

$$\frac{2A^L(1 - R^L f_w^L(1 - \mathbb{S}_i^L))}{\Phi^L \mathfrak{S}^L} F'^L(\mathbb{S}_n) = x t^{-\frac{1}{2}} \quad \text{for all } \mathbb{S}_n \in [\mathbb{S}_0^L, \mathbb{S}_i^L]. \quad (3.36)$$

3.3 Wetting Phase Influx Problem

The exact solution for the wetting phase influx problem can be derived using the analogous procedure as in the Section 3.2. It can be done by switching the non-wetting phase variables for the wetting-phase variables and vice versa and the \mathbb{S}_w -formulation instead of the \mathbb{S}_n -formulation is used.

The wetting phase influx problem is defined as the injection of the wetting phase in the positive direction along the x axis with non-negative total velocity u defined by (2.28) as $u = u_n + u_w$. Therefore assume $u_w(t, x) \geq 0$ for all $t \geq 0$ and $x \in (-\infty, \infty)$.

The derivation of the exact solution that have been already done for the non-wetting phase intrusion problem is briefly repeated in the following text.

3.3.1 Exact Solution

PROBLEM EQUATIONS

The equations (3.3) and (3.4) are transformed into

$$\Phi^R \mathfrak{S}^R \frac{\partial \mathbb{S}_w}{\partial t} = -u^R \frac{\partial f_w^R(\mathbb{S}_w)}{\partial x} + \frac{\partial}{\partial x} \left(D^R(\mathbb{S}_w) \frac{\partial \mathbb{S}_w}{\partial x} \right), \quad (3.37)$$

$$\Phi^L \mathfrak{S}^L \frac{\partial \mathbb{S}_w}{\partial t} = -u^L \frac{\partial f_w^L(\mathbb{S}_w)}{\partial x} + \frac{\partial}{\partial x} \left(D^L(\mathbb{S}_w) \frac{\partial \mathbb{S}_w}{\partial x} \right). \quad (3.38)$$

RIGHT DOMAIN PROBLEM

Consider wetting phase influx problem (the non-wetting phase displacement) in the domain Ω^R with boundary and initial conditions given by

$$\mathfrak{S}_w(t, 0) = \mathfrak{S}_0^R \quad \text{for all } t > 0, \quad (3.39)$$

$$\mathfrak{S}_w(t, \infty) = \mathfrak{S}_i^R \quad \text{for all } t > 0, \quad (3.40)$$

$$\mathfrak{S}_w(0, x) = \mathfrak{S}_i^R \quad \text{for all } x > 0, \quad (3.41)$$

where

$$\mathfrak{S}_0^R > \mathfrak{S}_i^R. \quad (3.42)$$

The wetting phase velocity is given by

$$u_w^R(t, 0) = A^R t^{-\frac{1}{2}}, \quad (3.43)$$

where $A^R > 0$ and the total velocity u^R satisfies for all $t \geq 0$ and $x \geq 0$

$$u^R(t, x) = u_n^R(t, x) + u_w^R(t, x) = R^R u_w^R(t, 0) = R^R A^R t^{-\frac{1}{2}}, \quad (3.44)$$

where $R^R \in [0, 1]$.

LEFT DOMAIN PROBLEM

The wetting phase flows out of the domain Ω^L with the velocity given by (3.43), while the non-wetting phase flows in with the negative velocity which yields from (3.44)

$$u_n^R(t, 0) = A^R (R^R - 1) t^{-\frac{1}{2}}. \quad (3.45)$$

The wetting phase displacement problem in the domain Ω^L is defined as follows

$$\mathfrak{S}_w(t, 0) = \mathfrak{S}_0^L \quad \text{for all } t > 0, \quad (3.46)$$

$$\mathfrak{S}_w(t, -\infty) = \mathfrak{S}_i^L \quad \text{for all } t > 0, \quad (3.47)$$

$$\mathfrak{S}_w(0, x) = \mathfrak{S}_i^L \quad \text{for all } x < 0, \quad (3.48)$$

where

$$\mathfrak{S}_0^L < \mathfrak{S}_i^L. \quad (3.49)$$

The influx non-wetting phase velocity in the wetting phase displacement is set as

$$u_n^L(t, 0) = A^L t^{-\frac{1}{2}}, \quad (3.50)$$

where $A^L < 0$. The total velocity in the domain Ω^L , defined as

$$u^L(t, x) = u_w^L(t, x) + u_n^L(t, x) = R^L u_n(t, 0) = R^L A^L t^{-\frac{1}{2}}, \quad (3.51)$$

must be equal to the total velocity in the domain Ω^R such that

$$u^R = u^L. \quad (3.52)$$

INTERFACE CONDITIONS

Again, it follows from (3.19) and (3.20) that

$$R^R = -\frac{R^L}{R^L - 1}, \quad (3.53)$$

or

$$R^L = -\frac{R^R}{R^R - 1}, \quad (3.54)$$

In this formulation, the *extended capillary pressure condition* (1.37), resp. (3.23) has the form

$$p_c^R(\mathbb{S}_0^R) = p_c^L(\mathbb{S}_0^L). \quad (3.55)$$

3.3.2 Admissible Range of Parameters

The inequalities (3.25) are transformed into

$$\mathbb{S}_w^{*L} \geq \mathbb{S}_0^L, \quad (3.56)$$

and together with the inequality (3.49) the limit condition for \mathbb{S}_0^L is obtained in the form

$$0 \leq \mathbb{S}_0^L < \mathbb{S}_{0min}^L = \min\{\mathbb{S}_w^{*L}, \mathbb{S}_i^L\}. \quad (3.57)$$

Altogether, the inequalities (3.56) and (3.42) yield boundary condition for the initial saturations \mathbb{S}_i^R and \mathbb{S}_i^L in the form (compare to (3.26))

$$p_c^R(\mathbb{S}_i^R) > p_c^L(\mathbb{S}_i^L). \quad (3.58)$$

3.3.3 Algorithm

In order to satisfy the total velocity interface condition (3.19), various values of $\mathbb{S}_0^L \in [0, \mathbb{S}_{0min}^L)$ are prescribed and the right domain boundary saturation \mathbb{S}_0^R is computed from (3.55).

WETTING PHASE INFLUX PROBLEM ALGORITHM

3.3. WETTING PHASE INFLUX PROBLEM

0. Let R^L be given. Let \mathfrak{S}_i^L and \mathfrak{S}_i^R be given such that the relationship (3.58) holds.

1. Choose some $\mathfrak{S}_0^L \in [0, \mathfrak{S}_{0min}^L)$.
2. Compute the McWhorter and Sunada exact solution for the wetting phase displacement with the setup parameters corresponding to the left domain and with

$$\mathfrak{S}_i := 1 - \mathfrak{S}_i^L, \quad (3.59)$$

$$\mathfrak{S}_0 := 1 - \mathfrak{S}_0^L, \quad (3.60)$$

$$R := R^L. \quad (3.61)$$

$$(3.62)$$

Set $A^L := -A$ and $F^L(\mathfrak{S}_w) := F'(1 - \mathfrak{S}_w)$.

3. Compute the right domain boundary saturation \mathfrak{S}_0^R from

$$p_c^L(\mathfrak{S}_0^L) = p_c^R(\mathfrak{S}_0^R).$$

4. Compute the McWhorter and Sunada exact solution for the non-wetting phase displacement with the setup parameters corresponding to the right domain and with

$$\mathfrak{S}_i := \mathfrak{S}_i^R, \quad (3.63)$$

$$\mathfrak{S}_0 := \mathfrak{S}_0^R, \quad (3.64)$$

$$R := -\frac{R^L}{R^L - 1} = R^R. \quad (3.65)$$

$$(3.66)$$

Set $A^R := A$ and $F^R(\mathfrak{S}_w) := F'(\mathfrak{S}_w)$.

5. If the total velocity interface condition (3.27) holds or the estimates of A^R and $A^L(1 + R^L)$ are below some bound ε_u

$$|A^R - A^L (R^L - 1)| < \varepsilon_u,$$

terminate the algorithm, otherwise skip back to 1..

The solution of the two-phase flow in heterogeneous medium problem (3.37) and (3.38) is subsequently obtained from

$$\frac{2A^R(1 - R^R f_w^R(\mathbb{S}_i^R))}{\Phi^R \vartheta^R} F'^R(\mathbb{S}_w) = x t^{-\frac{1}{2}} \quad \text{for all } \mathbb{S}_w \in [\mathbb{S}_i^R, \mathbb{S}_0^R], \quad (3.67)$$

$$\frac{2A^L(1 - R^L f_n^L(\mathbb{S}_i^L))}{\Phi^L \vartheta^L} F'^L(\mathbb{S}_w) = x t^{-\frac{1}{2}} \quad \text{for all } \mathbb{S}_w \in [\mathbb{S}_0^L, \mathbb{S}_i^L]. \quad (3.68)$$

3.4 Illustrative Calculations

3.4.1 Model Parameters

The unrealistic sands in Table 3.1 are used in this subsection to demonstrate applicability of the exact solution to a heterogeneous porous medium. The non-wetting phase intrusion problem discussed in Section 3.2 is studied.

	Par.	Units	fine sand (FS)	coarse sand (CS)
Porosity	Φ	[-]	0.38	0.40
Intrinsic Permeability	K	$[m^2]$	10^{-11}	10^{-10}
Residual Water Sat.	S_{wr}	[-]	0.10	0.08
Residual NAPL Sat.	S_{nr}	[-]	0	0
Water Viscosity	μ_w	$[kg\ m^{-1}\ s^{-1}]$	0.001	0.001
DNAPL Viscosity	μ_n	$[kg\ m^{-1}\ s^{-1}]$	0.001	0.001
Brooks-Corey	P_d	$[Pa]$	1000	900
	λ	[-]	3.86	3.86
van Genuchten	$\frac{1}{\alpha}$	$[Pa]$	1500	800
	m	[-]	0.60	0.40

Table 3.1: Parameter setup for two unrealistic porous materials - coarse and fine sands.

Different initial saturations \mathbb{S}_i^R and \mathbb{S}_i^L are distinguished in the two subdomains. Various values of $R^L \in [-10000, 1]$ are prescribed and the boundary value R_{min}^L is experimentally determined for the case of the algorithm failure due to absence of the intersection point of the curves $A^R(\mathbb{S}_0)$ and $(R^L - 1)A^L(\mathbb{S}_0)$ as in Figure 3.4. It shows the values of A^R and $A^L (R^L - 1)$ depending on \mathbb{S}_0^L for the maximal initial saturations setup (i.e. $\mathbb{S}_i^L = 1$ and $\mathbb{S}_i^R = 0$). If the intersection of the two curves is realized at \mathbb{S}_0^L , then $\kappa(\mathbb{S}_0^L) = 0$ and then the algorithm terminates successfully.

Figure 3.5 depicts the admissible range of initial saturations that can be prescribed for the heterogeneous exact solution. Each point of the filled area of the

(S_i^L, S_i^R) -plane represents possible setup for the problem. The bisection method is used to arrive at intersection of the $A^L(R^L - 1)$ and A^R curves in the step 1. of the algorithm (see Figure 3.4).

The capillary pressure-effective saturation curves corresponding to the values in Table 3.1 are depicted in Figure 3.3. The van Genuchten model functions are selected such that the capillary pressure are intersected. Consequently, the saturation jumps across the interface differs using the van Genuchten and Brooks-Corey model respectively. The exact solutions for various setup parameters R^L , S_i^R and S_i^L are depicted in Figures 3.6, 3.7, 3.8 and 3.9. All solutions are at time $t = 1000$ s and are obtained by using the modified iterative method variant A (2.72) with $\varepsilon_A = 10^{-15}$.

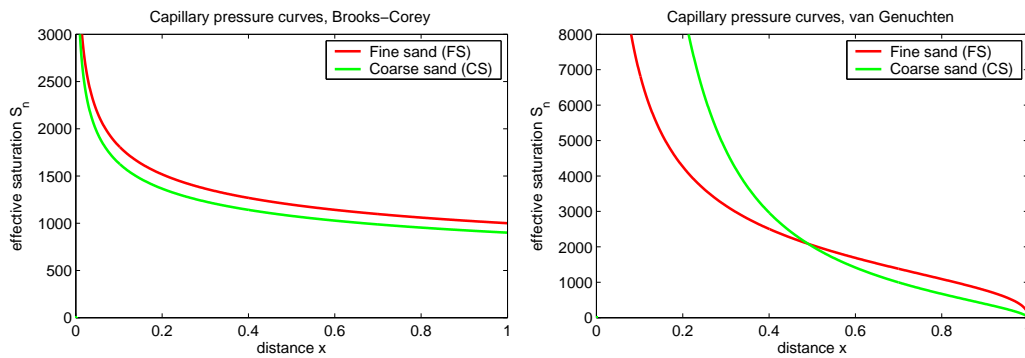


Figure 3.3: Capillary pressure curves for van Genuchten and Brooks-Corey model functions.

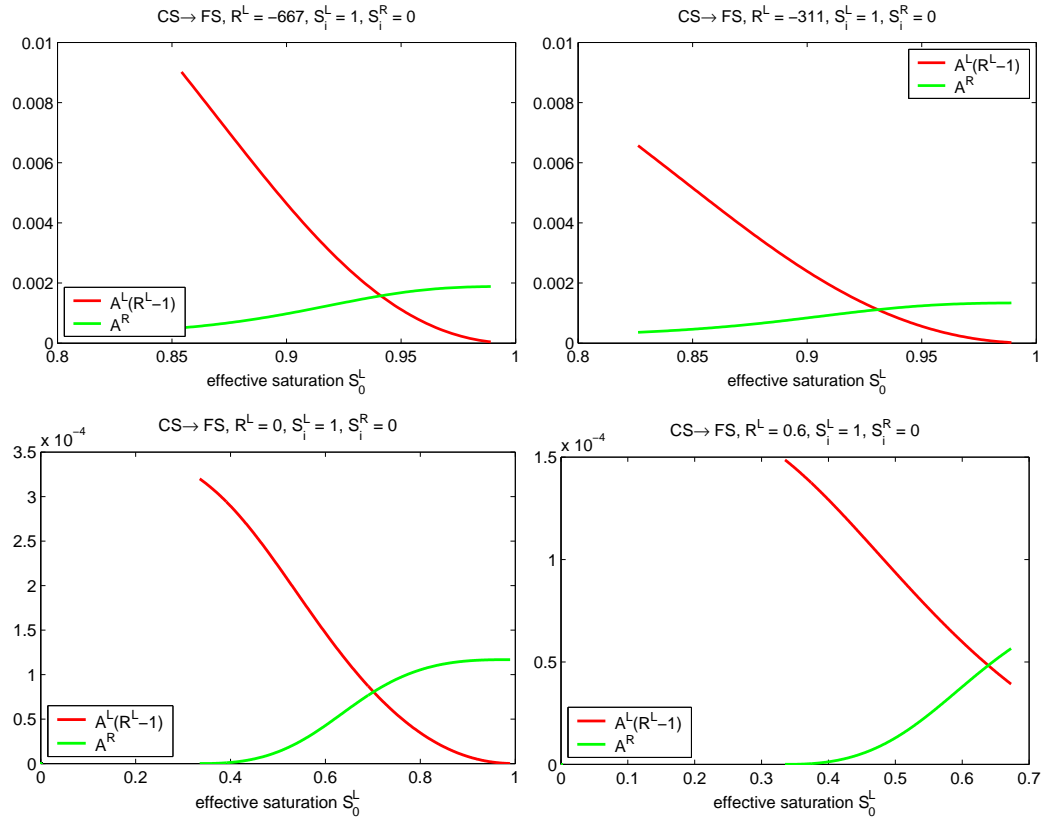


Figure 3.4: Values of A^R and $A^L(R^L - 1)$ depending on $S_0^L \in [1 - S_0^{*L}, S_i^L]$.

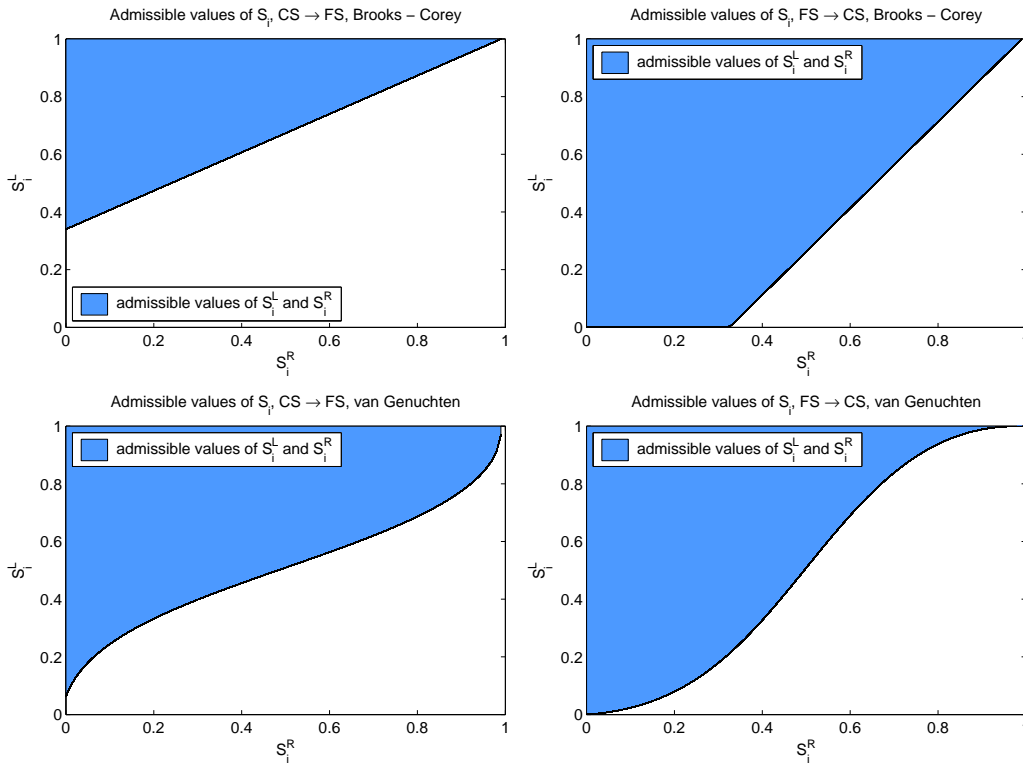


Figure 3.5: Admissible values of S_i^L and S_i^R in the (S_i^L, S_i^R) -plane that satisfy the condition (3.26) are delimited by the filled area. The Brooks and Corey model functions are depicted in upper figures and the van Genuchten model functions in the lower figures. The left-hand side figures correspond to the flow from the coarse sand (CS) to the fine sand (FS) and vice versa for the right-hand side figures.

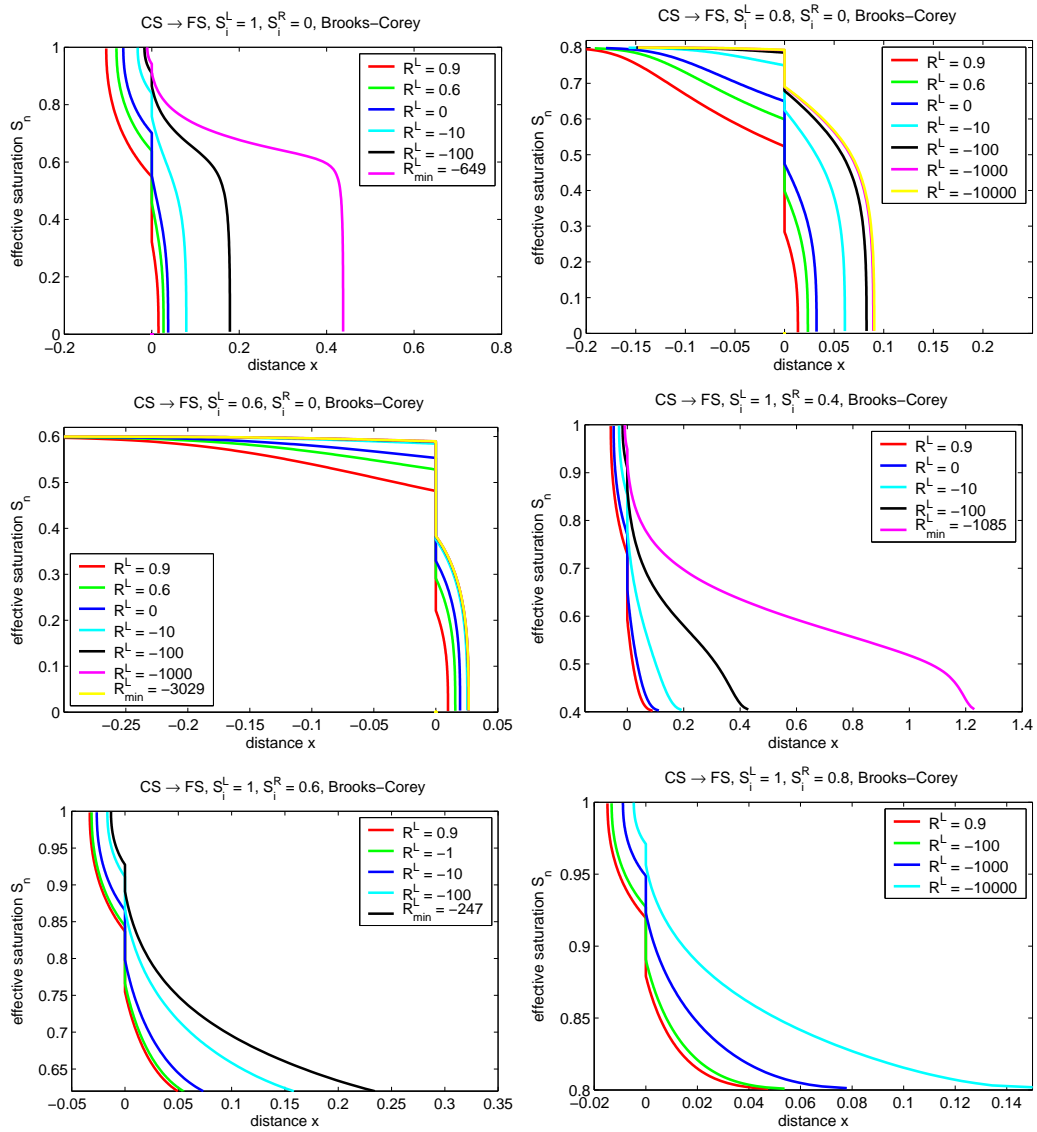


Figure 3.6: Exact solutions for a medium with a discontinuity for various R^L and initial setups at time $t = 1000$ s, Brooks-Corey model functions. The DNAPL flows from the coarse sand (CS) placed at $x < 0$ to the fine sand (FS) placed at $x > 0$.

3.4. ILLUSTRATIVE CALCULATIONS

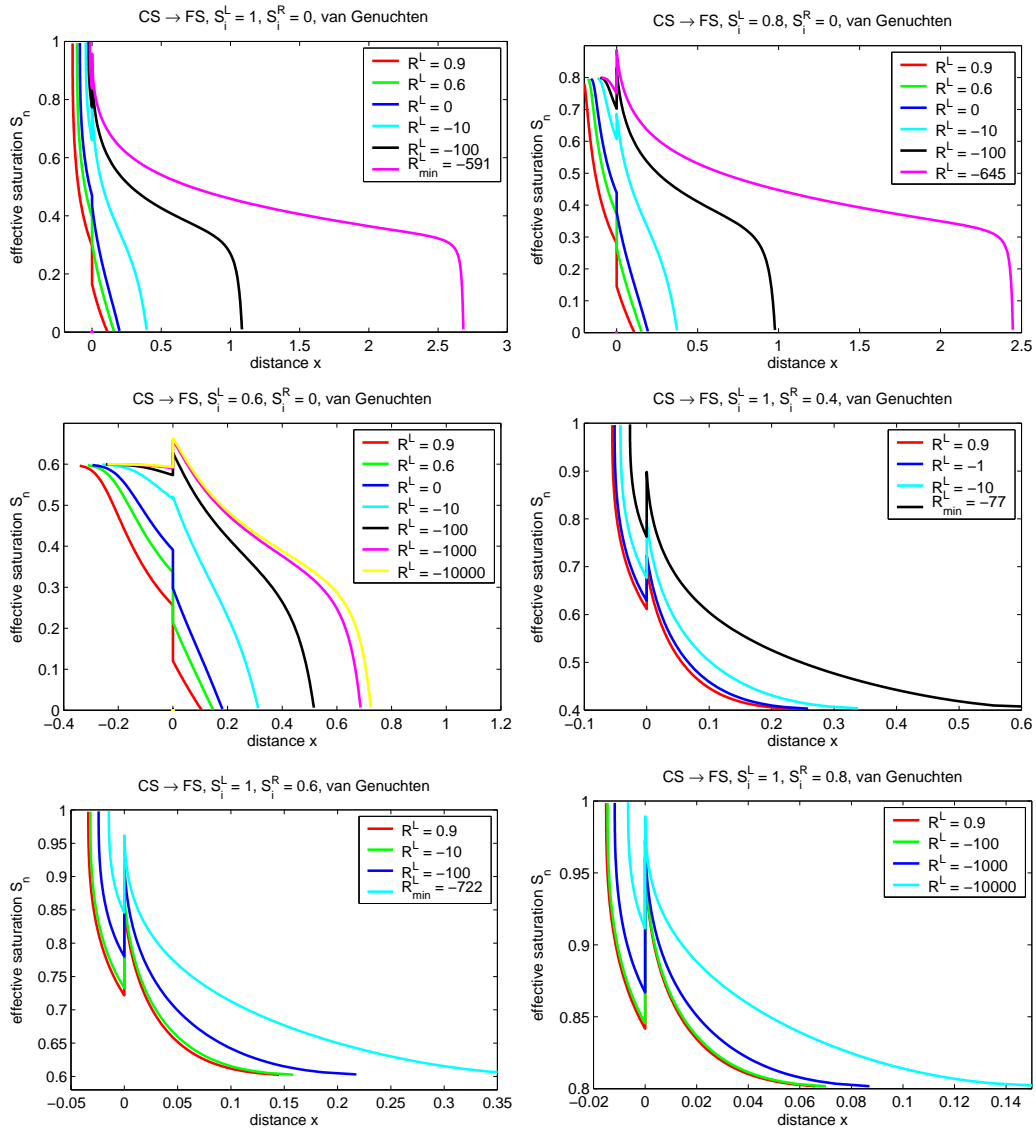


Figure 3.7: Exact solutions for a medium with a discontinuity for various R^L and initial setups at time $t = 1000$ s, van Genuchten model functions. The DNAPL flows from the coarse sand (CS) placed at $x < 0$ to the fine sand (FS) placed at $x > 0$.

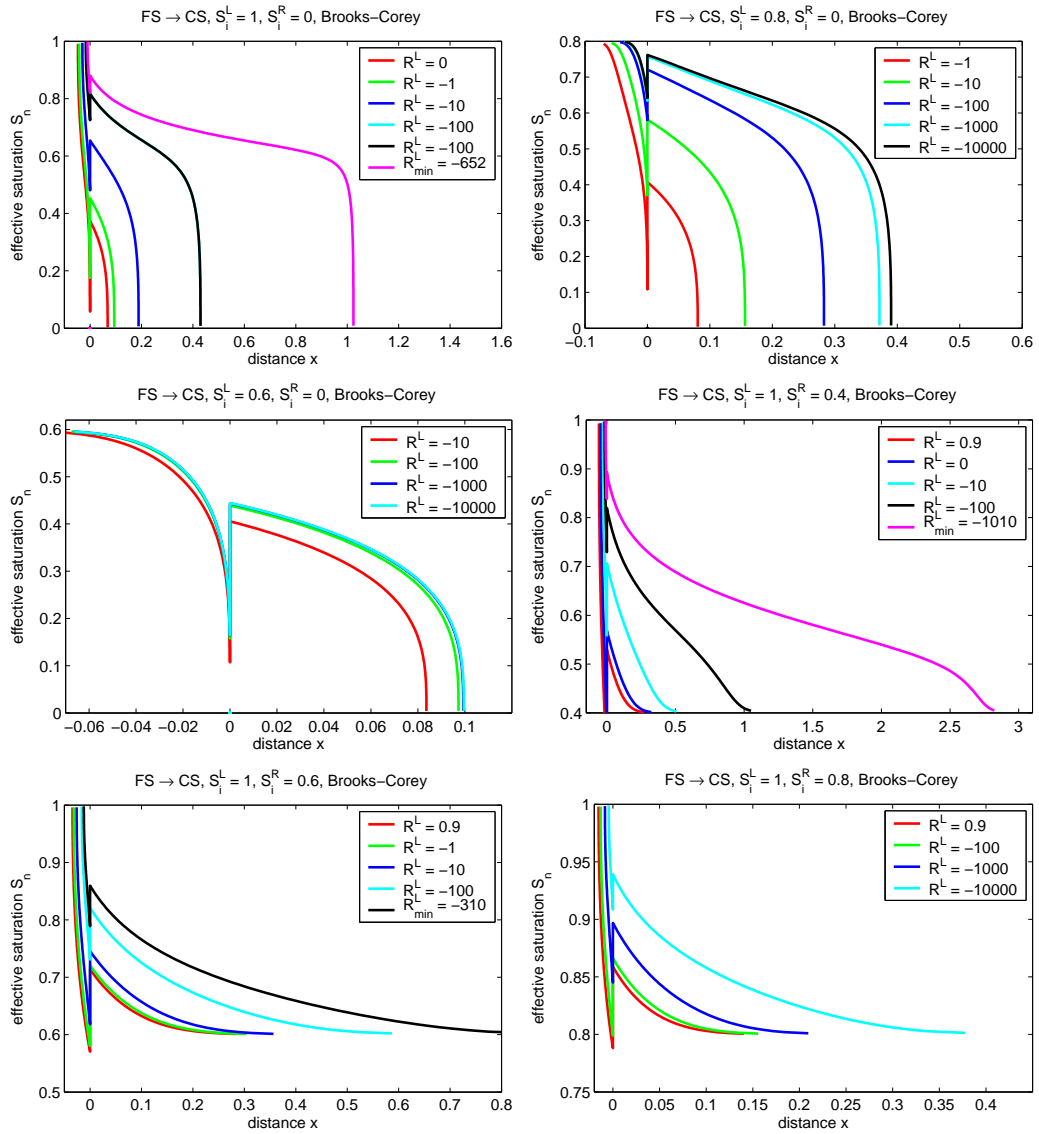


Figure 3.8: Exact solutions for a medium with a discontinuity for various R^L and initial setups at time $t = 1000$ s, Brooks-Corey model functions. The DNAPL flows from the fine sand (FS) placed at $x < 0$ to the coarse sand (CS) placed at $x > 0$.

3.4. ILLUSTRATIVE CALCULATIONS

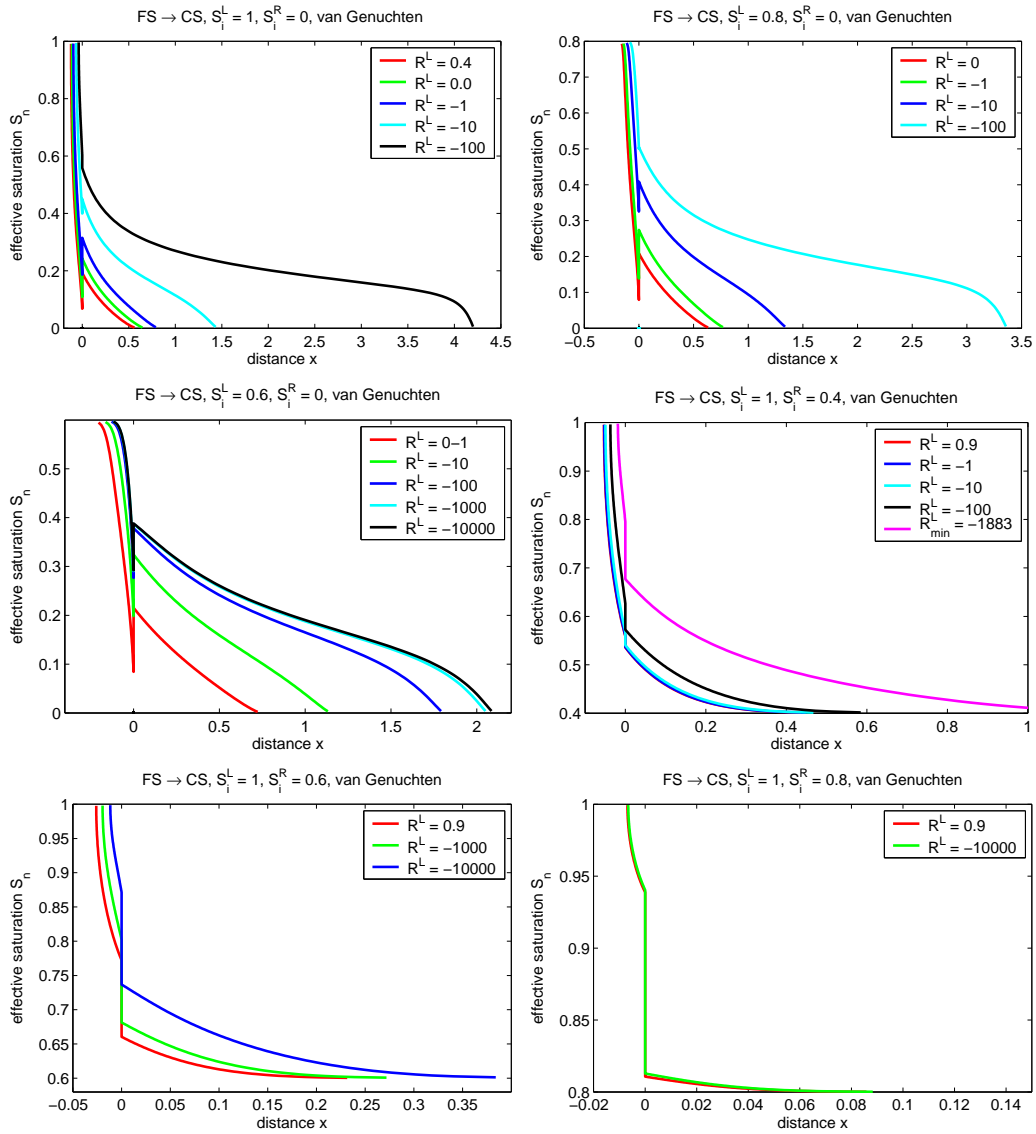


Figure 3.9: Exact solutions for a medium with a discontinuity for various R^L and initial setups at time $t = 1000$ s, van Genuchten model functions. The DNAPL flows from the fine sand (FS) placed at $x < 0$ to the coarse sand (CS) placed at $x > 0$.

3.4.2 Materials and Fluids with Significant Saturation Jumps across Interface

Realistic materials described in Das *et al.*, 2004 are used to compute exact solutions of a PCE contamination problem. The flow of the non-wetting phase from the fine sand to the coarse sand (FS \rightarrow CS) can not be obtained using the presented formulation. This is due to very large jumps in the saturations across the interface so that equation (3.19) does not admit any solution for none of the value of $R^L \in (-\infty, 1)$ and none of the wide range of possible initial saturations setups \mathbb{S}_i^R and \mathbb{S}_i^L . Refer to the left-hand part of Figure 3.10, where the white area corresponds to the admissible values of \mathbb{S}_i^R and \mathbb{S}_i^L for the fine sand to coarse sand flow.

On the other hand, the inverse placement of the porous media (CS \rightarrow FS) admits a solution for a very small range of initial saturations (the filled area of the left-hand part of Figure 3.10, inverse to the previous FS \rightarrow CS case). The exact solutions are depicted in the right-hand part of the Figure 3.10. The interfacial saturation \mathbb{S}_0^L is in near the maximal non-wetting saturation for all parameters R^L , again due to large jumps in the capillary pressure curves.

	Par.	Units	fine sand (FS)	coarse sand (CS)
Porosity	Φ	$[-]$	0.40	0.40
Intrinsic Permeability	K	$[m^2]$	$5 \cdot 10^{-12}$	10^{-9}
Residual Water Sat.	S_{wr}	$[-]$	0.098	0.078
Residual NAPL Sat.	S_{nr}	$[-]$	0	0
Water Viscosity	μ_w	$[kg\ m^{-1}s^{-1}]$	0.001	0.001
DNAPL Viscosity	μ_n	$[kg\ m^{-1}s^{-1}]$	0.0009	0.0009
Brooks-Corey	P_d	$[Pa]$	1325	370
	λ	$[-]$	2.49	2.86

Table 3.2: Parameter setup for two unrealistic porous materials - coarse and fine sands.

3.4. ILLUSTRATIVE CALCULATIONS

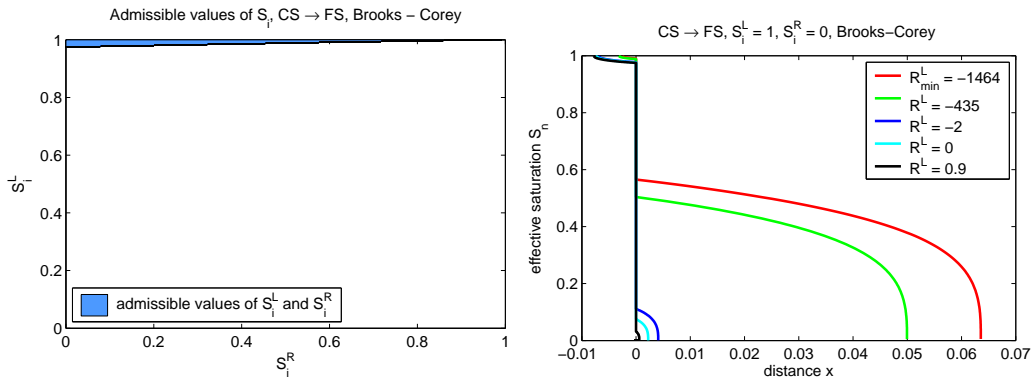


Figure 3.10: Exact solutions for the Brooks-Corey model functions at time $t = 1000$ s for various R^L .

3.4.3 Realistic Materials and Fluids

Realistic sands described in Walser *et al.*, 1999 and the DNAPL Soltrol 220 described in Chao *et al.*, 2000 are used. In this case, the exact solution can be obtained for both material compositions.

The ranges of admissible initial saturations are depicted in Figure 3.11 and the solutions for both flows from the coarse to fine sand and reversely are depicted in Figure 3.12.

	Par.	Units	fine sand (FS)	coarse sand (CS)
Porosity	Φ	$[-]$	0.40	0.40
Intrinsic Permeability	K	$[m^2]$	$5 \cdot 10^{-10}$	10^{-9}
Residual Water Sat.	S_{wr}	$[-]$	0.01	0.08
Residual NAPL Sat.	S_{nr}	$[-]$	0	0
Water Viscosity	μ_w	$[kg\ m^{-1}\ s^{-1}]$	0.001	0.001
DNAPL Viscosity	μ_n	$[kg\ m^{-1}\ s^{-1}]$	0.0035	0.0035
Brooks-Corey	P_d	$[Pa]$	1207	828
	λ	$[-]$	1.6	7.4

Table 3.3: Parameter setup for two realistic porous materials - coarse and fine sands.

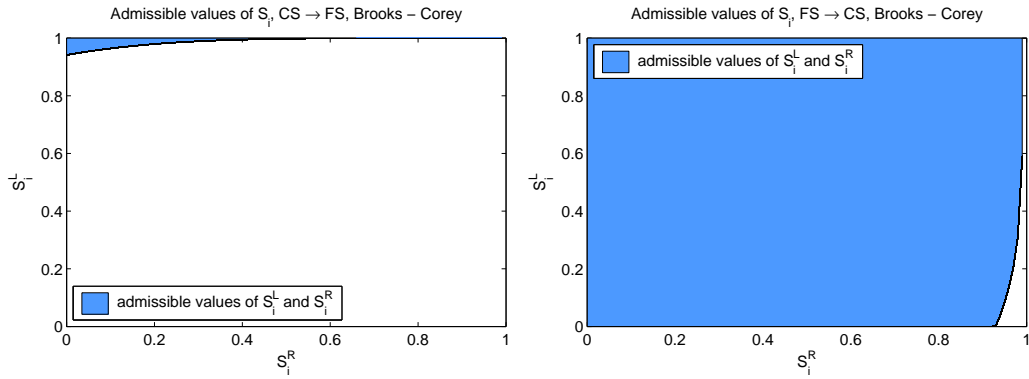


Figure 3.11: Admissible values of S_i^L and S_i^R in the (S_i^L, S_i^R) -plane that satisfy the condition (3.26) are delimited by the filled area, the Brooks and Corey model functions .

3.4. ILLUSTRATIVE CALCULATIONS

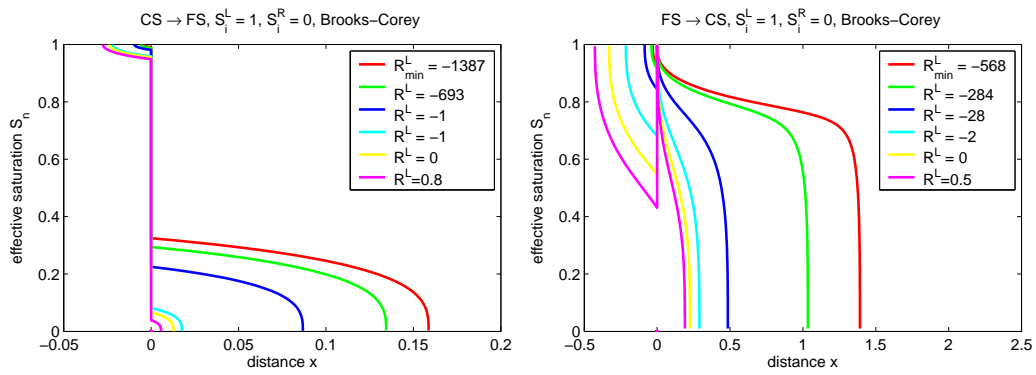


Figure 3.12: Exact solutions for the Brooks-Corey model functions at time $t = 1000$ s for various R^L .

Chapter 4

One-dimensional Numerical Methods

4.1 Two-Phase Flow Equation

The McWhorter and Sunada exact solution described in the previous chapter has to be solved numerically anyway. This fact motivates us to propose another straight method of obtaining the solution of the one-dimensional problem

$$\vartheta\Phi \frac{\partial \mathcal{S}}{\partial t} = -u(t) \frac{\partial f(\mathcal{S})}{\partial x} + \frac{\partial}{\partial x} \left(D(\mathcal{S}) \frac{\partial \mathcal{S}}{\partial x} \right), \quad (4.1)$$

where boundary and initial conditions will be discussed later.

Explicit numerical schemes based on the finite-difference method discretizing the spatial derivatives are used with subsequent solution of the ODE system by Runge-Kutta methods. It is also possible to use more complex and accurate numerical methods as well as implicit methods for solving the equation (4.1), but the objective is to demonstrate the applicability and existence of the exact solution using the simple numerical methods that have been already described in the literature, e.g. in Helmig, 1997 or Bastian, 1999.

GENERALIZED FLOW EQUATION

In order to demonstrate applicability of the numerical method in solving the one-dimensional heterogeneous medium problem discussed in Helmig, 1997, it is necessary to incorporate gravitational effects into the equation. Combining the equations (1.54) to (1.58), the one-dimensional two phase flow equation can be obtained in the form

$$\vartheta\Phi \frac{\partial \mathcal{S}}{\partial t} = -u(t) \frac{\partial f(\mathcal{S})}{\partial x} + \frac{\partial}{\partial x} \left(D(\mathcal{S}) \frac{\partial \mathcal{S}}{\partial x} + G(\mathcal{S}) \right), \quad (4.2)$$

where the term $G(\mathbf{S})$ incorporates the effect of the gravitational force in the equation either in the form

$$G(\mathbf{S}_w) = K(\rho_n - \rho_w) \frac{\lambda_w(\mathbf{S}_w)\lambda_n(\mathbf{S}_w)}{\lambda_w(\mathbf{S}_w) + \lambda_n(\mathbf{S}_w)} g, \quad (4.3)$$

for the wetting phase saturation formulation, or in the form

$$G(\mathbf{S}_n) = K(\rho_w - \rho_n) \frac{\lambda_w(1 - \mathbf{S}_n)\lambda_n(1 - \mathbf{S}_n)}{\lambda_w(1 - \mathbf{S}_w) + \lambda_n(1 - \mathbf{S}_n)} g, \quad (4.4)$$

for the non-wetting phase saturation formulation.

4.1.1 Spatial Discretization

The following spatial discretization of the equation (4.2) is used. Let h be given size of a uniform grid mesh Ω_h with $I + 1$ nodes that is a subset of the interval $[0, \infty)$

$$\Omega_h = \{ih : 0 \leq i \leq I\} \subset [0, \infty), \quad (4.5)$$

and let L be length of the one-dimensional domain such that $L = Ih$.

Suppose the discrete function $s = s_j(t) = \mathbf{S}(t, jh)$, which is the pointwise projection of the solution approximation on the mesh Ω_h at a given time t .

The semi-discretized flow equation (4.2) can be written in the form

$$\vartheta\Phi \frac{ds_j(t)}{dt} = - \frac{u_{dp\ j+\frac{1}{2}}(t) - u_{dp\ j-\frac{1}{2}}(t)}{h}, \quad (4.6)$$

for all $j \in \{0, 1, 2, \dots, I\}$.

The discrete velocities are computed from (1.65) as

$$u_{dp\ j+\frac{1}{2}} = f(s_*) u(t) - D_{j+\frac{1}{2}} - G(s_*), \quad (4.7)$$

for all $j \in \{0, 1, 2, \dots, I-1\}$, where the variable s_* is the upwinded saturation w.r.t. u (see Helmig, 1997) defined as follows:

$$\text{upwinded discretization: } s_* = \begin{cases} s_j & \text{if } u > 0 \\ \frac{s_{j+1} + s_j}{2} & \text{if } u = 0 \\ s_{j+1} & \text{if } u < 0 \end{cases} .$$

The term $D_{j+\frac{1}{2}}$ has to be specified separately both for the wetting and non-wetting phase saturation formulation.

WETTING PHASE SATURATION FORMULATION

According to Section 2.1, the equation (4.2) can be used for the non-wetting phase displacement problem using the following substitution

$$\mathbb{S} \equiv \mathbb{S}_w, \quad (4.8)$$

$$f(\mathbb{S}) = f(\mathbb{S}_w) = f_w(\mathbb{S}_w), \quad (4.9)$$

$$D(\mathbb{S}) = \mathfrak{D}(\mathbb{S}_w), \quad (4.10)$$

together with the definition (4.3) for the gravitational term $G(\mathbb{S})$.

The term $D_{j+\frac{1}{2}}$ reads as

$$D_{j+\frac{1}{2}} = K \frac{\lambda_w(s_*)\lambda_n(s_*)}{\lambda_w(s_*) + \lambda_n(s_*)} \frac{p_c(s_{j+1}) - p_c(s_j)}{h}. \quad (4.11)$$

WETTING PHASE DISPLACEMENT

In the opposite situation, the substitution is in the form

$$\mathbb{S} \equiv \mathbb{S}_n, \quad (4.12)$$

$$f(\mathbb{S}) = f(\mathbb{S}_n) = f_w(1 - \mathbb{S}_n), \quad (4.13)$$

$$D(\mathbb{S}) = \mathfrak{D}(1 - \mathbb{S}_n), \quad (4.14)$$

together with the definition (4.4) for the gravitational term $G(\mathbb{S})$.

The term $D_{j+\frac{1}{2}}$ stands for

$$D_{j+\frac{1}{2}} = -K \frac{\lambda_w(1 - s_*)\lambda_n(1 - s_*)}{\lambda_w(1 - s_*) + \lambda_n(1 - s_*)} \frac{p_c(1 - s_{j+1}) - p_c(1 - s_j)}{h}. \quad (4.15)$$

4.1.2 Initial and Boundary Conditions

It is possible to prescribe either Dirichlet boundary conditions at $x = 0$ or $x = L$, or the flux of the displacing (or displaced) phase at $x = 0$ or $x = L$. If the flux condition is provided at a boundary, e.g. at $x = 0$, the respective discretized velocity, e.g. $u_{dp -\frac{1}{2}}(t)$ equals directly to the prescribed velocity. The form of the discretized equation (4.6) does not require the knowledge of the value $s_0(t)$ in such cases. On the other hand, there is no need to compute the discretized velocity $u_{dp -\frac{1}{2}}(t)$, resp. $u_{dp m+\frac{1}{2}}(t)$, if the Dirichlet boundary condition is prescribed at the boundary at $x = 0$, resp. $x = L$.

The initial condition for the discretized function s is obtained using the point-wise projection of the initial state of the saturation $\mathbb{S}(0, x)$ in the domain $[0, \infty)$ on the discrete subset Ω_h , i.e.

$$s_j(0) = \mathbb{S}(0, hj) \quad \text{for all } j = 0, 1, \dots, I.$$

4.1.3 Runge-Kutta Methods for System of ODE

The semi-discretized system of the equations (4.6)

$$\frac{ds_j(t)}{dt} = -\frac{u_{dp\ j+\frac{1}{2}}(t) - u_{dp\ j-\frac{1}{2}}(t)}{h} \quad \text{for all } j \in \{0, 1, 2, \dots, m\}, \quad (4.16)$$

$$(4.17)$$

represents a system of ordinary differential equations with the respective initial and boundary conditions.

Describing this system formally as

$$s'(t) = Z(t, s(t)), \quad (4.18)$$

$$s(0) = \sigma_0, \quad (4.19)$$

where σ_0 is the initial saturation distribution vector, the Runge-Kutta numerical methods for a system of ODE can be applied, see Vitásek, 1994. The time quantity is discretized as $t = k\tau$ for $k = 0, 1, 2, \dots$ so that the vector $s(t)$ is discretized to $s^k = s(k\tau)$.

RK1 - EULER METHOD

The first order Runge-Kutta method, the *Euler method* (denoted as RK1) is exactly the explicit form of the finite difference method. This explicit numerical scheme reads

$$s^{k+1} = s^k + \tau Z(k\tau, s^k). \quad (4.20)$$

RK4 - STANDARD RUNGE-KUTTA METHOD

The fourth order Runge-Kutta method, commonly referred to as the *standard Runge-Kutta method* (denoted as RK4) is represented by the following system of equations :

$$s^{k+1} = s^k + \frac{\tau}{6}(\kappa_1 + 2\kappa_2 + 2\kappa_3 + \kappa_4), \quad (4.21)$$

$$\kappa_1 = Z(k\tau, s^k), \quad (4.22)$$

$$\kappa_2 = Z\left(k\tau + \frac{1}{2}\tau, s^k + \frac{1}{2}\tau\kappa_1\right), \quad (4.23)$$

$$\kappa_3 = Z\left(k\tau + \frac{1}{2}\tau, s^k + \frac{1}{2}\tau\kappa_2\right), \quad (4.24)$$

$$\kappa_4 = Z(k\tau + \tau, s^k + \tau\kappa_3). \quad (4.25)$$

4.1.4 Interface Implementation

In this subsection, the interface implementation is presented for the case of the wetting phase displacing problem, i.e. \mathcal{S}_n -formulation with $u_{dp} \equiv u_n$.

At the interface of two porous homogeneous media, the conditions (1.37) and (1.36) are used in the following way. Assume the interface is placed between the nodes j and $j + 1$ as it is depicted in Figure 4.1. Numerical implementation of the interface conditions (1.37) and (1.36) is provided by replacing $u_{n, j+\frac{1}{2}}$ in (4.6) by the interfacial phase velocity $u_{n, j+\frac{1}{2}}^{k, int}$. Since the total velocity is constant in space, the continuity of the total velocity across the interface is always satisfied.

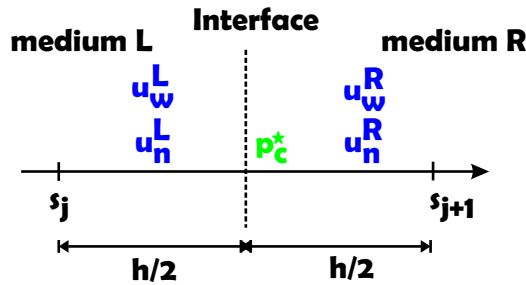


Figure 4.1: Interface between adjacent nodes.

Assume the non-wetting phase flows from the left-hand side to the right-hand side domain, i.e. $u_n(t, x) \geq 0$ for all x . The interfacial phase velocity $u_{n, j+\frac{1}{2}}^{k, int}$ is zero if

$$p_c^L(1 - s_j) \leq p_c^R(1) \quad \wedge \quad s_{j+1} = 0, \quad (4.26)$$

which yields from (1.37).

If the condition (4.26) does not hold, the interfacial velocity $u_{n, j+\frac{1}{2}}^{k, int}$ is computed by solving a system of linear equation for p_c^* . It is possible to approximate the left-hand side velocities u_w^L and u_n^L and the right-hand side velocities u_w^R and u_n^R as the function of the capillary pressure p_c^* (which is continuous across the interface) as

$$u_w^L = \frac{\lambda_w^L}{\lambda_w^L + \lambda_n^L} u + K \frac{\lambda_w^L \lambda_n^L}{\lambda_w^L + \lambda_n^L} \left(\frac{p_c^* - p_c^L(s_i)}{\frac{h}{2}} + (\rho_w - \rho_n)g \right), \quad (4.27)$$

$$u_w^R = \frac{\lambda_w^R}{\lambda_w^R + \lambda_n^R} u + K \frac{\lambda_w^R \lambda_n^R}{\lambda_w^R + \lambda_n^R} \left(\frac{p_c(s_{i+1}^R) - p_c^*}{\frac{h}{2}} + (\rho_w - \rho_n)g \right), \quad (4.28)$$

$$u_n^L = \frac{\lambda_n^L}{\lambda_w^L + \lambda_n^L} u - K \frac{\lambda_w^L \lambda_n^L}{\lambda_w^L + \lambda_n^L} \left(\frac{p_c^* - p_c^L(s_i)}{\frac{h}{2}} + (\rho_w - \rho_n)g \right), \quad (4.29)$$

$$u_n^R = \frac{\lambda_n^R}{\lambda_w^R + \lambda_n^R} u - K \frac{\lambda_w^R \lambda_n^R}{\lambda_w^R + \lambda_n^R} \left(\frac{p_c^R(s_{i+1}) - p_c^*}{\frac{h}{2}} + (\rho_w - \rho_n)g \right), \quad (4.30)$$

where

$$\begin{aligned} \lambda_w^L &= \lambda_w(1 - s_j), \\ \lambda_n^L &= \lambda_n(1 - s_j), \\ \lambda_w^R &= \lambda_w(1 - s_{j+1}), \\ \lambda_n^R &= \lambda_n(1 - s_{j+1}). \end{aligned}$$

The interface condition (1.36) yields

$$u_w^L = u_w^R,$$

so that the unknown variable p_c^* can be expressed and substituted into both expressions of u_n . The desired interfacial phase velocity is obtained in the form

$$u_n^{k \text{ int}} = u_n^L = u_n^R = \lambda_n^L \lambda_n^R \frac{(\lambda_w^L + \lambda_w^R)u + 2K\lambda_w^L \lambda_w^R \left(\frac{p_c^L(s_j) - p_c^R(s_{j+1})}{h} + (\rho_n - \rho_w)g \right)}{\lambda_w^L \lambda_w^R (\lambda_n^L + \lambda_n^R) + \lambda_n^L \lambda_n^R (\lambda_w^L + \lambda_w^R)}. \quad (4.31)$$

4.2 Applicability in Homogeneous Medium

4.2.1 Linearization

Using the numerical schemes in the form (4.6), one can encounter unbounded values due to infinite value of the limit

$$\lim_{\mathbb{S} \rightarrow 0} p_c(\mathbb{S}) = \infty.$$

The value of the velocity $u_{dp \ j+\frac{1}{2}}$ in (4.7) is infinite and thus numerically undefined if the non-wetting phase reaches its maximal saturation, i.e. $\mathbb{S}_n = 1$. Taking

advantage of the zero value of \mathfrak{D} for $\mathfrak{S}_n = 1$ due to $\lambda_w(0) = 0$, the following linearization of the capillary pressure - saturation relationship is proposed.

Let $\varepsilon_{p_c} > 0$ be arbitrary selected value, define

$$p_c^{lin}(\mathfrak{S}) = \begin{cases} p_c(\mathfrak{S}) & \text{for all } \varepsilon_{p_c} < \mathfrak{S} \leq 1, \\ p'_c(\varepsilon_{p_c})(\mathfrak{S} - \varepsilon_{p_c}) + p_c(\varepsilon_{p_c}) & \text{for all } 0 \leq \mathfrak{S} \leq \varepsilon_{p_c}, \end{cases} \quad (4.32)$$

Substitution of p_c^{lin} for p_c in all numerical schemes and choice of $\varepsilon_{p_c} = 0.01$ is used in all of the subsequent computations.

4.2.2 Applicability of McWhorter and Sunada Exact Solutions

PROBLEM FORMULATION

The McWhorter and Sunada problem requires the total velocity in the form $u(t) = AR t^{-\frac{1}{2}}$. The initial condition is discretized as

$$s_j(0) = \mathfrak{S}_j, \quad \text{for all } j \in \{1, 2, \dots, I - 1\}, \quad (4.33)$$

and the boundary conditions for all $t > 0$ read

$$s_0(t) = \mathfrak{S}_0 \quad (4.34)$$

$$s_m(t) = \mathfrak{S}_i. \quad (4.35)$$

The domain length L must be selected such that the front of the numerical solution does not reach the right hand side boundary at $x = L$, otherwise the numerical solution will not respect the semi-infinite McWhorter and Sunada problem formulation (L approximates the infinite boundary). The magnitude parameter A of the total velocity u is obtained by computing the quasi-analytical solution for a given parameters R , \mathfrak{S}_0 and \mathfrak{S}_i and thus the numerical solution depends on the analytical solution through the value of A ¹.

EXPERIMENTAL ORDER OF CONVERGENCE

The McWhorter and Sunada exact solution is mainly used to determine the *experimental order of convergence (EOC)* of more complex numerical schemes. Let h_a and h_b be two different mesh sizes and \mathfrak{S}_h^n be numerical solution on a mesh

¹The relationship between A and \mathfrak{S}_0 can be determined only by computing the McWhorter and Sunada exact solution, see Chapter 2.

with the mesh size h and \mathbb{S}^a be analytical solution. Then the experimental order of convergence is defined as follows (see Mikyška, 2005)

$$ECC(h_a, h_b) = \frac{\ln \|\mathbb{S}_{h_a}^n - \mathbb{S}^a\|_{L^p} - \ln \|\mathbb{S}_{h_b}^n - \mathbb{S}^a\|_{L^p}}{\ln h_a - \ln h_b}. \quad (4.36)$$

In the case of explicit numerical schemes like the scheme (4.6) presented in this chapter, the form of the total velocity term $u(t) = ARt^{-\frac{1}{2}}$ causes unwelcome numerical difficulties in practical applications due to infinite limit

$$\lim_{t \rightarrow 0^+} u(t).$$

The numerical implementation is possible only for finite values of $u(0)$, i.e. for $u(t) = AR(t + \varepsilon_t)^{-\frac{1}{2}}$. Therefore, the *ECC* should be regarded as a function of $\varepsilon_t > 0$.

4.2.3 Convergence analysis

TEST PROBLEM DESCRIPTION

A test problem is proposed to demonstrate how the numerical precision ε_t affects the *ECC* and to demonstrate applicability of the exact solution proposed by McWhorter and Sunada. As it was already discussed in Section 4.2.2, the experimental order of convergence depends on two mesh sizes h_a and h_b . In this section, the length of the domain L and the number of divisions I of the interval $[0, L]$ is used to compute the mesh sizes as

$$h = \frac{L}{I}.$$

The demonstration starts with $I_1 = 100$ divisions and then the grid is uniformly refined by doubling the number of divisions in each step.

Denoting $ECC_k = ECC(h_{k-1}, h_k)$, where

$$h_k = \frac{L}{kI_1},$$

the experimental order of convergence reads

$$ECC_k = \log_2 \frac{\|\mathbb{S}_{h_{k-1}}^n - \mathbb{S}^a\|_{L^p}}{\|\mathbb{S}_{h_k}^n - \mathbb{S}^a\|_{L^p}}. \quad (4.37)$$

The unidirectional ($R = 1$) displacement of the wetting phase is studied with and without dominant advection term, i.e. for the value of $\mathbb{S}_0 \in \{0.5, 0.7, 0.8, 0.9\}$.

4.2. APPLICABILITY IN HOMOGENEOUS MEDIUM

The exact solution is obtained for $\varepsilon_A = 10^{-15}$ and using 1000 nodes in the discretization of F .

The Dirichlet boundary conditions at $x = 0$ and $x = L$ are prescribed in the numerical problem.

Both van Genuchten and Brooks-Corey model functions are selected with the following setup:

Brooks-Corey :	$\lambda = 2,$	$p_d = 1000 \text{ Pa},$
van Genuchten :	$m = 0.75,$	$\alpha = 0.001 \text{ Pa}^{-1}.$
Residual saturations :	$S_{rw} = 0,$	$S_{rn} = 0,$
Fluid viscosities :	$\mu_w = 0.001 \text{ Pa s}$	$\mu_n = 0.001 \text{ Pa s},$
Miscellaneous :	$\Phi = 0.4,$	$K = 10^{-10} \text{ m}^{-2}.$

The tests proceed in the following way. First, the exact solution is obtained at $t = 1000 \text{ s}$ for a given value of $\mathcal{S}_0, R = 1$ and $\mathcal{S}_i = 0$. The resulting total velocity coefficient A is used in the numerical computation. The domain length L is set to a 1.3 multiple of the position of the front of the exact solution at $t = 1000 \text{ s}$ to assure the front of the numerical solution will not reach the right hand side boundary at $x = L$.

The time step τ is selected heuristically such that the numerical scheme is stable. The initial time step $\tau = 0.1 \text{ s}$ is selected and the numerical procedure is restarted with the reduced value of τ every time the instabilities manifest via oscillations of the numerical solution. Therefore, the time step is constant for each result. The resulting respective time steps are shown in Tables 4.1 and 4.10.

BROOKS-COREY MODEL FUNCTIONS

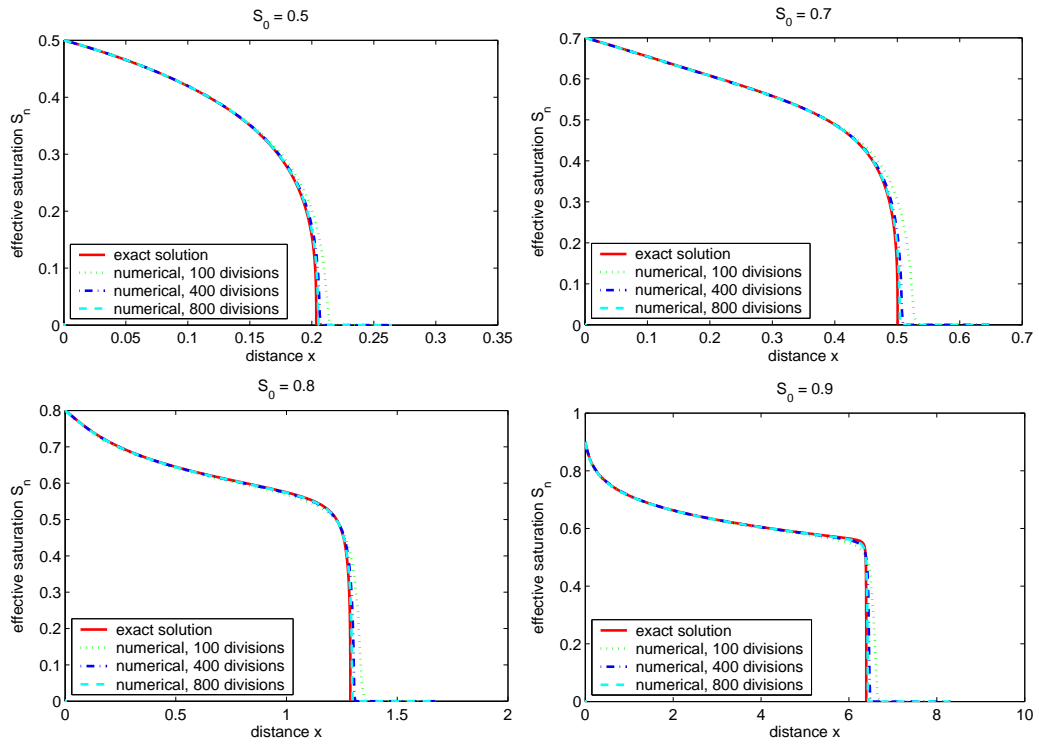


Figure 4.2: Exact and numerical solutions for the Brooks-Corey model functions at time $t = 1000$ s for various S_0 , homogeneous porous medium. Numerical solutions computed using the standard Runge Kutta RK4 method with $\varepsilon_t = 10^{-5}$.

4.2. APPLICABILITY IN HOMOGENEOUS MEDIUM

S_0	ε_t	RK	100	200	400	800	1600
0.5	1e-1	RK1,4	1.0e-1	1.0e-2	5.0e-3	2.0e-3	1.0e-3
	1e-2	RK1,4	1.0e-1	1.0e-2	5.0e-3	2.0e-3	1.0e-3
	1e-3	RK1	5.0e-2	1.0e-2	5.0e-3	1.0e-3	5.0e-4
		RK4	5.0e-2	1.0e-2	5.0e-3	2.0e-3	5.0e-4
	1e-4	RK1	2.5e-2	1.0e-2	2.5e-3	1.0e-3	2.5e-4
		RK4	2.5e-2	1.0e-2	5.0e-3	1.0e-3	5.0e-4
	1e-5	RK1	6.3e-3	2.5e-3	1.3e-3	5.0e-4	2.5e-4
		RK4	1.3e-2	5.0e-3	2.5e-3	1.0e-3	2.5e-4
1e-6	RK1	1.6e-3	1.3e-3	6.3e-4	2.5e-4	1.3e-4	
	RK4	1.3e-2	2.5e-3	1.3e-3	5.0e-4	2.5e-4	
0.7	1e-1	RK1,4	1.0e-1	1.0e-2	5.0e-3	2.0e-3	1.0e-3
	1e-2	RK1,4	1.0e-1	1.0e-2	5.0e-3	2.0e-3	1.0e-3
	1e-3	RK1	2.5e-2	1.0e-2	5.0e-3	2.0e-3	1.0e-3
		RK4	5.0e-2	1.0e-2	5.0e-3	2.0e-3	1.0e-3
	1e-4	RK1	1.3e-2	5.0e-3	2.5e-3	1.0e-3	5.0e-4
		RK4	2.5e-2	1.0e-2	5.0e-3	2.0e-3	1.0e-3
	1e-5	RK1	3.1e-3	1.3e-3	6.3e-4	5.0e-4	2.5e-4
		RK4	2.5e-2	1.0e-2	5.0e-3	1.0e-3	5.0e-4
1e-6	RK1	7.8e-4	6.3e-4	3.1e-4	1.3e-4	6.3e-5	
	RK4	6.3e-3	1.3e-3	6.3e-4	1.0e-3	1.3e-4	
0.8	1e-1	RK1,4	1.0e-1	1.0e-2	5.0e-3	2.0e-3	1.0e-3
	1e-2	RK1,4	1.0e-1	1.0e-2	5.0e-3	2.0e-3	1.0e-3
	1e-3	RK1	2.5e-2	1.0e-2	5.0e-3	2.0e-3	1.0e-3
		RK4	5.0e-2	1.0e-2	5.0e-3	2.0e-3	1.0e-3
	1e-4	RK1	1.3e-2	5.0e-3	2.5e-3	1.0e-3	5.0e-4
		RK4	2.5e-2	1.0e-2	5.0e-3	2.0e-3	1.0e-3
	1e-5	RK1	3.1e-3	1.3e-3	6.3e-4	5.0e-4	2.5e-4
		RK4	6.3e-3	1.0e-2	5.0e-3	1.0e-3	5.0e-4
1e-6	RK1	7.8e-4	6.3e-4	3.1e-4	1.3e-4	6.3e-5	
	RK4	6.3e-3	1.3e-3	6.3e-4	2.5e-4	1.3e-4	
0.9	1e-1	RK1,4	1.0e-1	1.0e-2	5.0e-3	2.0e-3	1.0e-3
	1e-2	RK1,4	1.0e-1	1.0e-2	5.0e-3	2.0e-3	1.0e-3
	1e-3	RK1	2.5e-2	1.0e-2	5.0e-3	2.0e-3	1.0e-3
		RK4	5.0e-2	1.0e-2	5.0e-3	2.0e-3	1.0e-3
	1e-4	RK1	1.3e-2	5.0e-3	2.5e-3	1.0e-3	5.0e-4
		RK4	2.5e-2	1.0e-2	5.0e-3	2.0e-3	1.0e-3
	1e-5	RK1	3.1e-3	1.3e-3	6.3e-4	5.0e-4	2.5e-4
		RK4	6.3e-3	1.0e-2	5.0e-3	1.0e-3	5.0e-4
1e-6	RK1	7.8e-4	6.3e-4	3.1e-4	1.3e-4	6.3e-5	
	RK4	6.3e-3	1.3e-3	6.3e-4	2.5e-4	1.3e-4	

Table 4.1: Time steps τ used in the numerical computations, Brooks-Corey model functions.

Runge Kutta RK1 method, I = 100, 200, 400, 800 and 1600 divisions, L_1 norms									
ε_t	100	ECC_1	200	ECC_2	400	ECC_3	800	ECC_4	1600
1e-1	2.0e-3	1.02	1.0e-3	0.99	5.0e-4	1.10	2.3e-4	1.23	1.0e-4
1e-2	2.0e-3	0.93	1.1e-3	0.92	5.6e-4	0.97	2.9e-4	1.00	1.4e-4
1e-3	2.2e-3	1.01	1.1e-3	0.89	5.9e-4	0.97	3.0e-4	0.95	1.5e-4
1e-4	2.4e-3	1.01	1.2e-3	1.00	5.8e-4	0.93	3.1e-4	0.96	1.6e-4
1e-5	2.2e-3	0.97	1.1e-3	0.93	5.9e-4	0.95	3.1e-4	0.94	1.6e-4
1e-6	2.2e-3	0.86	1.2e-3	0.95	6.1e-4	0.97	3.1e-4	0.95	1.6e-4
Runge Kutta RK4 method, I = 100, 200, 400, 800 and 1600 divisions, L_1 norms									
ε_t	100	ECC_1	200	ECC_2	400	ECC_3	800	ECC_4	1600
1e-1	1.9e-3	0.93	1.0e-3	0.99	5.0e-4	1.10	2.3e-4	1.25	9.8e-5
1e-2	2.0e-3	0.92	1.1e-3	0.92	5.5e-4	0.95	2.9e-4	1.00	1.4e-4
1e-3	2.0e-3	0.90	1.1e-3	0.91	5.7e-4	0.92	3.0e-4	0.95	1.5e-4
1e-4	2.0e-3	0.90	1.1e-3	0.90	5.8e-4	0.95	3.0e-4	0.93	1.6e-4
1e-5	2.0e-3	0.91	1.1e-3	0.91	5.8e-4	0.93	3.0e-4	0.95	1.6e-4
1e-6	2.2e-3	1.03	1.1e-3	0.92	5.8e-4	0.94	3.0e-4	0.93	1.6e-4

Table 4.2: Experimental order of convergence computed from the L_1 norms for the Brooks-Corey model functions and $S_0 = 0.5$.

Runge Kutta RK1 method, I = 100, 200, 400, 800 and 1600 divisions, L_1 norms									
ε_t	100	ECC_1	200	ECC_2	400	ECC_3	800	ECC_4	1600
1e-1	5.8e-3	1.01	2.9e-3	0.85	1.6e-3	0.24	1.3e-3	-0.26	1.6e-3
1e-2	7.2e-3	1.16	3.2e-3	0.99	1.6e-3	1.02	8.0e-4	0.85	4.4e-4
1e-3	7.2e-3	0.99	3.6e-3	0.96	1.9e-3	1.02	9.2e-4	1.02	4.5e-4
1e-4	8.1e-3	1.01	4.0e-3	0.96	2.1e-3	1.02	1.0e-3	0.99	5.1e-4
1e-5	7.9e-3	1.00	3.9e-3	0.95	2.0e-3	0.86	1.1e-3	0.98	5.7e-4
1e-6	7.5e-3	0.80	4.3e-3	0.95	2.2e-3	1.01	1.1e-3	0.97	5.7e-4
Runge Kutta RK4 method, I = 100, 200, 400, 800 and 1600 divisions, L_1 norms									
ε_t	100	ECC_1	200	ECC_2	400	ECC_3	800	ECC_4	1600
1e-1	5.6e-3	0.97	2.9e-3	0.84	1.6e-3	0.23	1.4e-3	-0.26	1.6e-3
1e-2	6.1e-3	0.95	3.1e-3	0.98	1.6e-3	1.00	7.9e-4	0.81	4.5e-4
1e-3	6.4e-3	0.95	3.3e-3	0.94	1.7e-3	0.98	8.7e-4	1.02	4.3e-4
1e-4	6.7e-3	0.94	3.5e-3	0.93	1.8e-3	0.96	9.4e-4	0.96	4.8e-4
1e-5	8.2e-3	1.00	4.1e-3	0.96	2.1e-3	1.09	9.8e-4	0.96	5.0e-4
1e-6	8.0e-3	1.13	3.6e-3	0.93	1.9e-3	0.75	1.1e-3	1.16	5.1e-4

Table 4.3: Experimental order of convergence computed from the L_1 norms for the Brooks-Corey model functions and $S_0 = 0.7$.

4.2. APPLICABILITY IN HOMOGENEOUS MEDIUM

Runge Kutta RK1 method, I = 100, 200, 400, 800 and 1600 divisions, L_1 norms									
ε_t	100	ECC_1	200	ECC_2	400	ECC_3	800	ECC_4	1600
1e-1	1.8e-2	0.96	9.3e-3	0.63	6.0e-3	-0.10	6.5e-3	-0.12	7.0e-3
1e-2	2.2e-2	1.02	1.1e-2	0.97	5.4e-3	0.97	2.8e-3	0.56	1.9e-3
1e-3	2.4e-2	0.94	1.2e-2	0.94	6.4e-3	1.01	3.2e-3	1.03	1.5e-3
1e-4	2.4e-2	0.89	1.3e-2	0.92	6.8e-3	0.94	3.5e-3	0.98	1.8e-3
1e-5	2.5e-2	0.89	1.3e-2	0.91	7.1e-3	0.97	3.6e-3	0.95	1.9e-3
1e-6	2.5e-2	0.92	1.3e-2	0.91	7.0e-3	0.88	3.8e-3	0.94	2.0e-3
Runge Kutta RK4 method, I = 100, 200, 400, 800 and 1600 divisions, L_1 norms									
ε_t	100	ECC_1	200	ECC_2	400	ECC_3	800	ECC_4	1600
1e-1	1.8e-2	0.93	9.3e-3	0.62	6.1e-3	-0.10	6.5e-3	-0.12	7.1e-3
1e-2	2.0e-2	0.92	1.0e-2	0.96	5.4e-3	0.95	2.8e-3	0.53	1.9e-3
1e-3	2.1e-2	0.92	1.1e-2	0.92	5.9e-3	0.96	3.0e-3	1.00	1.5e-3
1e-4	2.2e-2	0.91	1.2e-2	0.91	6.3e-3	0.95	3.3e-3	0.96	1.7e-3
1e-5	2.2e-2	0.79	1.3e-2	0.92	6.7e-3	0.96	3.5e-3	0.95	1.8e-3
1e-6	2.4e-2	0.97	1.2e-2	0.90	6.7e-3	0.94	3.5e-3	0.93	1.8e-3

Table 4.4: Experimental order of convergence computed from the L_1 norms for the Brooks-Corey model functions and $S_0 = 0.8$.

Runge Kutta RK1 method, I = 100, 200, 400, 800 and 1600 divisions, L_1 norms									
ε_t	100	ECC_1	200	ECC_2	400	ECC_3	800	ECC_4	1600
1e-1	9.1e-2	1.01	4.5e-2	0.53	3.1e-2	-0.19	3.6e-2	-0.10	3.8e-2
1e-2	1.1e-1	1.00	5.6e-2	0.98	2.8e-2	1.03	1.4e-2	0.46	1.0e-2
1e-3	1.2e-1	0.90	6.6e-2	0.92	3.5e-2	0.99	1.8e-2	1.05	8.5e-3
1e-4	1.4e-1	1.05	6.9e-2	0.91	3.7e-2	0.88	2.0e-2	0.96	1.0e-2
1e-5	1.3e-1	0.87	7.2e-2	0.88	3.9e-2	0.91	2.1e-2	0.96	1.1e-2
1e-6	1.3e-1	0.75	7.8e-2	0.93	4.1e-2	0.98	2.1e-2	0.92	1.1e-2
Runge Kutta RK4 method, I = 100, 200, 400, 800 and 1600 divisions, L_1 norms									
ε_t	100	ECC_1	200	ECC_2	400	ECC_3	800	ECC_4	1600
1e-1	8.9e-2	0.97	4.5e-2	0.52	3.2e-2	-0.18	3.6e-2	-0.10	3.8e-2
1e-2	1.0e-1	0.90	5.5e-2	0.97	2.8e-2	1.00	1.4e-2	0.43	1.0e-2
1e-3	1.1e-1	0.90	5.9e-2	0.89	3.2e-2	0.94	1.7e-2	1.01	8.3e-3
1e-4	1.2e-1	0.89	6.4e-2	0.88	3.5e-2	0.91	1.9e-2	0.93	9.7e-3
1e-5	1.2e-1	0.74	7.1e-2	0.92	3.7e-2	0.91	2.0e-2	0.91	1.1e-2
1e-6	1.3e-1	0.99	6.8e-2	0.86	3.7e-2	0.91	2.0e-2	0.90	1.1e-2

Table 4.5: Experimental order of convergence computed from the L_1 norms for the Brooks-Corey model functions and $S_0 = 0.9$.

Runge Kutta RK1 method, I = 100, 200, 400, 800 and 1600 divisions, L_2 norms									
ε_t	100	ECC_1	200	ECC_2	400	ECC_3	800	ECC_4	1600
1e-1	1.3e-2	0.69	8.2e-3	0.69	5.1e-3	0.75	3.0e-3	0.83	1.7e-3
1e-2	1.3e-2	0.64	8.5e-3	0.66	5.4e-3	0.69	3.3e-3	0.72	2.0e-3
1e-3	1.4e-2	0.69	8.6e-3	0.65	5.5e-3	0.70	3.4e-3	0.70	2.1e-3
1e-4	1.4e-2	0.69	8.9e-3	0.70	5.5e-3	0.68	3.4e-3	0.70	2.1e-3
1e-5	1.4e-2	0.67	8.8e-3	0.67	5.5e-3	0.69	3.4e-3	0.69	2.1e-3
1e-6	1.4e-2	0.61	9.0e-3	0.68	5.6e-3	0.70	3.5e-3	0.70	2.1e-3
Runge Kutta RK4 method, I = 100, 200, 400, 800 and 1600 divisions, L_2 norms									
ε_t	100	ECC_1	200	ECC_2	400	ECC_3	800	ECC_4	1600
1e-1	1.3e-2	0.65	8.2e-3	0.69	5.1e-3	0.75	3.0e-3	0.84	1.7e-3
1e-2	1.3e-2	0.64	8.4e-3	0.66	5.3e-3	0.69	3.3e-3	0.72	2.0e-3
1e-3	1.3e-2	0.63	8.5e-3	0.65	5.4e-3	0.67	3.4e-3	0.70	2.1e-3
1e-4	1.3e-2	0.63	8.5e-3	0.65	5.4e-3	0.68	3.4e-3	0.69	2.1e-3
1e-5	1.3e-2	0.63	8.6e-3	0.65	5.4e-3	0.67	3.4e-3	0.70	2.1e-3
1e-6	1.4e-2	0.70	8.6e-3	0.66	5.5e-3	0.68	3.4e-3	0.69	2.1e-3

Table 4.6: Experimental order of convergence computed from the L_2 norms for the Brooks-Corey model functions and $S_0 = 0.5$.

Runge Kutta RK1 method, I = 100, 200, 400, 800 and 1600 divisions, L_2 norms									
ε_t	100	ECC_1	200	ECC_2	400	ECC_3	800	ECC_4	1600
1e-1	2.6e-2	0.89	1.4e-2	1.11	6.5e-3	1.07	3.1e-3	-1.04	6.3e-3
1e-2	3.3e-2	0.88	1.8e-2	0.72	1.1e-2	0.87	6.0e-3	1.17	2.7e-3
1e-3	3.3e-2	0.68	2.1e-2	0.66	1.3e-2	0.73	7.9e-3	0.75	4.7e-3
1e-4	3.7e-2	0.69	2.3e-2	0.67	1.4e-2	0.72	8.7e-3	0.70	5.3e-3
1e-5	3.6e-2	0.68	2.2e-2	0.65	1.4e-2	0.60	9.4e-3	0.70	5.8e-3
1e-6	3.5e-2	0.53	2.4e-2	0.66	1.5e-2	0.71	9.3e-3	0.69	5.8e-3
Runge Kutta RK4 method, I = 100, 200, 400, 800 and 1600 divisions, L_2 norms									
ε_t	100	ECC_1	200	ECC_2	400	ECC_3	800	ECC_4	1600
1e-1	2.4e-2	0.82	1.4e-2	1.12	6.4e-3	1.01	3.2e-3	-1.02	6.4e-3
1e-2	2.8e-2	0.66	1.8e-2	0.73	1.1e-2	0.87	5.8e-3	1.19	2.5e-3
1e-3	3.0e-2	0.66	1.9e-2	0.65	1.2e-2	0.70	7.4e-3	0.77	4.3e-3
1e-4	3.1e-2	0.64	2.0e-2	0.64	1.3e-2	0.68	8.1e-3	0.68	5.0e-3
1e-5	3.7e-2	0.69	2.3e-2	0.67	1.5e-2	0.79	8.4e-3	0.68	5.2e-3
1e-6	3.6e-2	0.80	2.1e-2	0.64	1.3e-2	0.51	9.4e-3	0.84	5.3e-3

Table 4.7: Experimental order of convergence computed from the L_2 norms for the Brooks-Corey model functions and $S_0 = 0.7$.

4.2. APPLICABILITY IN HOMOGENEOUS MEDIUM

Runge Kutta RK1 method, I = 100, 200, 400, 800 and 1600 divisions, L_2 norms									
ε_t	100	ECC_1	200	ECC_2	400	ECC_3	800	ECC_4	1600
1e-1	5.0e-2	1.06	2.4e-2	1.18	1.1e-2	-0.95	2.1e-2	-0.45	2.8e-2
1e-2	7.1e-2	0.88	3.9e-2	0.78	2.3e-2	1.08	1.1e-2	1.39	4.1e-3
1e-3	7.4e-2	0.65	4.8e-2	0.65	3.0e-2	0.75	1.8e-2	0.85	1.0e-2
1e-4	7.9e-2	0.59	5.3e-2	0.62	3.4e-2	0.69	2.1e-2	0.71	1.3e-2
1e-5	8.0e-2	0.61	5.3e-2	0.60	3.5e-2	0.60	2.3e-2	0.68	1.4e-2
1e-6	7.9e-2	0.52	5.5e-2	0.60	3.6e-2	0.64	2.3e-2	0.66	1.5e-2
Runge Kutta RK4 method, I = 100, 200, 400, 800 and 1600 divisions, L_2 norms									
ε_t	100	ECC_1	200	ECC_2	400	ECC_3	800	ECC_4	1600
1e-1	4.7e-2	0.98	2.4e-2	1.14	1.1e-2	-0.95	2.1e-2	-0.44	2.8e-2
1e-2	5.8e-2	0.65	3.7e-2	0.77	2.2e-2	1.08	1.0e-2	1.30	4.2e-3
1e-3	6.4e-2	0.62	4.1e-2	0.62	2.7e-2	0.71	1.6e-2	0.85	9.2e-3
1e-4	6.9e-2	0.60	4.5e-2	0.60	3.0e-2	0.66	1.9e-2	0.68	1.2e-2
1e-5	6.9e-2	0.37	5.3e-2	0.62	3.5e-2	0.76	2.0e-2	0.66	1.3e-2
1e-6	8.1e-2	0.74	4.8e-2	0.59	3.2e-2	0.65	2.1e-2	0.65	1.3e-2

Table 4.8: Experimental order of convergence computed from the L_2 norms for the Brooks-Corey model functions and $S_0 = 0.8$.

Runge Kutta RK1 method, I = 100, 200, 400, 800 and 1600 divisions, L_2 norms									
ε_t	100	ECC_1	200	ECC_2	400	ECC_3	800	ECC_4	1600
1e-1	1.3e-1	1.11	6.0e-2	0.22	5.2e-2	-0.85	9.4e-2	-0.26	1.1e-1
1e-2	1.9e-1	0.78	1.1e-1	0.72	6.6e-2	1.17	2.9e-2	0.17	2.6e-2
1e-3	2.0e-1	0.55	1.4e-1	0.55	9.4e-2	0.67	5.9e-2	0.81	3.4e-2
1e-4	2.1e-1	0.49	1.5e-1	0.51	1.1e-1	0.56	7.2e-2	0.61	4.7e-2
1e-5	2.1e-1	0.50	1.5e-1	0.49	1.1e-1	0.51	7.6e-2	0.56	5.1e-2
1e-6	2.1e-1	0.44	1.6e-1	0.49	1.1e-1	0.51	7.8e-2	0.54	5.4e-2
Runge Kutta RK4 method, I = 100, 200, 400, 800 and 1600 divisions, L_2 norms									
ε_t	100	ECC_1	200	ECC_2	400	ECC_3	800	ECC_4	1600
1e-1	1.2e-1	0.99	6.0e-2	0.17	5.3e-2	-0.83	9.4e-2	-0.26	1.1e-1
1e-2	1.5e-1	0.57	1.0e-1	0.73	6.3e-2	1.17	2.8e-2	0.04	2.7e-2
1e-3	1.7e-1	0.53	1.2e-1	0.52	8.2e-2	0.61	5.4e-2	0.81	3.1e-2
1e-4	1.9e-1	0.51	1.3e-1	0.50	9.3e-2	0.56	6.3e-2	0.59	4.2e-2
1e-5	1.8e-1	0.29	1.5e-1	0.51	1.1e-1	0.62	6.9e-2	0.56	4.7e-2
1e-6	2.1e-1	0.62	1.4e-1	0.48	1.0e-1	0.53	6.9e-2	0.54	4.8e-2

Table 4.9: Experimental order of convergence computed from the L_2 norms for the Brooks-Corey model functions and $S_0 = 0.9$.

VAN GENUCHTEN MODEL FUNCTIONS

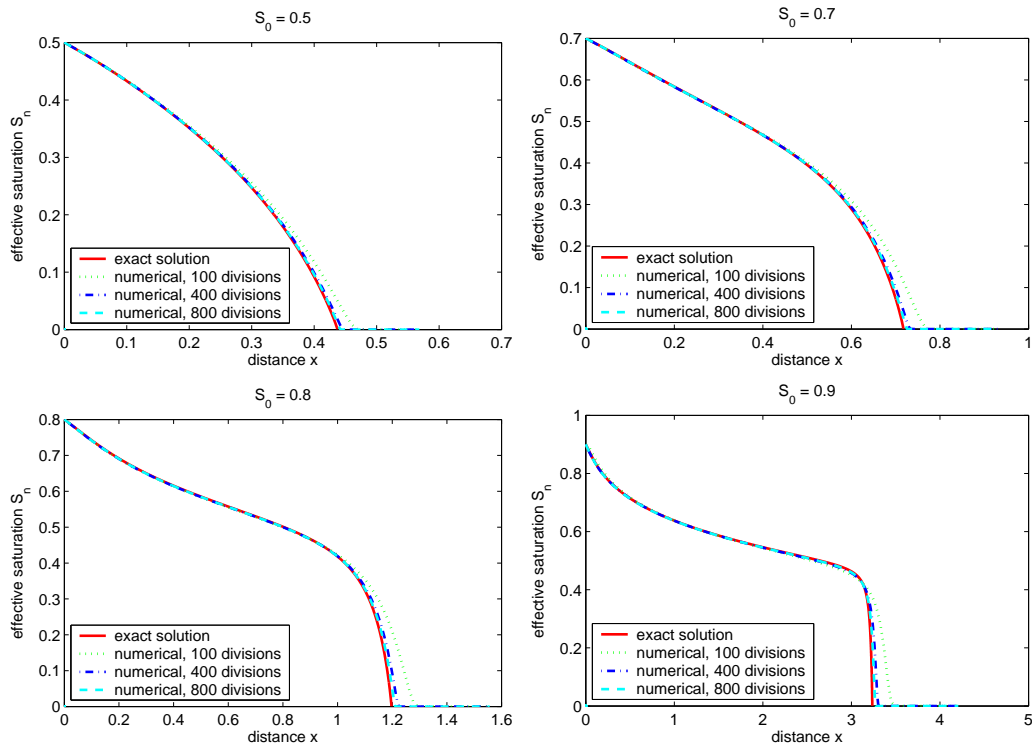


Figure 4.3: Exact and numerical solutions for the van Genuchten model functions at time $t = 1000$ s for various S_0 , homogeneous porous medium. Numerical solutions computed using the standard Runge Kutta RK4 method with $\varepsilon_t = 10^{-5}$.

4.2. APPLICABILITY IN HOMOGENEOUS MEDIUM

S_0	ε_t	RK	100	200	400	800	1600
0.5	1e-1	RK1,4	1.0e-1	1.0e-2	5.0e-3	2.0e-3	1.0e-3
	1e-2	RK1,4	1.0e-1	1.0e-2	5.0e-3	2.0e-3	1.0e-3
	1e-3	RK1	5.0e-2	1.0e-2	5.0e-3	2.0e-3	1.0e-3
		RK4	1.0e-1	1.0e-2	5.0e-3	2.0e-3	5.0e-4
	1e-4	RK1	2.5e-2	1.0e-2	5.0e-3	2.0e-3	5.0e-4
		RK4	5.0e-2	1.0e-2	5.0e-3	2.0e-3	5.0e-4
	1e-5	RK1	6.3e-3	2.5e-3	1.3e-3	1.0e-3	2.5e-4
		RK4	5.0e-2	5.0e-3	2.5e-3	2.0e-3	5.0e-4
1e-6	RK1	3.1e-3	1.3e-3	6.3e-4	2.5e-4	1.3e-4	
	RK4	6.3e-3	2.5e-3	1.3e-3	2.0e-3	2.5e-4	
0.7	1e-1	RK1,4	1.0e-1	1.0e-2	5.0e-3	2.0e-3	1.0e-3
	1e-2	RK1,4	1.0e-1	1.0e-2	5.0e-3	2.0e-3	1.0e-3
	1e-3	RK1	5.0e-2	1.0e-2	5.0e-3	2.0e-3	1.0e-3
		RK4	1.0e-1	1.0e-2	5.0e-3	2.0e-3	1.0e-3
	1e-4	RK1	1.3e-2	5.0e-3	2.5e-3	2.0e-3	5.0e-4
		RK4	2.5e-2	1.0e-2	5.0e-3	2.0e-3	1.0e-3
	1e-5	RK1	3.1e-3	2.5e-3	1.3e-3	5.0e-4	2.5e-4
		RK4	2.5e-2	5.0e-3	2.5e-3	1.0e-3	5.0e-4
1e-6	RK1	1.6e-3	6.3e-4	3.1e-4	1.3e-4	6.3e-5	
	RK4	3.1e-3	5.0e-3	2.5e-3	1.0e-3	5.0e-4	
0.8	1e-1	RK1,4	1.0e-1	1.0e-2	5.0e-3	2.0e-3	1.0e-3
	1e-2	RK1,4	1.0e-1	1.0e-2	5.0e-3	2.0e-3	1.0e-3
	1e-3	RK1	2.5e-2	1.0e-2	5.0e-3	2.0e-3	1.0e-3
		RK4	5.0e-2	1.0e-2	5.0e-3	2.0e-3	1.0e-3
	1e-4	RK1	1.3e-2	5.0e-3	2.5e-3	1.0e-3	5.0e-4
		RK4	2.5e-2	1.0e-2	5.0e-3	2.0e-3	1.0e-3
	1e-5	RK1	3.1e-3	1.3e-3	6.3e-4	5.0e-4	2.5e-4
		RK4	2.5e-2	1.0e-2	5.0e-3	1.0e-3	5.0e-4
1e-6	RK1	7.8e-4	6.3e-4	3.1e-4	1.3e-4	6.3e-5	
	RK4	6.3e-3	1.3e-3	6.3e-4	1.0e-3	5.0e-4	
0.9	1e-1	RK1,4	1.0e-1	1.0e-2	5.0e-3	2.0e-3	1.0e-3
	1e-2	RK1,4	1.0e-1	1.0e-2	5.0e-3	2.0e-3	1.0e-3
	1e-3	RK1	2.5e-2	1.0e-2	5.0e-3	2.0e-3	1.0e-3
		RK4	5.0e-2	1.0e-2	5.0e-3	2.0e-3	1.0e-3
	1e-4	RK1	1.3e-2	5.0e-3	2.5e-3	1.0e-3	5.0e-4
		RK4	2.5e-2	1.0e-2	5.0e-3	2.0e-3	1.0e-3
	1e-5	RK1	3.1e-3	1.3e-3	6.3e-4	5.0e-4	2.5e-4
		RK4	2.5e-2	1.0e-2	5.0e-3	1.0e-3	5.0e-4
1e-6	RK1	7.8e-4	6.3e-4	3.1e-4	1.3e-4	6.3e-5	
	RK4	6.3e-3	1.3e-3	6.3e-4	1.0e-3	1.3e-4	

Table 4.10: Time steps τ used in the numerical computations, van Genuchten model functions.

CHAPTER 4. ONE-DIMENSIONAL NUMERICAL METHODS

Runge Kutta RK1 method, I = 100, 200, 400, 800 and 1600 divisions, L_1 norms									
ε_t	100	ECC_1	200	ECC_2	400	ECC_3	800	ECC_4	1600
1e-1	3.4e-3	1.06	1.6e-3	1.06	7.8e-4	1.23	3.3e-4	1.40	1.3e-4
1e-2	3.8e-3	1.10	1.8e-3	0.93	9.4e-4	0.98	4.8e-4	1.09	2.2e-4
1e-3	4.0e-3	1.08	1.9e-3	0.91	1.0e-3	0.93	5.2e-4	1.01	2.6e-4
1e-4	4.3e-3	1.03	2.1e-3	0.95	1.1e-3	0.97	5.6e-4	1.02	2.8e-4
1e-5	4.1e-3	1.01	2.0e-3	0.95	1.1e-3	0.89	5.7e-4	1.05	2.7e-4
1e-6	4.6e-3	1.06	2.2e-3	0.98	1.1e-3	1.01	5.5e-4	0.97	2.8e-4
Runge Kutta RK4 method, I = 100, 200, 400, 800 and 1600 divisions, L_1 norms									
ε_t	100	ECC_1	200	ECC_2	400	ECC_3	800	ECC_4	1600
1e-1	3.1e-3	0.97	1.6e-3	1.07	7.7e-4	1.23	3.3e-4	1.37	1.3e-4
1e-2	3.4e-3	0.93	1.8e-3	0.94	9.1e-4	0.99	4.6e-4	1.04	2.2e-4
1e-3	3.6e-3	0.99	1.8e-3	0.92	9.5e-4	0.94	5.0e-4	0.97	2.5e-4
1e-4	3.6e-3	0.98	1.8e-3	0.91	9.8e-4	0.93	5.1e-4	0.97	2.6e-4
1e-5	4.3e-3	1.22	1.9e-3	0.92	9.9e-4	0.90	5.3e-4	0.98	2.7e-4
1e-6	3.7e-3	0.96	1.9e-3	0.93	1.0e-3	0.82	5.7e-4	1.09	2.7e-4

Table 4.11: Experimental order of convergence computed from the L_1 norms for the van Genuchten model functions and $\mathcal{S}_0 = 0.5$.

Runge Kutta RK1 method, I = 100, 200, 400, 800 and 1600 divisions, L_1 norms									
ε_t	100	ECC_1	200	ECC_2	400	ECC_3	800	ECC_4	1600
1e-1	7.5e-3	1.03	3.7e-3	0.95	1.9e-3	0.48	1.4e-3	-0.19	1.6e-3
1e-2	9.1e-3	1.14	4.1e-3	1.00	2.1e-3	1.05	9.9e-4	1.00	5.0e-4
1e-3	1.0e-2	1.17	4.6e-3	0.96	2.4e-3	1.02	1.2e-3	1.02	5.7e-4
1e-4	1.0e-2	1.01	5.0e-3	0.96	2.6e-3	0.87	1.4e-3	1.13	6.5e-4
1e-5	9.9e-3	0.81	5.6e-3	0.97	2.9e-3	1.03	1.4e-3	0.98	7.2e-4
1e-6	1.1e-2	1.02	5.5e-3	0.95	2.8e-3	1.02	1.4e-3	0.97	7.1e-4
Runge Kutta RK4 method, I = 100, 200, 400, 800 and 1600 divisions, L_1 norms									
ε_t	100	ECC_1	200	ECC_2	400	ECC_3	800	ECC_4	1600
1e-1	7.2e-3	0.98	3.7e-3	0.94	1.9e-3	0.47	1.4e-3	-0.19	1.6e-3
1e-2	7.8e-3	0.95	4.0e-3	0.99	2.0e-3	1.04	9.8e-4	0.97	5.0e-4
1e-3	8.5e-3	1.02	4.2e-3	0.95	2.2e-3	0.99	1.1e-3	1.03	5.4e-4
1e-4	8.5e-3	0.94	4.4e-3	0.94	2.3e-3	0.97	1.2e-3	0.97	6.1e-4
1e-5	1.0e-2	1.15	4.7e-3	0.94	2.4e-3	0.98	1.2e-3	0.96	6.3e-4
1e-6	8.9e-3	0.64	5.7e-3	0.97	2.9e-3	1.03	1.4e-3	0.99	7.2e-4

Table 4.12: Experimental order of convergence computed from the L_1 norms for the van Genuchten model functions and $\mathcal{S}_0 = 0.7$.

4.2. APPLICABILITY IN HOMOGENEOUS MEDIUM

Runge Kutta RK1 method, I = 100, 200, 400, 800 and 1600 divisions, L_1 norms									
ε_t	100	ECC_1	200	ECC_2	400	ECC_3	800	ECC_4	1600
1e-1	1.8e-2	0.92	9.4e-3	0.81	5.4e-3	0.24	4.5e-3	-0.15	5.0e-3
1e-2	2.0e-2	0.98	1.0e-2	0.95	5.2e-3	0.97	2.7e-3	0.80	1.5e-3
1e-3	2.1e-2	0.92	1.1e-2	0.93	5.7e-3	0.98	2.9e-3	1.00	1.5e-3
1e-4	2.1e-2	0.87	1.2e-2	0.92	6.1e-3	0.96	3.1e-3	0.97	1.6e-3
1e-5	2.2e-2	0.91	1.2e-2	0.91	6.2e-3	0.91	3.3e-3	0.95	1.7e-3
1e-6	2.2e-2	0.87	1.2e-2	0.90	6.3e-3	0.93	3.3e-3	0.94	1.7e-3
Runge Kutta RK4 method, I = 100, 200, 400, 800 and 1600 divisions, L_1 norms									
ε_t	100	ECC_1	200	ECC_2	400	ECC_3	800	ECC_4	1600
1e-1	1.8e-2	0.90	9.4e-3	0.80	5.4e-3	0.24	4.6e-3	-0.15	5.1e-3
1e-2	1.9e-2	0.90	1.0e-2	0.94	5.2e-3	0.96	2.7e-3	0.78	1.6e-3
1e-3	1.9e-2	0.90	1.0e-2	0.91	5.5e-3	0.95	2.8e-3	0.99	1.4e-3
1e-4	2.0e-2	0.90	1.1e-2	0.91	5.7e-3	0.95	3.0e-3	0.95	1.5e-3
1e-5	2.1e-2	0.85	1.2e-2	0.92	6.1e-3	0.98	3.1e-3	0.95	1.6e-3
1e-6	2.2e-2	0.97	1.1e-2	0.90	5.9e-3	0.87	3.2e-3	0.95	1.7e-3

Table 4.13: Experimental order of convergence computed from the L_1 norms for the van Genuchten model functions and $S_0 = 0.8$.

Runge Kutta RK1 method, I = 100, 200, 400, 800 and 1600 divisions, L_1 norms									
ε_t	100	ECC_1	200	ECC_2	400	ECC_3	800	ECC_4	1600
1e-1	6.1e-2	0.87	3.3e-2	0.82	1.9e-2	0.23	1.6e-2	-0.12	1.7e-2
1e-2	6.3e-2	0.80	3.6e-2	0.90	1.9e-2	0.95	1.0e-2	0.84	5.6e-3
1e-3	6.9e-2	0.84	3.9e-2	0.88	2.1e-2	0.93	1.1e-2	0.97	5.6e-3
1e-4	7.0e-2	0.86	3.8e-2	0.86	2.1e-2	0.86	1.2e-2	0.93	6.1e-3
1e-5	6.9e-2	0.79	4.0e-2	0.86	2.2e-2	0.99	1.1e-2	0.91	5.9e-3
1e-6	7.2e-2	0.88	3.9e-2	0.89	2.1e-2	0.83	1.2e-2	0.91	6.3e-3
Runge Kutta RK4 method, I = 100, 200, 400, 800 and 1600 divisions, L_1 norms									
ε_t	100	ECC_1	200	ECC_2	400	ECC_3	800	ECC_4	1600
1e-1	6.1e-2	0.87	3.3e-2	0.82	1.9e-2	0.23	1.6e-2	-0.11	1.7e-2
1e-2	6.5e-2	0.85	3.6e-2	0.89	1.9e-2	0.94	1.0e-2	0.82	5.7e-3
1e-3	6.7e-2	0.85	3.7e-2	0.86	2.0e-2	0.91	1.1e-2	0.95	5.6e-3
1e-4	6.9e-2	0.85	3.8e-2	0.86	2.1e-2	0.89	1.1e-2	0.92	6.0e-3
1e-5	7.2e-2	0.92	3.8e-2	0.86	2.1e-2	0.82	1.2e-2	0.91	6.3e-3
1e-6	6.9e-2	0.80	4.0e-2	0.85	2.2e-2	0.97	1.1e-2	0.82	6.3e-3

Table 4.14: Experimental order of convergence computed from the L_1 norms for the van Genuchten model functions and $S_0 = 0.9$.

Runge Kutta RK1 method, I = 100, 200, 400, 800 and 1600 divisions, L_2 norms									
ε_t	100	ECC_1	200	ECC_2	400	ECC_3	800	ECC_4	1600
1e-1	8.4e-3	0.94	4.4e-3	0.96	2.3e-3	1.08	1.1e-3	1.32	4.3e-4
1e-2	9.1e-3	0.97	4.7e-3	0.89	2.5e-3	0.93	1.3e-3	1.01	6.6e-4
1e-3	9.4e-3	0.96	4.8e-3	0.87	2.6e-3	0.90	1.4e-3	0.97	7.2e-4
1e-4	9.9e-3	0.93	5.2e-3	0.90	2.8e-3	0.93	1.5e-3	0.97	7.4e-4
1e-5	9.6e-3	0.92	5.1e-3	0.90	2.7e-3	0.88	1.5e-3	1.00	7.4e-4
1e-6	1.0e-2	0.95	5.3e-3	0.92	2.8e-3	0.96	1.5e-3	0.95	7.5e-4
Runge Kutta RK4 method, I = 100, 200, 400, 800 and 1600 divisions, L_2 norms									
ε_t	100	ECC_1	200	ECC_2	400	ECC_3	800	ECC_4	1600
1e-1	8.0e-3	0.88	4.4e-3	0.96	2.2e-3	1.09	1.1e-3	1.30	4.3e-4
1e-2	8.4e-3	0.86	4.6e-3	0.89	2.5e-3	0.94	1.3e-3	0.98	6.6e-4
1e-3	8.7e-3	0.90	4.7e-3	0.88	2.5e-3	0.91	1.4e-3	0.95	7.0e-4
1e-4	8.8e-3	0.89	4.8e-3	0.87	2.6e-3	0.91	1.4e-3	0.94	7.2e-4
1e-5	1.0e-2	1.05	4.8e-3	0.88	2.6e-3	0.89	1.4e-3	0.95	7.3e-4
1e-6	9.0e-3	0.88	4.9e-3	0.89	2.6e-3	0.83	1.5e-3	1.02	7.3e-4

Table 4.15: Experimental order of convergence computed from the L_2 norms for the van Genuchten model functions and $\mathcal{S}_0 = 0.5$.

Runge Kutta RK1 method, I = 100, 200, 400, 800 and 1600 divisions, L_2 norms									
ε_t	100	ECC_1	200	ECC_2	400	ECC_3	800	ECC_4	1600
1e-1	1.7e-2	1.03	8.4e-3	1.17	3.7e-3	1.02	1.8e-3	-0.23	2.2e-3
1e-2	2.1e-2	1.05	1.0e-2	0.93	5.4e-3	1.07	2.6e-3	1.26	1.1e-3
1e-3	2.4e-2	1.03	1.2e-2	0.88	6.4e-3	0.95	3.3e-3	0.98	1.7e-3
1e-4	2.4e-2	0.89	1.3e-2	0.88	7.0e-3	0.83	3.9e-3	1.06	1.9e-3
1e-5	2.3e-2	0.72	1.4e-2	0.88	7.6e-3	0.95	3.9e-3	0.94	2.0e-3
1e-6	2.5e-2	0.89	1.4e-2	0.87	7.4e-3	0.95	3.9e-3	0.93	2.0e-3
Runge Kutta RK4 method, I = 100, 200, 400, 800 and 1600 divisions, L_2 norms									
ε_t	100	ECC_1	200	ECC_2	400	ECC_3	800	ECC_4	1600
1e-1	1.6e-2	0.97	8.3e-3	1.17	3.7e-3	1.00	1.9e-3	-0.24	2.2e-3
1e-2	1.8e-2	0.85	1.0e-2	0.93	5.3e-3	1.07	2.5e-3	1.27	1.0e-3
1e-3	2.0e-2	0.92	1.1e-2	0.87	5.9e-3	0.93	3.1e-3	1.00	1.5e-3
1e-4	2.0e-2	0.83	1.1e-2	0.86	6.3e-3	0.91	3.3e-3	0.92	1.8e-3
1e-5	2.4e-2	1.01	1.2e-2	0.86	6.6e-3	0.91	3.5e-3	0.92	1.8e-3
1e-6	2.1e-2	0.58	1.4e-2	0.88	7.6e-3	0.95	3.9e-3	0.94	2.0e-3

Table 4.16: Experimental order of convergence computed from the L_2 norms for the van Genuchten model functions and $\mathcal{S}_0 = 0.7$.

4.2. APPLICABILITY IN HOMOGENEOUS MEDIUM

Runge Kutta RK1 method, I = 100, 200, 400, 800 and 1600 divisions, L_2 norms									
ε_t	100	ECC_1	200	ECC_2	400	ECC_3	800	ECC_4	1600
1e-1	3.3e-2	1.03	1.6e-2	1.22	7.0e-3	0.45	5.1e-3	-0.51	7.3e-3
1e-2	4.3e-2	0.99	2.2e-2	0.92	1.2e-2	1.13	5.3e-3	1.38	2.0e-3
1e-3	4.5e-2	0.80	2.6e-2	0.83	1.4e-2	0.95	7.5e-3	1.03	3.7e-3
1e-4	4.8e-2	0.78	2.8e-2	0.82	1.6e-2	0.91	8.5e-3	0.93	4.5e-3
1e-5	4.8e-2	0.79	2.8e-2	0.80	1.6e-2	0.79	9.3e-3	0.91	4.9e-3
1e-6	4.7e-2	0.66	3.0e-2	0.80	1.7e-2	0.88	9.3e-3	0.89	5.0e-3
Runge Kutta RK4 method, I = 100, 200, 400, 800 and 1600 divisions, L_2 norms									
ε_t	100	ECC_1	200	ECC_2	400	ECC_3	800	ECC_4	1600
1e-1	3.2e-2	0.97	1.6e-2	1.21	7.0e-3	0.43	5.2e-3	-0.50	7.3e-3
1e-2	3.7e-2	0.80	2.1e-2	0.92	1.1e-2	1.12	5.2e-3	1.36	2.0e-3
1e-3	3.9e-2	0.78	2.3e-2	0.82	1.3e-2	0.91	7.0e-3	1.03	3.4e-3
1e-4	4.2e-2	0.76	2.5e-2	0.80	1.4e-2	0.88	7.7e-3	0.91	4.1e-3
1e-5	4.9e-2	0.77	2.8e-2	0.82	1.6e-2	0.98	8.2e-3	0.90	4.4e-3
1e-6	4.9e-2	0.90	2.6e-2	0.79	1.5e-2	0.70	9.3e-3	0.91	4.9e-3

Table 4.17: Experimental order of convergence computed from the L_2 norms for the van Genuchten model functions and $\mathcal{S}_0 = 0.8$.

Runge Kutta RK1 method, I = 100, 200, 400, 800 and 1600 divisions, L_2 norms									
ε_t	100	ECC_1	200	ECC_2	400	ECC_3	800	ECC_4	1600
1e-1	8.7e-2	0.89	4.7e-2	1.25	2.0e-2	-0.01	2.0e-2	-0.71	3.3e-2
1e-2	1.1e-1	0.76	6.6e-2	0.76	3.9e-2	1.04	1.9e-2	1.53	6.6e-3
1e-3	1.2e-1	0.61	7.7e-2	0.66	4.9e-2	0.79	2.8e-2	0.93	1.5e-2
1e-4	1.2e-1	0.57	8.3e-2	0.63	5.4e-2	0.73	3.3e-2	0.80	1.9e-2
1e-5	1.2e-1	0.58	8.4e-2	0.61	5.5e-2	0.67	3.4e-2	0.77	2.0e-2
1e-6	1.2e-1	0.51	8.7e-2	0.61	5.7e-2	0.69	3.5e-2	0.75	2.1e-2
Runge Kutta RK4 method, I = 100, 200, 400, 800 and 1600 divisions, L_2 norms									
ε_t	100	ECC_1	200	ECC_2	400	ECC_3	800	ECC_4	1600
1e-1	8.3e-2	0.84	4.7e-2	1.25	2.0e-2	-0.03	2.0e-2	-0.70	3.3e-2
1e-2	9.8e-2	0.62	6.4e-2	0.75	3.8e-2	1.03	1.9e-2	1.51	6.5e-3
1e-3	1.0e-1	0.59	7.0e-2	0.64	4.5e-2	0.75	2.6e-2	0.92	1.4e-2
1e-4	1.1e-1	0.58	7.5e-2	0.62	4.9e-2	0.71	3.0e-2	0.79	1.7e-2
1e-5	1.2e-1	0.56	8.4e-2	0.63	5.4e-2	0.77	3.2e-2	0.76	1.9e-2
1e-6	1.3e-1	0.67	7.9e-2	0.60	5.2e-2	0.58	3.5e-2	0.87	1.9e-2

Table 4.18: Experimental order of convergence computed from the L_2 norms for the van Genuchten model functions and $\mathcal{S}_0 = 0.9$.

DISCUSSION OF RESULTS

Tables 4.2, 4.3, 4.4, 4.5, 4.6, 4.7, 4.8 and 4.9 resp. Tables 4.11, 4.12, 4.13, 4.14, 4.15, 4.16, 4.17 and 4.18 show results obtained using the Brooks-Corey, resp. van Genuchten model functions using the L_1 and the L_2 norms.

As expected, the experimental order of convergence depends on ε_t , but this dependence can be neglected, approximately by the value of $\varepsilon_t = 10^{-3}$. If ε_t is not small enough, a negative experimental order of convergence is obtained as it can be observed for example in Table 4.2 in the case of ECC_4 . In such a case, the numerical solution does not converge to the quasi-analytical solution.

The numerical method uses the first order spatial discretization, which is in agreement with the presented results and also with the results in Bastian, 1999.

Figures 4.2 and 4.3 illustrate the convergence of the numerical solution to the exact solution.

4.3 Applicability in Heterogeneous Media

4.3.1 Convergence analysis

PROBLEM FORMULATION

The following parameters and boundary and initial conditions has to be setup in order to be able to compare the numerical solution to the exact solution obtained by the method described in Chapter 3, Sections 3.2.2 and 3.3.3. Suppose the one-dimensional non-wetting phase intrusion problem (4.2) without gravity (e.g. $G \equiv 0$) with the mirror boundary conditions

$$u_{n-\frac{1}{2}} = u_{n+\frac{1}{2}}, \quad (4.38)$$

$$u_{n+m+\frac{1}{2}} = u_{n+m-\frac{1}{2}}. \quad (4.39)$$

The interface is placed at $x = 0$ as it is depicted in Figure 4.4. The discretized function s is defined as $s_j(t) = \mathbb{S}_n(t, hj - \frac{1}{2}L)$, where L is a sufficiently large length of the domain Ω such that the numerical solution preserves its initial state in the vicinity of the boundary $\partial\Omega$, i.e. at $x = -\frac{1}{2}L$ and $x = \frac{1}{2}L$, for all $t \in [0, T]$, where T is the final time of the numerical simulation. The initial state is described as

$$s_j(0) = \mathbb{S}_i^L \quad \text{for all } 0 \leq j < \frac{1}{2}I, \quad (4.40)$$

$$s_j(0) = \mathbb{S}_i^R \quad \text{for all } \frac{1}{2}I \leq j \leq I. \quad (4.41)$$

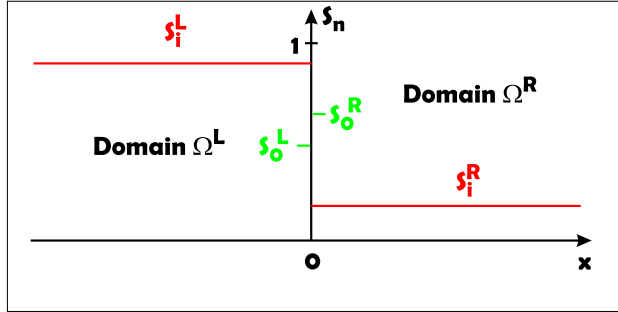


Figure 4.4: Initial state of the porous medium with a discontinuity.

The product of the magnitude parameter A and the ratio parameter R of the total velocity

$$u(t) = ARt^{-\frac{1}{2}},$$

is equal in both subdomains L and R , i.e.

$$A^R R^R = A^L R^L,$$

and must be computed using the exact solution obtention algorithm.

The unrealistic sands already used in Section 3.4.1 are selected to demonstrate convergence and to determine experimental order of convergence EOC of the numerical scheme in the heterogeneous case.

The exact solution is obtained for a given initial saturation setup $S_i^L = 0.9$ and $S_i^R = 0.1$ for the non-wetting phase formulation, i.e. the non-wetting phase intrusion problem. 1000 nodes are used to discretize the functions F , resp. G in the exact solution computation and the parameter $\varepsilon_A = 10^{-15}$ is set. The numerical solutions are computed on a series of mesh sizes characterised by $I \in \{100, 200, 400, 800, 1600\}$ and compared to the exact solution in the L_1 norm.

Based on the previous study of the influence of the initial numerical time ε_t , $\varepsilon_t = 10^{-5}$ is selected in all numerical computations in this section.

The time step τ is selected heuristically such that the numerical stability is assured in the same way as in the homogeneous case (see Section 4.2.3). The time steps τ for the respective cases are shown in Tables 4.20, 4.23, 4.26 and 4.29.

	Par.	Units	fine sand (FS)	coarse sand (CS)
Porosity	Φ	[-]	0.38	0.40
Intrinsic Permeability	K	$[m^2]$	10^{-11}	10^{-10}
Residual Water Sat.	S_{wr}	[-]	0.10	0.08
Residual NAPL Sat.	S_{nr}	[-]	0	0
Water Viscosity	μ_w	$[kg\ m^{-1}s^{-1}]$	0.001	0.001
DNAPL Viscosity	μ_n	$[kg\ m^{-1}s^{-1}]$	0.001	0.001
Brooks-Corey	P_d	$[Pa]$	1000	900
	λ	[-]	3.86	3.86
van Genuchten	$\frac{1}{\alpha}$	$[Pa]$	1500	800
	m	[-]	0.60	0.40

Table 4.19: Parameter setup for two unrealistic porous materials - coarse and fine sands.

BROOKS-COREY MODEL FUNCTIONS, CS \rightarrow FS

R^L	RK	100	200	400	800	1600
-1000.0	RK1	6.3e-3	3.1e-3	1.6e-3	6.3e-4	5.0e-4
	RK4	5.0e-2	2.5e-2	1.3e-2	5.0e-3	1.0e-3
-100.0	RK1	6.3e-3	3.1e-3	1.6e-3	1.3e-3	5.0e-4
	RK4	5.0e-2	2.5e-2	1.3e-2	2.5e-3	1.0e-3
-10.0	RK1	1.3e-2	6.3e-3	3.1e-3	1.3e-3	1.0e-3
	RK4	2.5e-2	1.3e-2	6.3e-3	1.0e-2	2.0e-3
-1.0	RK1	2.5e-2	1.3e-2	6.3e-3	5.0e-3	2.0e-3
	RK4	5.0e-2	2.5e-2	1.3e-2	5.0e-3	2.0e-3
0.0	RK1	1.0e-1	5.0e-2	5.0e-2	1.0e-2	2.0e-3
	RK4	1.0e-1	5.0e-2	5.0e-2	1.0e-2	2.0e-3
0.1	RK1	2.5e-2	1.3e-2	6.3e-3	2.5e-3	2.0e-3
	RK4	1.0e-1	5.0e-2	2.5e-2	1.0e-2	2.0e-3

Table 4.20: Time steps τ used in the numerical computations, Brooks-Corey model functions, CS \rightarrow FS.

Runge Kutta RK1 method, I = 100, 200, 400, 800 and 1600 divisions, L_1 norms									
R^L	100	ECC_1	200	ECC_2	400	ECC_3	800	ECC_4	1600
0.1	3.8e-3	0.51	2.7e-3	0.67	1.7e-3	0.74	1.0e-3	0.82	5.7e-4
0	4.0e-3	0.53	2.8e-3	0.68	1.7e-3	0.76	1.0e-3	0.81	5.8e-4
-1	5.1e-3	0.59	3.4e-3	0.76	2.0e-3	0.69	1.2e-3	1.12	5.7e-4
-10	4.8e-3	0.51	3.4e-3	0.77	2.0e-3	1.03	9.6e-4	0.66	6.1e-4
-100	1.6e-2	1.13	7.3e-3	0.91	3.9e-3	0.91	2.1e-3	0.89	1.1e-3
-1000	3.7e-2	0.81	2.1e-2	0.89	1.2e-2	0.89	6.2e-3	0.97	3.2e-3
-1942	4.5e-2	0.81	2.6e-2	0.86	1.4e-2	0.89	7.6e-3	0.98	3.9e-3

Runge Kutta RK4 method, I = 100, 200, 400, 800 and 1600 divisions, L_1 norms									
R^L	100	ECC_1	200	ECC_2	400	ECC_3	800	ECC_4	1600
0.1	3.9e-3	0.52	2.7e-3	0.67	1.7e-3	0.74	1.0e-3	0.79	5.9e-4
0	4.0e-3	0.53	2.8e-3	0.68	1.7e-3	0.76	1.0e-3	0.81	5.8e-4
-1	4.2e-3	0.55	2.9e-3	0.73	1.7e-3	0.84	9.7e-4	0.89	5.3e-4
-10	2.9e-3	0.36	2.2e-3	0.66	1.4e-3	0.42	1.1e-3	1.35	4.1e-4
-100	1.6e-2	1.14	7.2e-3	0.93	3.8e-3	0.93	2.0e-3	0.91	1.1e-3
-1000	3.3e-2	0.82	1.9e-2	0.90	1.0e-2	0.79	5.8e-3	0.86	3.2e-3
-1942	4.0e-2	0.86	2.2e-2	0.88	1.2e-2	0.78	7.1e-3	0.84	3.9e-3

Table 4.21: Experimental order of convergence computed from the L_1 norms for the Brooks-Corey model functions, coarse to fine sand flow (CS \rightarrow FS).

4.3. APPLICABILITY IN HETEROGENEOUS MEDIA

Runge Kutta RK1 method, I = 100, 200, 400, 800 and 1600 divisions, L_2 norms									
R^L	100	ECC_1	200	ECC_2	400	ECC_3	800	ECC_4	1600
0.1	1.1e-2	0.48	7.7e-3	0.61	5.0e-3	0.66	3.2e-3	0.69	2.0e-3
0	1.1e-2	0.49	7.9e-3	0.62	5.1e-3	0.67	3.2e-3	0.69	2.0e-3
-1	1.4e-2	0.53	9.4e-3	0.69	5.8e-3	0.65	3.7e-3	0.93	2.0e-3
-10	1.6e-2	0.51	1.1e-2	0.68	7.0e-3	0.89	3.8e-3	0.68	2.3e-3
-100	4.2e-2	0.72	2.5e-2	0.71	1.5e-2	0.62	1.0e-2	0.90	5.4e-3
-1000	8.4e-2	0.53	5.8e-2	0.58	3.9e-2	0.69	2.4e-2	0.62	1.6e-2
-1942	9.5e-2	0.51	6.7e-2	0.56	4.5e-2	0.66	2.9e-2	0.60	1.9e-2

Runge Kutta RK4 method, I = 100, 200, 400, 800 and 1600 divisions, L_2 norms									
R^L	100	ECC_1	200	ECC_2	400	ECC_3	800	ECC_4	1600
0.1	1.1e-2	0.48	7.7e-3	0.62	5.1e-3	0.66	3.2e-3	0.68	2.0e-3
0	1.1e-2	0.49	7.9e-3	0.62	5.1e-3	0.67	3.2e-3	0.69	2.0e-3
-1	1.2e-2	0.50	8.4e-3	0.67	5.3e-3	0.74	3.2e-3	0.75	1.9e-3
-10	1.1e-2	0.35	8.7e-3	0.63	5.6e-3	0.49	4.0e-3	1.11	1.8e-3
-100	4.4e-2	0.72	2.7e-2	0.72	1.6e-2	1.00	8.0e-3	0.86	4.4e-3
-1000	8.3e-2	0.54	5.7e-2	0.60	3.8e-2	0.65	2.4e-2	0.83	1.4e-2
-1942	9.4e-2	0.53	6.5e-2	0.58	4.4e-2	0.63	2.8e-2	0.79	1.6e-2

Table 4.22: Experimental order of convergence computed from the L_2 norms for the Brooks-Corey model functions, coarse to fine sand flow (CS \rightarrow FS).

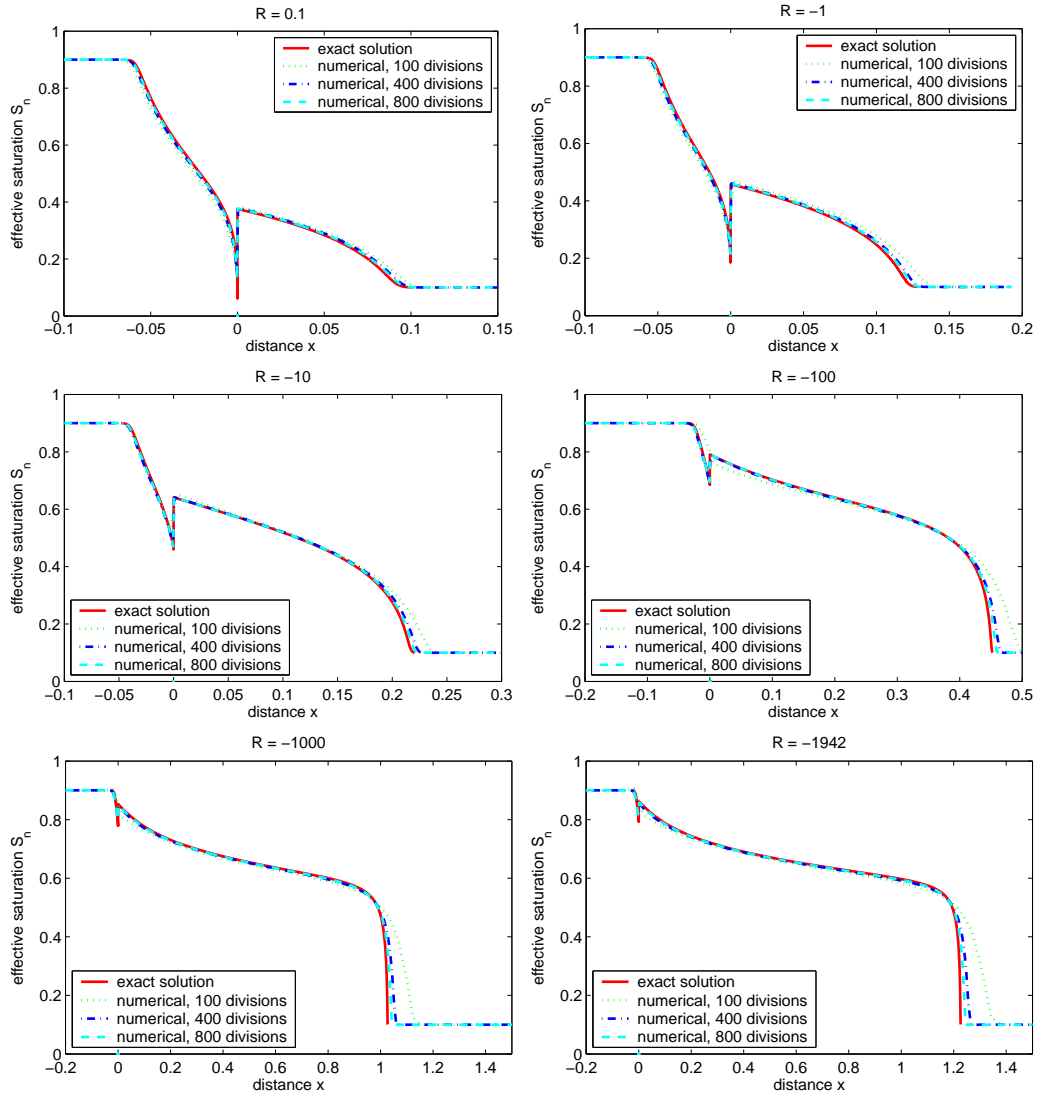


Figure 4.5: Exact and numerical solutions for the Brooks-Corey model functions at time $t = 1000$ s for various S_0 , heterogeneous porous medium, coarse to fine sand flow (CS \rightarrow FS). Numerical solutions computed using the standard Runge Kutta RK4 method with $\varepsilon_t = 10^{-5}$.

BROOKS-COREY MODEL FUNCTIONS, FS \rightarrow CS

R^L	RK	100	200	400	800	1600
-1000.0	RK1	1.6e-3	7.8e-4	3.9e-4	1.6e-4	6.3e-5
	RK4	3.1e-3	1.6e-3	7.8e-4	3.1e-4	5.0e-4
-100.0	RK1	1.6e-3	7.8e-4	3.9e-4	1.6e-4	6.3e-5
	RK4	3.1e-3	1.6e-3	7.8e-4	3.1e-4	5.0e-4
-10.0	RK1	1.6e-3	7.8e-4	3.9e-4	3.1e-4	1.3e-4
	RK4	1.3e-2	6.3e-3	3.1e-3	1.3e-3	2.5e-4
-1.0	RK1	6.3e-3	3.1e-3	1.6e-3	1.3e-3	5.0e-4
	RK4	5.0e-2	2.5e-2	1.3e-2	2.5e-3	1.0e-3
0.0	RK1	1.0e-1	5.0e-2	5.0e-2	1.0e-2	2.0e-3
	RK4	1.0e-1	5.0e-2	5.0e-2	1.0e-2	2.0e-3
0.1	RK1	1.0e-1	5.0e-2	2.5e-2	1.0e-2	2.0e-3
	RK4	1.0e-1	5.0e-2	5.0e-2	1.0e-2	2.0e-3
0.2	RK1	5.0e-2	2.5e-2	1.3e-2	5.0e-3	2.0e-3
	RK4	1.0e-1	5.0e-2	5.0e-2	1.0e-2	2.0e-3
0.3	RK1	2.5e-2	1.3e-2	6.3e-3	5.0e-3	2.0e-3
	RK4	1.0e-1	5.0e-2	5.0e-2	1.0e-2	2.0e-3
0.4	RK1	2.5e-2	1.3e-2	6.3e-3	2.5e-3	2.0e-3
	RK4	1.0e-1	5.0e-2	2.5e-2	1.0e-2	2.0e-3
0.5	RK1	2.5e-2	1.3e-2	6.3e-3	2.5e-3	1.0e-3
	RK4	1.0e-1	5.0e-2	2.5e-2	1.0e-2	2.0e-3
0.6	RK1	1.3e-2	6.3e-3	3.1e-3	2.5e-3	1.0e-3
	RK4	1.0e-1	5.0e-2	2.5e-2	1.0e-2	2.0e-3
0.8	RK1	1.3e-2	6.3e-3	3.1e-3	1.3e-3	5.0e-4
	RK4	5.0e-2	2.5e-2	1.3e-2	5.0e-3	2.0e-3
0.9	RK1	6.3e-3	3.1e-3	1.6e-3	6.3e-4	5.0e-4
	RK4	5.0e-2	2.5e-2	1.3e-2	5.0e-3	2.0e-3

Table 4.23: Time steps τ used in the numerical computations, Brooks-Corey model functions, FS \rightarrow CS.

Runge Kutta RK1 method, I = 100, 200, 400, 800 and 1600 divisions, L_1 norms									
R^L	100	ECC_1	200	ECC_2	400	ECC_3	800	ECC_4	1600
0.9	1.4e-3	1.17	6.0e-4	0.70	3.7e-4	0.69	2.3e-4	1.06	1.1e-4
0.8	5.6e-3	2.88	7.6e-4	0.88	4.1e-4	0.80	2.4e-4	1.02	1.2e-4
0.6	1.2e-3	0.63	7.4e-4	0.69	4.6e-4	0.84	2.6e-4	0.92	1.4e-4
0.5	4.5e-3	2.56	7.7e-4	0.83	4.3e-4	0.70	2.7e-4	0.96	1.4e-4
0.4	1.5e-3	0.97	7.5e-4	0.63	4.8e-4	0.85	2.7e-4	0.87	1.5e-4
0.3	6.1e-3	2.62	9.8e-4	1.25	4.2e-4	0.59	2.8e-4	0.93	1.5e-4
0.2	1.2e-3	0.57	8.2e-4	0.70	5.1e-4	0.93	2.7e-4	0.90	1.4e-4
0.1	1.2e-3	0.50	8.6e-4	0.72	5.2e-4	0.88	2.8e-4	1.01	1.4e-4
0	1.4e-3	0.70	8.8e-4	0.84	4.9e-4	0.90	2.6e-4	0.94	1.4e-4
-1	1.2e-3	0.79	6.8e-4	0.63	4.4e-4	0.73	2.7e-4	0.87	1.5e-4
-10	1.9e-3	0.76	1.1e-3	0.83	6.2e-4	0.96	3.2e-4	0.83	1.8e-4
-100	4.0e-3	0.83	2.3e-3	0.83	1.3e-3	0.83	7.2e-4	0.87	4.0e-4
-1000	9.1e-3	0.87	5.0e-3	0.86	2.7e-3	0.85	1.5e-3	0.87	8.3e-4
-8906	1.1e-2	0.87	6.2e-3	0.86	3.4e-3	0.85	1.9e-3	0.87	1.0e-3
Runge Kutta RK4 method, I = 100, 200, 400, 800 and 1600 divisions, L_1 norms									
R^L	100	ECC_1	200	ECC_2	400	ECC_3	800	ECC_4	1600
0.9	3.6e-3	2.56	6.1e-4	0.72	3.7e-4	0.91	2.0e-4	1.07	9.4e-5
0.8	1.5e-3	1.23	6.3e-4	0.64	4.0e-4	0.91	2.1e-4	1.02	1.1e-4
0.6	2.7e-3	2.09	6.4e-4	0.60	4.2e-4	0.76	2.5e-4	1.06	1.2e-4
0.5	1.2e-3	0.75	7.4e-4	0.67	4.6e-4	0.87	2.5e-4	1.04	1.2e-4
0.4	1.1e-3	0.47	8.1e-4	1.13	3.7e-4	0.53	2.6e-4	1.01	1.3e-4
0.3	1.3e-3	0.57	8.5e-4	0.82	4.8e-4	0.89	2.6e-4	0.99	1.3e-4
0.2	1.3e-3	0.64	8.6e-4	0.78	5.0e-4	0.95	2.6e-4	0.97	1.3e-4
0.1	1.4e-3	0.68	8.7e-4	0.80	5.0e-4	0.94	2.6e-4	0.96	1.3e-4
0	1.4e-3	0.70	8.8e-4	0.84	4.9e-4	0.91	2.6e-4	0.94	1.4e-4
-1	1.3e-3	0.59	8.5e-4	0.77	5.0e-4	0.79	2.9e-4	0.92	1.5e-4
-10	1.7e-3	0.71	1.0e-3	0.80	5.9e-4	0.76	3.5e-4	0.89	1.9e-4
-100	4.2e-3	0.80	2.4e-3	0.84	1.4e-3	0.87	7.4e-4	0.96	3.8e-4
-1000	8.6e-3	0.80	5.0e-3	0.83	2.8e-3	0.86	1.5e-3	0.94	8.1e-4
-8906	1.1e-2	0.80	6.2e-3	0.82	3.5e-3	0.85	1.9e-3	0.93	1.0e-3

Table 4.24: Experimental order of convergence computed from the L_1 norms for the Brooks-Corey model functions, fine to coarse sand flow (FS \rightarrow CS).

4.3. APPLICABILITY IN HETEROGENEOUS MEDIA

Runge Kutta RK1 method, I = 100, 200, 400, 800 and 1600 divisions, L_2 norms									
R^L	100	ECC_1	200	ECC_2	400	ECC_3	800	ECC_4	1600
0.9	6.1e-3	0.89	3.3e-3	0.51	2.3e-3	0.57	1.6e-3	0.60	1.0e-3
0.8	2.2e-2	2.68	3.5e-3	0.70	2.1e-3	0.54	1.5e-3	0.63	9.4e-4
0.6	4.6e-3	0.50	3.2e-3	0.54	2.2e-3	0.72	1.4e-3	0.63	8.8e-4
0.5	1.6e-2	2.36	3.1e-3	0.67	2.0e-3	0.51	1.4e-3	0.67	8.7e-4
0.4	5.2e-3	0.75	3.1e-3	0.50	2.2e-3	0.64	1.4e-3	0.74	8.5e-4
0.3	2.1e-2	2.53	3.7e-3	0.99	1.9e-3	0.44	1.4e-3	0.67	8.6e-4
0.2	4.5e-3	0.42	3.4e-3	0.56	2.3e-3	0.85	1.3e-3	0.55	8.7e-4
0.1	4.6e-3	0.39	3.5e-3	0.59	2.3e-3	0.70	1.4e-3	0.72	8.8e-4
0	6.5e-3	0.59	4.3e-3	0.72	2.6e-3	0.78	1.5e-3	0.77	8.9e-4
-1	5.9e-3	0.42	4.4e-3	0.65	2.8e-3	0.76	1.7e-3	0.80	9.5e-4
-10	9.4e-3	0.64	6.1e-3	0.74	3.6e-3	0.83	2.0e-3	0.81	1.2e-3
-100	1.8e-2	0.59	1.2e-2	0.65	7.8e-3	0.72	4.7e-3	0.80	2.7e-3
-1000	3.2e-2	0.52	2.2e-2	0.57	1.5e-2	0.63	9.7e-3	0.70	6.0e-3
-8906	3.7e-2	0.50	2.6e-2	0.54	1.8e-2	0.61	1.2e-2	0.67	7.5e-3
Runge Kutta RK4 method, I = 100, 200, 400, 800 and 1600 divisions, L_2 norms									
R^L	100	ECC_1	200	ECC_2	400	ECC_3	800	ECC_4	1600
0.9	1.7e-2	2.28	3.4e-3	0.57	2.3e-3	0.55	1.6e-3	0.59	1.0e-3
0.8	5.9e-3	0.91	3.1e-3	0.49	2.2e-3	0.59	1.5e-3	0.64	9.4e-4
0.6	9.7e-3	1.74	2.9e-3	0.50	2.1e-3	0.55	1.4e-3	0.66	8.9e-4
0.5	4.7e-3	0.55	3.2e-3	0.52	2.2e-3	0.64	1.4e-3	0.69	8.8e-4
0.4	4.6e-3	0.39	3.5e-3	0.97	1.8e-3	0.34	1.4e-3	0.71	8.8e-4
0.3	5.2e-3	0.46	3.8e-3	0.78	2.2e-3	0.60	1.5e-3	0.73	8.8e-4
0.2	5.8e-3	0.53	4.0e-3	0.73	2.4e-3	0.71	1.5e-3	0.74	8.8e-4
0.1	6.2e-3	0.56	4.2e-3	0.72	2.5e-3	0.75	1.5e-3	0.76	8.9e-4
0	6.5e-3	0.59	4.3e-3	0.72	2.6e-3	0.78	1.5e-3	0.77	8.9e-4
-1	7.0e-3	0.56	4.7e-3	0.71	2.9e-3	0.81	1.6e-3	0.81	9.4e-4
-10	8.9e-3	0.61	5.8e-3	0.72	3.5e-3	0.79	2.0e-3	0.82	1.2e-3
-100	1.8e-2	0.58	1.2e-2	0.65	7.7e-3	0.73	4.7e-3	0.82	2.6e-3
-1000	3.1e-2	0.51	2.2e-2	0.56	1.5e-2	0.63	9.5e-3	0.70	5.8e-3
-8906	3.6e-2	0.49	2.5e-2	0.54	1.8e-2	0.60	1.2e-2	0.67	7.3e-3

Table 4.25: Experimental order of convergence computed from the L_2 norms for the Brooks-Corey model functions, fine to coarse sand flow (FS \rightarrow CS).

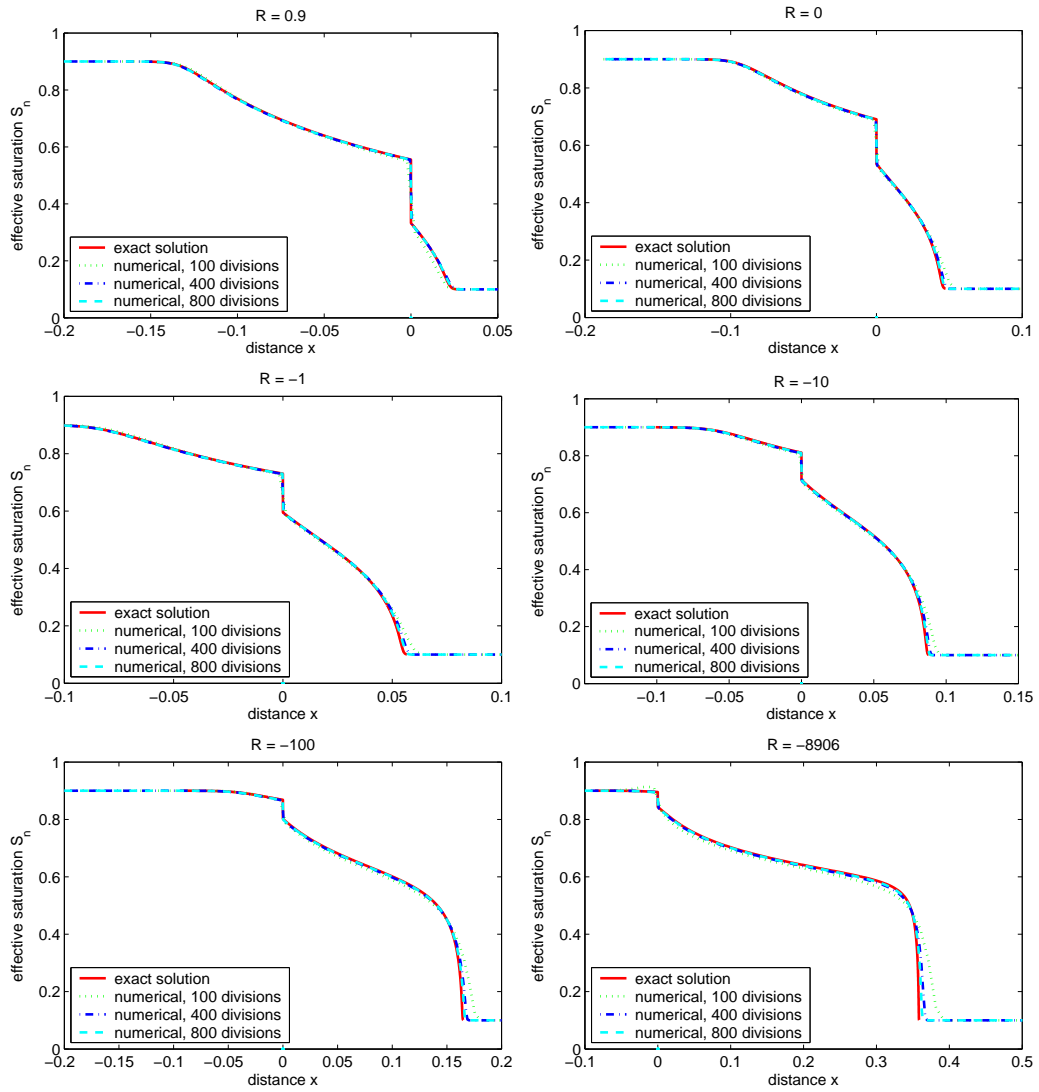


Figure 4.6: Exact and numerical solutions for the Brooks-Corey model functions at time $t = 1000$ s for various S_0 , heterogeneous porous medium, coarse to fine sand flow (FS \rightarrow CS). Numerical solutions computed using the standard Runge Kutta RK4 method with $\varepsilon_t = 10^{-5}$.

VAN GENUCHTEN MODEL FUNCTIONS, CS \rightarrow FS

R^L	RK	100	200	400	800	1600
-10.0	RK1	5.0e-2	2.5e-2	1.3e-2	5.0e-3	2.0e-3
	RK4	1.0e-1	5.0e-2	2.5e-2	1.0e-2	2.0e-3
-1.0	RK1	1.0e-1	5.0e-2	5.0e-2	1.0e-2	2.0e-3
	RK4	1.0e-1	5.0e-2	5.0e-2	1.0e-2	2.0e-3
0.0	RK1	1.0e-1	5.0e-2	5.0e-2	1.0e-2	2.0e-3
	RK4	1.0e-1	5.0e-2	5.0e-2	1.0e-2	2.0e-3
0.1	RK1	1.0e-1	5.0e-2	2.5e-2	1.0e-2	2.0e-3
	RK4	1.0e-1	5.0e-2	5.0e-2	1.0e-2	2.0e-3
0.2	RK1	5.0e-2	2.5e-2	1.3e-2	1.0e-2	2.0e-3
	RK4	1.0e-1	5.0e-2	5.0e-2	1.0e-2	2.0e-3
0.3	RK1	5.0e-2	2.5e-2	1.3e-2	5.0e-3	2.0e-3
	RK4	1.0e-1	5.0e-2	5.0e-2	1.0e-2	2.0e-3
0.4	RK1	2.5e-2	1.3e-2	6.3e-3	2.5e-3	2.0e-3
	RK4	1.0e-1	5.0e-2	5.0e-2	1.0e-2	2.0e-3
0.5	RK1	2.5e-2	1.3e-2	6.3e-3	2.5e-3	1.0e-3
	RK4	1.0e-1	5.0e-2	5.0e-2	1.0e-2	2.0e-3
0.6	RK1	1.3e-2	6.3e-3	3.1e-3	2.5e-3	1.0e-3
	RK4	1.0e-1	5.0e-2	2.5e-2	1.0e-2	2.0e-3
0.8	RK1	1.3e-2	6.3e-3	3.1e-3	1.3e-3	5.0e-4
	RK4	5.0e-2	2.5e-2	1.3e-2	1.0e-2	2.0e-3
0.9	RK1	6.3e-3	3.1e-3	1.6e-3	1.3e-3	5.0e-4
	RK4	5.0e-2	2.5e-2	1.3e-2	1.0e-2	2.0e-3

Table 4.26: Time steps τ used in the numerical computations, van Genuchten model functions, CS \rightarrow FS.

Runge Kutta RK1 method, I = 100, 200, 400, 800 and 1600 divisions, L_1 norms									
R^L	100	ECC_1	200	ECC_2	400	ECC_3	800	ECC_4	1600
0.9	1.5e-2	2.09	3.5e-3	1.97	8.9e-4	1.34	3.5e-4	1.05	1.7e-4
0.8	2.6e-2	2.32	5.3e-3	2.18	1.2e-3	1.82	3.3e-4	0.44	2.4e-4
0.6	1.2e-1	2.35	2.3e-2	2.37	4.4e-3	2.41	8.3e-4	1.90	2.2e-4
0.5	1.1e-1	2.16	2.5e-2	2.40	4.8e-3	2.52	8.3e-4	1.52	2.9e-4
0.4	1.1e-1	2.08	2.6e-2	2.42	4.8e-3	2.53	8.4e-4	1.49	3.0e-4
0.3	1.1e-1	1.97	2.7e-2	2.44	5.0e-3	2.56	8.4e-4	1.42	3.2e-4
0.2	1.0e-1	1.89	2.8e-2	2.45	5.1e-3	2.57	8.6e-4	1.37	3.3e-4
0.1	1.0e-1	1.81	2.8e-2	2.44	5.2e-3	2.54	9.0e-4	1.35	3.5e-4
0	9.6e-2	1.71	2.9e-2	2.42	5.5e-3	2.45	1.0e-3	1.42	3.7e-4
-1	6.8e-2	1.04	3.3e-2	2.10	7.7e-3	2.07	1.8e-3	1.83	5.2e-4
-10	4.0e-2	0.08	3.8e-2	1.66	1.2e-2	0.94	6.2e-3	2.28	1.3e-3
-100	1.2e-1	1.01	5.8e-2	1.00	2.9e-2	1.14	1.3e-2	1.45	4.8e-3
-1000	2.0e-1	1.05	9.5e-2	1.02	4.7e-2	0.50	3.3e-2	1.21	1.4e-2
-2079	2.6e-1	1.04	1.3e-1	1.03	6.3e-2	0.53	4.4e-2	1.31	1.8e-2
Runge Kutta RK4 method, I = 100, 200, 400, 800 and 1600 divisions, L_1 norms									
R^L	100	ECC_1	200	ECC_2	400	ECC_3	800	ECC_4	1600
0.9	1.7e-2	2.12	3.8e-3	2.02	9.4e-4	1.21	4.1e-4	1.50	1.4e-4
0.8	2.3e-2	2.29	4.7e-3	2.11	1.1e-3	1.56	3.7e-4	1.05	1.8e-4
0.6	1.1e-1	2.41	2.2e-2	2.43	4.0e-3	2.54	6.9e-4	1.80	2.0e-4
0.5	1.1e-1	2.26	2.3e-2	2.52	4.1e-3	2.51	7.1e-4	1.67	2.2e-4
0.4	1.1e-1	2.05	2.6e-2	2.60	4.3e-3	2.34	8.5e-4	1.71	2.6e-4
0.3	1.0e-1	1.96	2.7e-2	2.56	4.6e-3	2.38	8.7e-4	1.58	2.9e-4
0.2	1.0e-1	1.88	2.8e-2	2.43	5.1e-3	2.49	9.1e-4	1.49	3.2e-4
0.1	9.8e-2	1.80	2.8e-2	2.43	5.2e-3	2.48	9.4e-4	1.43	3.5e-4
0	9.6e-2	1.71	2.9e-2	2.42	5.5e-3	2.45	1.0e-3	1.42	3.7e-4
-1	7.7e-2	1.12	3.5e-2	2.38	6.8e-3	2.24	1.4e-3	1.47	5.2e-4
-10	4.5e-2	0.08	4.3e-2	1.80	1.2e-2	2.14	2.8e-3	1.50	9.9e-4
-100	5.4e-2	0.54	3.7e-2	0.43	2.8e-2	0.87	1.5e-2	1.44	5.6e-3
-1000	1.4e-1	0.78	8.4e-2	0.61	5.5e-2	1.04	2.7e-2	0.61	1.8e-2
-2079	1.9e-1	0.78	1.1e-1	0.55	7.5e-2	1.15	3.4e-2	0.67	2.1e-2

Table 4.27: Experimental order of convergence computed from the L_1 norms for the van Genuchten model functions, coarse to fine sand flow (CS \rightarrow FS).

4.3. APPLICABILITY IN HETEROGENEOUS MEDIA

Runge Kutta RK1 method, I = 100, 200, 400, 800 and 1600 divisions, L_2 norms									
R^L	100	ECC_1	200	ECC_2	400	ECC_3	800	ECC_4	1600
0.9	2.7e-2	1.90	7.3e-3	1.12	3.4e-3	0.65	2.2e-3	0.58	1.4e-3
0.8	4.8e-2	2.18	1.1e-2	1.58	3.6e-3	0.71	2.2e-3	0.53	1.5e-3
0.6	2.0e-1	2.13	4.4e-2	2.28	9.1e-3	1.84	2.6e-3	0.77	1.5e-3
0.5	1.9e-1	1.96	4.9e-2	2.30	9.9e-3	1.93	2.6e-3	0.75	1.5e-3
0.4	1.9e-1	1.91	4.9e-2	2.36	9.6e-3	1.93	2.5e-3	0.69	1.6e-3
0.3	1.8e-1	1.81	5.1e-2	2.36	1.0e-2	1.97	2.6e-3	0.70	1.6e-3
0.2	1.8e-1	1.75	5.2e-2	2.39	1.0e-2	1.98	2.5e-3	0.67	1.6e-3
0.1	1.7e-1	1.67	5.4e-2	2.41	1.0e-2	1.96	2.6e-3	0.70	1.6e-3
0	1.7e-1	1.57	5.6e-2	2.34	1.1e-2	2.04	2.7e-3	0.75	1.6e-3
-1	1.4e-1	0.99	7.0e-2	1.89	1.9e-2	2.26	3.9e-3	1.22	1.7e-3
-10	7.7e-2	-0.09	8.2e-2	1.68	2.6e-2	1.43	9.5e-3	2.39	1.8e-3
-100	1.2e-1	0.99	6.0e-2	0.68	3.7e-2	0.85	2.1e-2	2.51	3.6e-3
-1000	7.2e-2	0.94	3.8e-2	0.89	2.0e-2	-0.21	2.3e-2	1.09	1.1e-2
-2079	8.5e-2	0.92	4.5e-2	0.85	2.5e-2	-0.32	3.1e-2	1.62	1.0e-2
Runge Kutta RK4 method, I = 100, 200, 400, 800 and 1600 divisions, L_2 norms									
R^L	100	ECC_1	200	ECC_2	400	ECC_3	800	ECC_4	1600
0.9	3.2e-2	1.94	8.3e-3	1.27	3.4e-3	0.65	2.2e-3	0.62	1.4e-3
0.8	4.2e-2	2.18	9.3e-3	1.43	3.5e-3	0.66	2.2e-3	0.60	1.4e-3
0.6	1.9e-1	2.19	4.2e-2	2.31	8.6e-3	1.80	2.5e-3	0.73	1.5e-3
0.5	1.9e-1	2.05	4.6e-2	2.46	8.3e-3	1.73	2.5e-3	0.73	1.5e-3
0.4	1.8e-1	1.87	5.1e-2	2.51	8.9e-3	1.74	2.7e-3	0.79	1.5e-3
0.3	1.8e-1	1.79	5.2e-2	2.46	9.4e-3	1.83	2.7e-3	0.77	1.6e-3
0.2	1.8e-1	1.72	5.3e-2	2.34	1.1e-2	1.98	2.7e-3	0.76	1.6e-3
0.1	1.7e-1	1.65	5.4e-2	2.34	1.1e-2	2.01	2.7e-3	0.74	1.6e-3
0	1.7e-1	1.57	5.6e-2	2.34	1.1e-2	2.04	2.7e-3	0.75	1.6e-3
-1	1.4e-1	1.06	6.8e-2	2.34	1.3e-2	2.16	3.0e-3	0.82	1.7e-3
-10	7.9e-2	-0.09	8.4e-2	1.90	2.2e-2	2.52	3.9e-3	1.31	1.6e-3
-100	3.2e-2	-0.02	3.2e-2	-0.16	3.6e-2	1.01	1.8e-2	2.33	3.5e-3
-1000	6.5e-2	0.65	4.2e-2	0.26	3.5e-2	1.01	1.7e-2	0.35	1.4e-2
-2079	7.7e-2	0.63	5.0e-2	0.18	4.4e-2	1.23	1.9e-2	0.45	1.4e-2

Table 4.28: Experimental order of convergence computed from the L_2 norms for the van Genuchten model functions, coarse to fine sand flow (CS \rightarrow FS).

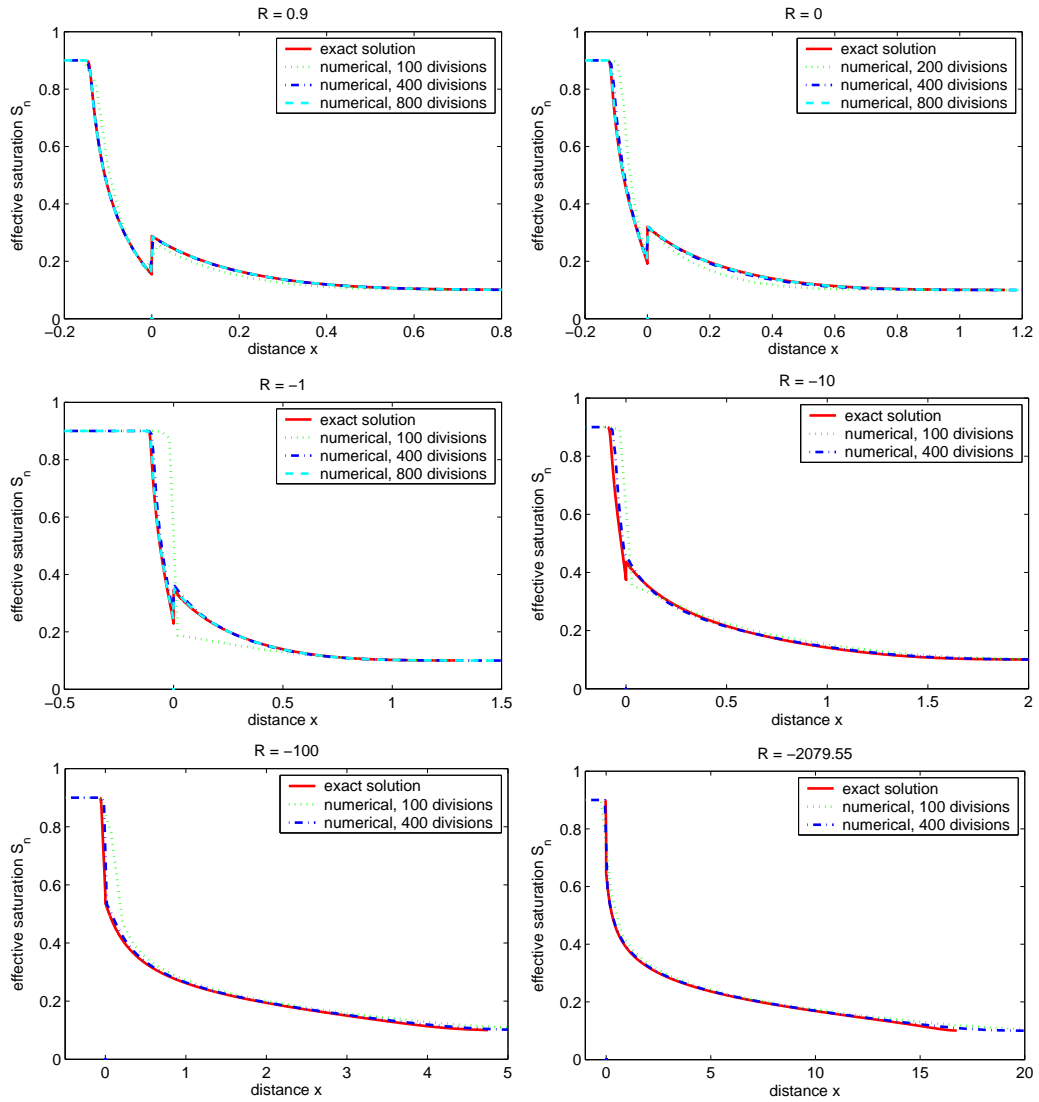


Figure 4.7: Exact and numerical solutions for the van Genuchten model functions at time $t = 1000$ s for various S_0 , heterogeneous porous medium, coarse to fine sand flow (CS \rightarrow FS). Numerical solutions computed using the standard Runge Kutta RK4 method with $\varepsilon_t = 10^{-5}$.

VAN GENUCHTEN MODEL FUNCTIONS, FS \rightarrow CS

R^L	RK	100	200	400	800	1600
-100.0	RK1	1.3e-2	6.3e-3	3.1e-3	1.3e-3	1.0e-3
	RK4	1.0e-1	5.0e-2	2.5e-2	1.0e-2	2.0e-3
-10.0	RK1	2.5e-2	1.3e-2	6.3e-3	2.5e-3	1.0e-3
	RK4	5.0e-2	2.5e-2	1.3e-2	5.0e-3	2.0e-3
-1.0	RK1	5.0e-2	2.5e-2	1.3e-2	1.0e-2	2.0e-3
	RK4	1.0e-1	5.0e-2	2.5e-2	1.0e-2	2.0e-3
0.0	RK1	1.0e-1	5.0e-2	5.0e-2	1.0e-2	2.0e-3
	RK4	1.0e-1	5.0e-2	5.0e-2	1.0e-2	2.0e-3
0.1	RK1	5.0e-2	2.5e-2	1.3e-2	5.0e-3	2.0e-3
	RK4	1.0e-1	5.0e-2	5.0e-2	1.0e-2	2.0e-3
0.2	RK1	2.5e-2	1.3e-2	6.3e-3	2.5e-3	1.0e-3
	RK4	1.0e-1	5.0e-2	2.5e-2	1.0e-2	2.0e-3
0.3	RK1	1.3e-2	6.3e-3	3.1e-3	1.3e-3	5.0e-4
	RK4	5.0e-2	2.5e-2	1.3e-2	1.0e-2	2.0e-3
0.4	RK1	6.3e-3	3.1e-3	1.6e-3	1.3e-3	5.0e-4
	RK4	5.0e-2	2.5e-2	1.3e-2	5.0e-3	2.0e-3
0.5	RK1	6.3e-3	3.1e-3	1.6e-3	6.3e-4	2.5e-4
	RK4	2.5e-2	1.3e-2	6.3e-3	5.0e-3	2.0e-3
0.6	RK1	6.3e-3	3.1e-3	7.8e-4	6.3e-4	2.5e-4
	RK4	2.5e-2	1.3e-2	6.3e-3	2.5e-3	2.0e-3
0.8	RK1	3.1e-3	1.6e-3	7.8e-4	3.1e-4	1.3e-4
	RK4	1.3e-2	6.3e-3	3.1e-3	1.3e-3	1.0e-3
0.9	RK1	1.6e-3	7.8e-4	3.9e-4	3.1e-4	1.3e-4
	RK4	1.3e-2	6.3e-3	3.1e-3	1.3e-3	5.0e-4

Table 4.29: Time steps τ used in the numerical computations, van Genuchten model functions, FS \rightarrow CS.

Runge Kutta RK1 method, I = 100, 200, 400, 800 and 1600 divisions, L_1 norms									
R^L	100	ECC_1	200	ECC_2	400	ECC_3	800	ECC_4	1600
0.9	8.0e-4	1.00	4.0e-4	1.02	2.0e-4	1.23	8.5e-5	1.14	3.8e-5
0.8	7.4e-3	1.00	3.7e-3	1.00	1.8e-3	1.01	9.2e-4	0.94	4.8e-4
0.6	7.7e-4	0.68	4.8e-4	0.84	2.7e-4	1.02	1.3e-4	0.97	6.7e-5
0.5	9.1e-4	1.17	4.1e-4	0.66	2.6e-4	0.60	1.7e-4	1.00	8.5e-5
0.4	1.4e-3	1.53	4.7e-4	0.62	3.1e-4	0.92	1.6e-4	0.91	8.7e-5
0.3	4.2e-3	2.46	7.5e-4	1.90	2.0e-4	0.55	1.4e-4	0.45	1.0e-4
0.2	1.3e-2	2.39	2.4e-3	2.39	4.6e-4	2.06	1.1e-4	0.11	1.0e-4
0.1	1.4e-2	2.36	2.8e-3	2.35	5.4e-4	2.22	1.2e-4	0.47	8.4e-5
0	1.5e-2	2.32	3.0e-3	2.34	5.9e-4	2.34	1.2e-4	0.72	7.1e-5
-1	1.4e-2	2.08	3.4e-3	1.42	1.3e-3	0.30	1.0e-3	2.28	2.1e-4
-10	2.3e-2	1.59	7.7e-3	1.24	3.2e-3	1.28	1.3e-3	1.17	5.9e-4
-100	3.3e-2	0.50	2.3e-2	0.99	1.2e-2	0.84	6.5e-3	1.10	3.0e-3
-666	8.3e-2	0.68	5.2e-2	0.63	3.3e-2	0.66	2.1e-2	0.97	1.1e-2
Runge Kutta RK4 method, I = 100, 200, 400, 800 and 1600 divisions, L_1 norms									
R^L	100	ECC_1	200	ECC_2	400	ECC_3	800	ECC_4	1600
0.9	5.9e-4	0.99	3.0e-4	1.02	1.5e-4	1.17	6.5e-5	1.08	3.1e-5
0.8	7.5e-3	1.06	3.6e-3	1.00	1.8e-3	0.96	9.2e-4	1.01	4.6e-4
0.6	6.4e-4	0.74	3.8e-4	0.78	2.2e-4	0.68	1.4e-4	1.02	6.9e-5
0.5	9.1e-4	0.95	4.7e-4	0.74	2.8e-4	0.97	1.4e-4	0.94	7.5e-5
0.4	1.7e-3	2.23	3.5e-4	0.52	2.5e-4	0.47	1.8e-4	1.16	7.9e-5
0.3	3.4e-3	2.41	6.5e-4	1.38	2.5e-4	0.72	1.5e-4	0.95	7.8e-5
0.2	1.2e-2	2.42	2.3e-3	2.63	3.8e-4	1.92	9.9e-5	0.54	6.8e-5
0.1	1.4e-2	2.36	2.8e-3	2.47	5.0e-4	2.23	1.1e-4	0.61	6.9e-5
0	1.5e-2	2.32	3.0e-3	2.34	5.9e-4	2.33	1.2e-4	0.71	7.1e-5
-1	1.7e-2	2.17	3.7e-3	2.12	8.5e-4	1.85	2.4e-4	1.19	1.0e-4
-10	2.5e-2	1.80	7.3e-3	1.52	2.6e-3	1.23	1.1e-3	0.84	6.1e-4
-100	3.3e-2	0.76	2.0e-2	0.91	1.0e-2	0.86	5.7e-3	0.55	3.9e-3
-666	1.0e-1	0.79	6.0e-2	0.53	4.1e-2	1.13	1.9e-2	0.52	1.3e-2

Table 4.30: Experimental order of convergence computed from the L_1 norms for the van Genuchten model functions, fine to coarse sand flow (FS \rightarrow CS).

4.3. APPLICABILITY IN HETEROGENEOUS MEDIA

Runge Kutta RK1 method, I = 100, 200, 400, 800 and 1600 divisions, L_2 norms									
R^L	100	ECC_1	200	ECC_2	400	ECC_3	800	ECC_4	1600
0.9	3.4e-3	0.69	2.1e-3	0.61	1.4e-3	0.60	9.0e-4	0.59	6.0e-4
0.8	1.9e-2	0.85	1.0e-2	0.81	5.9e-3	0.75	3.5e-3	0.63	2.3e-3
0.6	2.8e-3	0.71	1.7e-3	0.66	1.1e-3	0.67	6.7e-4	0.62	4.4e-4
0.5	2.5e-3	0.83	1.4e-3	0.59	9.5e-4	0.52	6.6e-4	0.70	4.1e-4
0.4	2.9e-3	1.06	1.4e-3	0.57	9.4e-4	0.71	5.8e-4	0.67	3.6e-4
0.3	9.4e-3	2.42	1.7e-3	1.32	7.0e-4	0.56	4.8e-4	0.48	3.4e-4
0.2	2.8e-2	2.36	5.5e-3	2.40	1.0e-3	1.37	4.0e-4	0.38	3.1e-4
0.1	3.1e-2	2.32	6.3e-3	2.41	1.2e-3	1.71	3.6e-4	0.56	2.5e-4
0	3.3e-2	2.22	7.1e-3	2.27	1.5e-3	2.11	3.4e-4	0.77	2.0e-4
-1	3.8e-2	1.76	1.1e-2	1.52	3.9e-3	0.78	2.3e-3	2.45	4.1e-4
-10	4.5e-2	1.68	1.4e-2	1.29	5.8e-3	1.24	2.4e-3	0.94	1.3e-3
-100	4.4e-2	0.38	3.4e-2	0.94	1.8e-2	0.80	1.0e-2	0.85	5.6e-3
-666	7.9e-2	0.41	5.9e-2	0.42	4.4e-2	0.52	3.1e-2	0.62	2.0e-2
Runge Kutta RK4 method, I = 100, 200, 400, 800 and 1600 divisions, L_2 norms									
R^L	100	ECC_1	200	ECC_2	400	ECC_3	800	ECC_4	1600
0.9	3.1e-3	0.65	2.0e-3	0.59	1.3e-3	0.57	9.0e-4	0.58	6.0e-4
0.8	1.9e-2	0.90	1.0e-2	0.81	5.8e-3	0.72	3.5e-3	0.65	2.2e-3
0.6	2.5e-3	0.73	1.5e-3	0.61	1.0e-3	0.55	6.9e-4	0.64	4.4e-4
0.5	2.5e-3	0.74	1.5e-3	0.63	9.9e-4	0.69	6.1e-4	0.64	3.9e-4
0.4	3.7e-3	1.58	1.2e-3	0.57	8.3e-4	0.47	6.0e-4	0.78	3.5e-4
0.3	7.6e-3	2.36	1.5e-3	0.97	7.6e-4	0.61	4.9e-4	0.68	3.1e-4
0.2	2.8e-2	2.37	5.4e-3	2.69	8.4e-4	1.10	3.9e-4	0.57	2.6e-4
0.1	3.2e-2	2.27	6.5e-3	2.50	1.2e-3	1.70	3.6e-4	0.63	2.3e-4
0	3.3e-2	2.22	7.1e-3	2.27	1.5e-3	2.10	3.4e-4	0.77	2.0e-4
-1	3.8e-2	1.98	9.6e-3	1.89	2.6e-3	2.00	6.5e-4	1.65	2.1e-4
-10	4.9e-2	2.02	1.2e-2	1.56	4.1e-3	1.04	2.0e-3	0.71	1.2e-3
-100	4.4e-2	0.51	3.1e-2	0.84	1.7e-2	0.85	9.6e-3	0.76	5.6e-3
-666	9.4e-2	0.57	6.3e-2	0.51	4.4e-2	0.58	3.0e-2	0.57	2.0e-2

Table 4.31: Experimental order of convergence computed from the L_2 norms for the van Genuchten model functions, fine to coarse sand flow (FS \rightarrow CS).

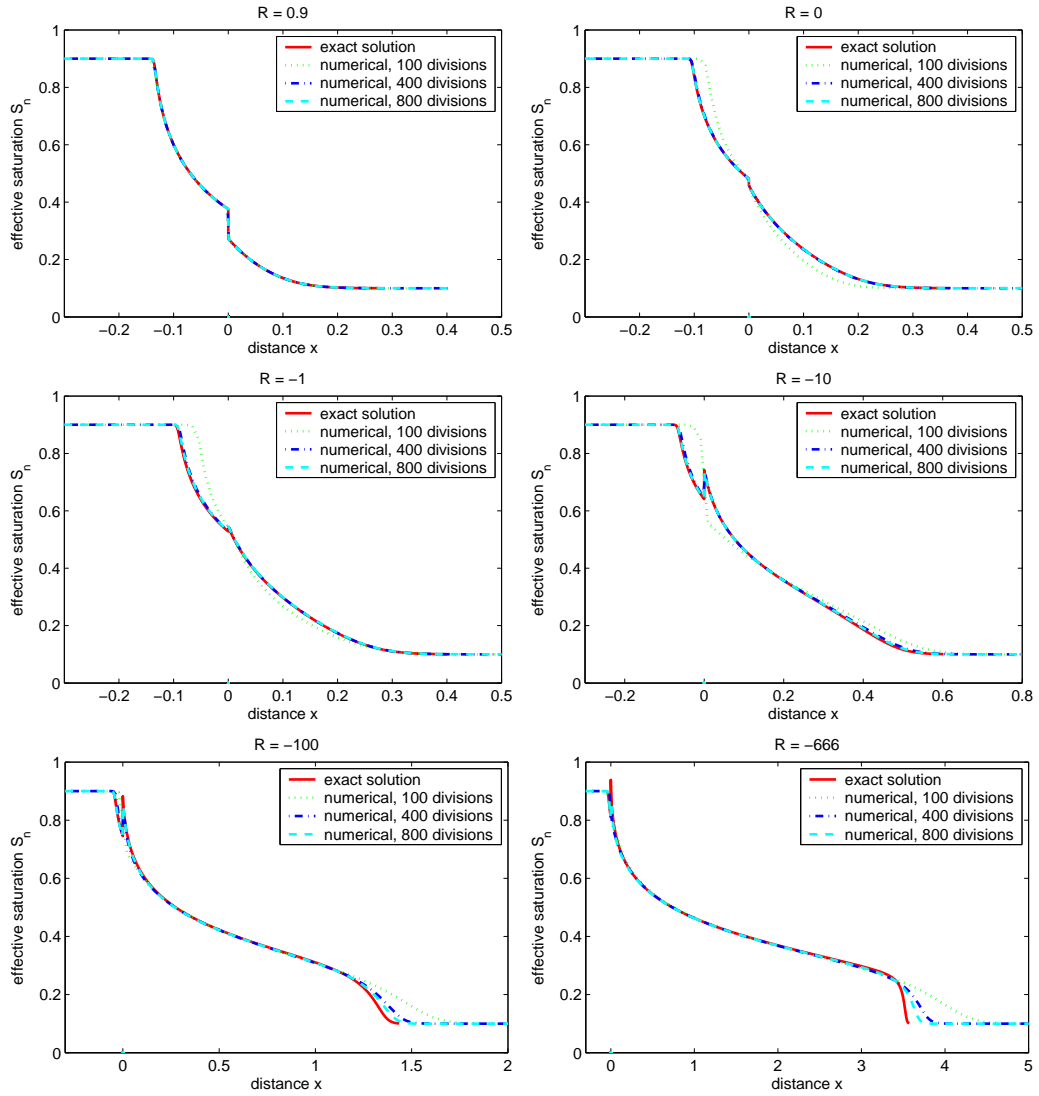


Figure 4.8: Exact and numerical solutions for the van Genuchten model functions at time $t = 1000$ s for various S_0 , heterogeneous porous medium, coarse to fine sand flow (FS \rightarrow CS). Numerical solutions computed using the standard Runge Kutta RK4 method with $\varepsilon_t = 10^{-5}$.

DISCUSSION OF RESULTS

Tables 4.21, 4.22, 4.24 and 4.25, resp. Tables 4.27, 4.28, 4.30 and 4.31 contain the experimental orders of convergence for various R^L and mesh division I computed using the L_1 and L_2 norms and using the Brooks and Corey, resp. van Genuchten model functions.

The fluid behaviour at the interface between the two subdomains is implemented in the numerical scheme via the continuous velocity of the displaced phase (4.31). The exact solution obtained using the algorithm described in Section 3.2.2, resp. Section 3.3.3 is using a couple of the Dirichlet boundary conditions \mathbb{S}_0^R and \mathbb{S}_0^L at $x = 0$ and the solution is composed of two exact solutions for the homogeneous porous media. The numerical solution depends on the exact solution only through the value of $A R$. With this respect, the interface implementation is independent of the exact solution. The resulting EOCs presented in Tables 4.21 to 4.31 confirm that the interface implementation (4.31) is correct.

The numerical method uses first order of the spatial discretization, which agree to the presented results.

4.3.2 Two Phase Flow in Heterogeneous Porous Media

The example used in Helmig, 1997 on the page 275 is selected in order to demonstrate applicability of the numerical scheme discussed in this chapter. A DNAPL is injected into a vertically placed fully water-saturated column consisting of two different sands. The situation is depicted in Figure 4.9. Note that the vertical axis x is oriented in the direction of the gravitational acceleration vector g and the origin $x = 0$ corresponds to the top of the column. The gravitational acceleration value is set as $g = 9.81 \text{ ms}^{-2}$.

The fluid and sand properties are shown in Table 4.32. According to Helmig, 1997, the van Genuchten and the Brooks and Corey model parameters correspond to the same soils ².

The input flux of the DNAPL, prescribed at $x = 0$, is given by

$$q_n(t, 0) = 0.05 \text{ kg s}^{-1} \text{ m}^{-2},$$

i.e. the input velocity of the DNAPL is given by

$$u_n(t, 0) = \frac{q_n(t, 0)}{\rho_n}.$$

²The issue concerning the van Genuchten and the Brooks-Corey parameter equivalence is described in Morel-Seytoux *et al.*, 1996

	Par.	Units	fine sand (FS)	coarse sand (CS)
Porosity	Φ	$[-]$	0.39	0.40
Intrinsic Permeability	K	$[m^2]$	$5.26 \cdot 10^{-11}$	$5.04 \cdot 10^{-10}$
Residual Water Sat.	S_{wr}	$[-]$	0.10	0.08
Residual NAPL Sat.	S_{nr}	$[-]$	0	0
Water Viscosity	μ_w	$[kg\ m^{-1}\ s^{-1}]$	0.001	0.001
DNAPL Viscosity	μ_n	$[kg\ m^{-1}\ s^{-1}]$	0.001	0.001
Water Density	ρ_w	$[kg\ m^{-3}]$	1000	1000
DNAPL Density	ρ_n	$[kg\ m^{-3}]$	1400	1400
Brooks-Corey	P_d	$[Pa]$	1324	370
	λ	$[-]$	2.49	3.86
van Genuchten	α	$[Pa^{-1}]$	$5.81 \cdot 10^{-4}$	$2.25 \cdot 10^{-3}$
	m	$[-]$	5.34	8.06

Table 4.32: Parameter setup : coarse and fine sands (see Helmig, 1997, pages 276-277).

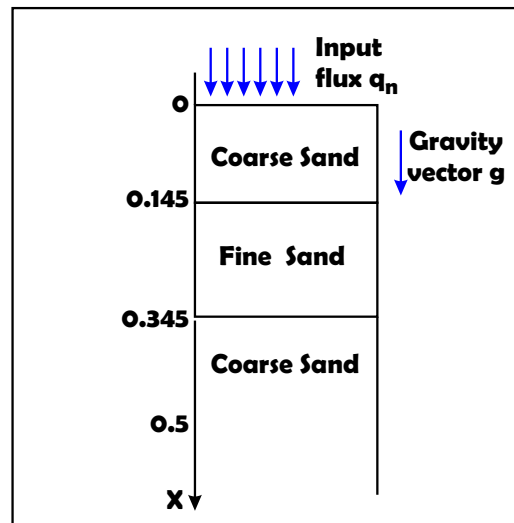


Figure 4.9: Test problem setup

The solutions are plotted in Figures 4.10 and 4.11 at the same time periods as in Helmig, 1997. Although both the Brooks-Corey and van Genuchten functions model the same soils, the barrier effect captured by the Brooks and Corey model functions causes the front of the solutions to be at different distances at $t = 1650$ s. These figures illustrate the fundamental difference between the two approaches to the modeling of the capillary pressure - saturation relationships.

4.3. APPLICABILITY IN HETEROGENEOUS MEDIA

Both Brooks-Corey and van Genuchten solutions agree to the results depicted in Helmig, 1997 on the pages 283-289. Consequently, the interface implementation (4.31) gives correct interface approximation in numerical schemes.

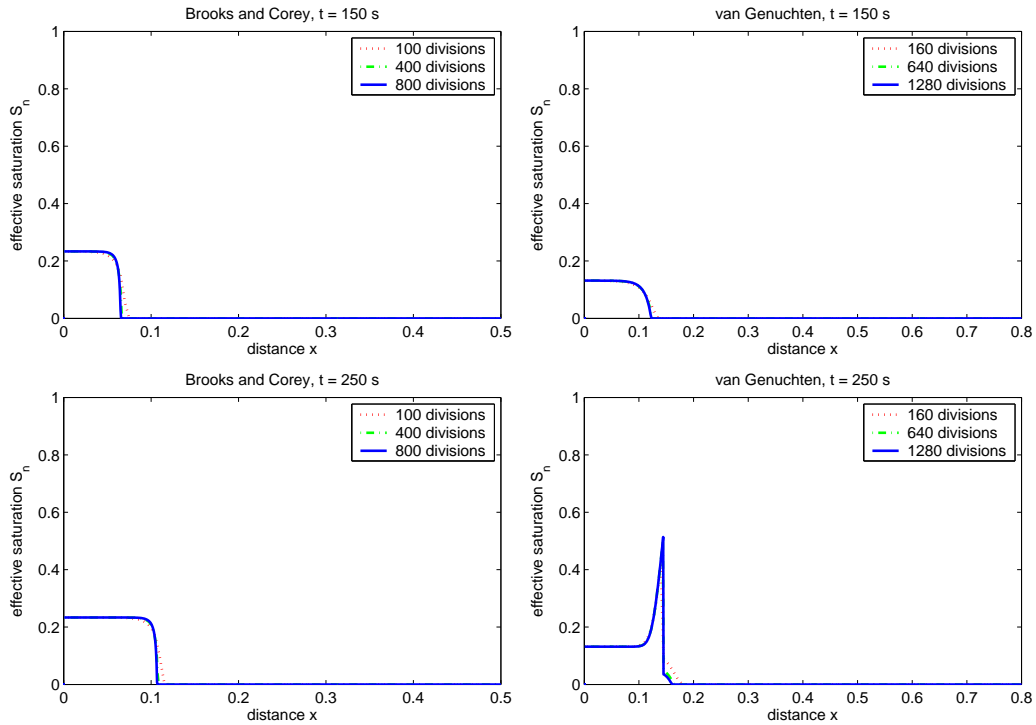


Figure 4.10: Numerical solutions at time $t = 150$ s and $t = 250$ s.

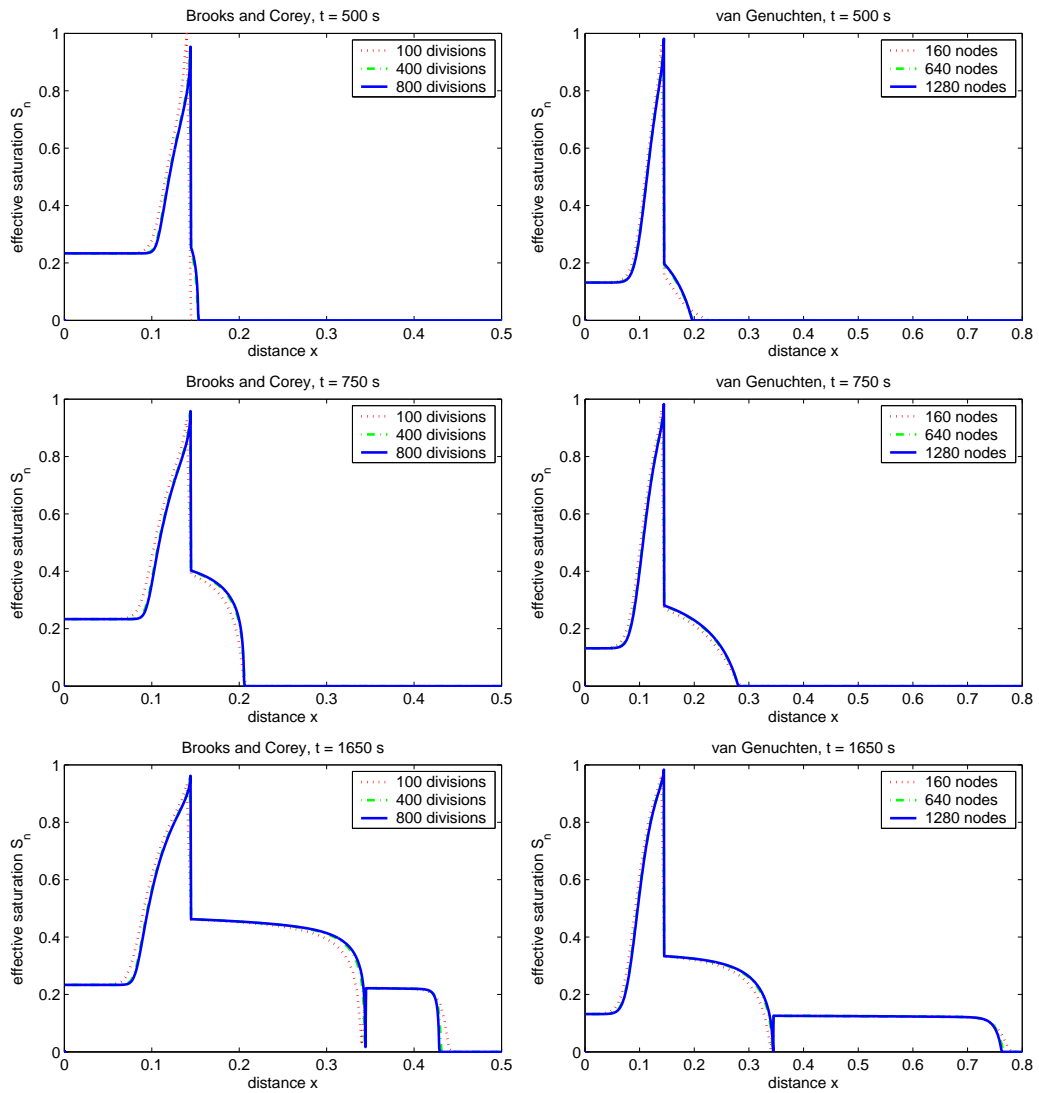


Figure 4.11: Numerical solutions at time $t = 500$ s, $t = 750$ s and $t = 1650$ s.

Conclusions

The presented work is devoted to a detailed discussion of the benchmark solution based on the work by McWhorter and Sunada (1990). The author proposes a reliable procedure of resolution of the implicit functional relationship which is the result of the analytical treatment of the advection - diffusion equation. This algorithm extends the use of the semi-analytical approach for a wider range of entry saturations compared to the original algorithm proposed by McWhorter and Sunada (1990). The use of the algorithm is limited by the round-off errors of the numerical computations only for the case $S_0 \rightarrow 1$ and $R \rightarrow 1$ simultaneously.

From the author's analysis, it follows that the original iterative method proposed by McWhorter and Sunada (1990) can be used to obtain solutions of the unidirectional displacement problem ($R=1$) only in a restricted interval of the entry saturations S_0 . This restriction is given by complications encountered in the first iteration. The modified iterative method removes this issue and offers the solution for larger range of entry saturations.

If $R \in [0, 1]$, the variant A (equation (2.72)) of the modified iterative scheme can be used to compute the solution for any admissible parameters except the values of S_0 extremely close to 1 while the variant B (equation (2.73)) occasionally fails if $S_i > 0$. Therefore the iterative method described by the variant A (equation (2.72)) can be used exclusively for safe computation of the McWhorter and Sunada quasi-analytical solution for $R \in [0, 1]$.

The author concludes that the McWhorter and Sunada exact solution can be derived for negative values of R as a consequence of the problem formulation and the definition of the ratio parameter R . In this situation, both variants A and B (equations (2.72) and (2.73)) of the modified iterative scheme fails for $R < R_{crit} < 0$, but the original iterative scheme works and thus can be used exclusively for safe obtention of the McWhorter and Sunada quasi-analytical solution for negative R .

The comparison of the McWhorter-Sunada fractional flow function F with the Buckley-Leverett fractional flow function F_{BL} allows us to determine the limit of A as $S_0 \rightarrow 1$ and therefore to confirm the statement given by McWhorter and Sunada (1990) compared to the results by Chen et al. (1992) and McWhorter and Sunada (1992).

The McWhorter and Sunada exact solutions can be applied to the two-phase flow heterogeneous porous medium problem discussed in van Duijn & de Neef, 1998. We developed a method that allows to obtain quasi-analytical solutions for the advection and diffusion governed two-phase flow in porous media with a discontinuity and verified its applicability using the first order numerical methods.

The results contribute to a detailed analysis of the analytical benchmark solution often useful for verification of more complex numerical models and in providing a tool for comparison under conditions of high wetting-phase high saturations. Such a code verification was conducted by Mikyška and Illangasekare (2005) where this improved solution was used.

References

- Anderson, M.P., & Woessner, W.W. 2002. *Applied Groundwater Modeling, Simulation of Flow and Advective Transport*. San Diego: Elsevier,.
- Bastian, P. 1999. *Numerical Computation of Multiphase Flows in Porous Media*. Christian-Albrechts-Universität Kiel.
- Bear, J., & Verruijt, A. 1990. *Modeling Groundwater Flow and Pollution*. Dordrecht: D. Reidel, Holland.
- Brooks, R. H., & Corey, A. T. 1964. Hydraulic properties of porous media. *Hydrology Paper*, **3**, 27.
- Chao, W. L., Parlange, J. Y., & Steenhuis, T. S. 2000. An Analysis of the Movement of Wetting and Nonwetting Fluids in Homogeneous Porous Media. *Transport in Porous Media*, **41**, 121–135.
- Collins, R. E. 1976. *Flow of Fluids through Porous Materials*. Tulsa: The Petroleum Publishing Company.
- Das, D. B., Hassanizadeh, S. M., Rotter, B. E., & Ataie-Ashtiani, B. 2004. A Numerical Study of Micro-heterogeneity Effects on Upscaled Properties of Two-phase Flow in Porous Media. *Transport in Porous Media*, **56**, 329–350.
- Fučík, R. 2004. *Numerical solution of multiphase porous media flow, Research work*. Prague: FNSPE of Czech Technical University Prague.
- Fučík, R. 2005. *Numerical analysis of multiphase porous media flow, Research project*. Prague: FNSPE of Czech Technical University Prague.
- Fučík, R., Mikyška, J., & Illangasekare, T. H. 2004a. Evaluation of saturation-dependent flux on two-phase flow using generalized semi-analytic solution. *Pages 25–37 of: Proceedings on the Czech Japanese Seminar in Applied Mathematics FNSPE CVUT Prague*.

REFERENCES

- Fučík, R., Beneš, M., Mikyška, J., & Illangasekare, T. H. 2004b. Generalization of the benchmark solution for the two-phase porous-media flow. *Pages 181–184 of: Finite Elements Models, MODFLOW, and More : Solving Groundwater problems.*
- Hassanizadeh, S. M., & Gray, W. G. 1993. Thermodynamic Basis of Capillary Pressure in Porous Media. *Water Resources Research*, **29:10**, 3389–3405.
- Helmig, R. 1997. *Multiphase Flow and Transport Processes in the Subsurface : A Contribution to the Modeling of Hydrosystems*. Berlin: Springer Verlag.
- Hornung, U. 1997. *Homogenization and Porous Media*. New York: Springer.
- Huyakorn, P. S., & Pinder, G. F. 1983. *Computational Methods in Subsurface Flow*. New York, London, Paris, San Diego, San Francisco, São Paulo, Sydney, Tokyo, Toronto: Academic Press, A Subsidiary of Harcourt Brace Jovanovich, Publishers.
- Kazda, I. 1997. *Podzemní hydraulika v ekologických a inženýrských aplikacích*. Praha: Academia.
- LeVeque, R. J. 1990. *Numerical Methods for Conservation Laws*. Basel, Boston, Berlin: Birkhausen Verlag.
- LeVeque, R. J. 2002. *Methods for Hyperbolic Problems*. Cambridge, New York, Melbourne, Madrid, Cape Town: Cambridge University Press.
- Mikyška, J. 2005. *Numerical Model for Simulation of Behaviour of Non-Aqueous Phase Liquids in Heterogeneous Porous Media Containing Sharp Texture Transitions, Ph.D. Thesis*. Prague: FNSPE of Czech Technical University.
- Mikyška, J., & Illangasekare, T. H. 2005. Application of a Multiphase Flow Model for Simulations of NAPL Behavior at Inclined Material Interfaces. *Pages 117–127 of: Proceedings of Czech-Japanese Seminar in Applied Mathematics 2004, editors M. Beneš, J. Mikyška, T. Oberhuber*. ISBN 80-01-03181-0.
- Mikyška, J., Beneš, M., Turner, A., & Illangasekare, T. H. 2004. Development and Validation of a Multiphase Flow Model for Applications in NAPL Behaviour in Highly Heterogeneous Aquifer Formations. *Pages 215–218 of: Proceedings on FEM_MODFLOW and More, editors K. Kovář, Z. Hrkal and J. Bruthans*.
- Morel-Seytoux, H. J., Meyer, P. D., Nachabe, M., Touma, J., van Genuchten, M. T., & Lenhard, R. J. 1996. Parameter equivalence for the Brooks-Corey

- and van Genuchten soil characteristics: Preserving the effective capillary drive. *Water Resources Research*, **32:5**, 1251–1258.
- Sunada, D. K., & McWhorter, D. B. 1990. Exact Integral Solutions for Two-Phase Flow. *Water Resources Research*, **26**, 399–413.
- Sunada, D. K., & McWhorter, D. B. 1992. Reply. *Water Resources Research*, **28**, 1479.
- Turner, A. D. 2004. *Behavior of dense non-aqueous phase liquids at soil interfaces of heterogeneous formations: Experimental methods and physical model testing. Numerical Computation of Multiphase Flows in Porous Media. Master's thesis.* Colorado School of Mines, Golden, Colorado.
- van Duijn, C. J., & de Neef, M. J. 1998. Similarity solution for capillary redistribution of two phases in a porous medium with a single discontinuity. *Advances in Water Resources*, **21**, 451–461.
- van Genuchten, M. T. 1980. A closed-form equation for predicting the hydraulic conductivity of unsaturated soils. *Soil Science Society of America Journal*, **44**, 892–898.
- Vitásek, E. 1994. *Základy teorie numerických metod pro řešení diferenciálních rovnic.* Praha: Academia.
- Walser, G. S., Illangasekare, T. H., & Corey, A. T. 1999. Retention of liquid contaminants in layered soils. *Journal of Contaminant Hydrology*, **39**, 91–108.
- Z.-X. Chen, G. S. Bodvarsson, & Witherspoon, P. A. 1992. Comment on 'Exact Integral Solutions for Two-Phase Flow'. *Water Resources Research*, **28**, 1477–1478.

Index

- averaging, 7
- barrier effect, 66
- bi-directional displacement, 24
- Brooks and Corey model, 14, 17
- capillarity, 12
- capillary pressure, 13
- characteristics, 28
- compound wave, 29
- contact angle, 12
- continuity theorem, 8, 11
- convex hull, 30
- Darcy law, 8
- density, 4, 8
- displacement
 - bidirectional, 35
 - unidirectional, 35
- DNAPL pooling, 14
- drainage, 15
- dual formulation, 30
- dual formulations, 24
- dynamic viscosity, 4, 8
- entropy condition, 29
- entry pressure, 14
- equal area rule, 30, 32
- Euler method, 88
- experimental order of convergence, 91
- extended capillary pressure condition, 19
- fountain, 8
- fractional flow function, 22
- heterogeneity, 7
- homogenization, 7
- imbibition, 15
- ink bottle effect, 15
- integral equation
 - modified, 47
 - original, 40
- interface condition, 18
- macroscale, 5
- macroscopic apparent velocity, 8
- mass conservation law, 8, 18
- microscale, 5
- mobility, 11
- molecular scale, 5
- NAPL, 5
 - DNAPL, 5
 - LNAPL, 5
- Newtonian fluid, 8
- non-wetting phase, 12
- permeability
 - absolute, 8, 11, 20
 - relative, 11, 16
- phase, 4
- porosity, 6, 8
- porous medium, 3
 - heterogeneous, 7
 - homogeneous, 7
- postshock value, 29
- pressure, 8

Rankine-Hugoniot condition, 30
rarefaction wave, 29
representative elementary volume, 7
REV, 7, 10
Reynolds number, 8

saturation, 9
 effective saturation, 10
 residual saturation, 10
shock speed, 29
 fractional, 29
sinks, 8
sources, 8
surface tension, 12
surfactant, 10

total velocity, 21
total velocity condition, 35
two-phase flow equation in 1D, 23
 with gravity, 85

unidirectional displacement, 24
upwinding, 86

van Genuchten model, 14, 18

weak solution, 29
wetting phase, 12

Young's equation, 12